Harvesting Energy from Microbial Fuel Cells and their Impedance Analysis

Doctoral Dissertation
Doctoral Program in Electronic Engineering (31st Cycle)

Harvesting Energy from Microbial Fuel Cells and their Impedance Analysis

Daniyal Ahmed
* * * * * *

Supervisors
Dr. M. Quaglio, Supervisor
Prof. F. Pirri, Co-Supervisor

Doctoral Examination Committee:
Prof. F. Adani, Referee, Università degli Studi di Milano.
Dr. S. Marasso, Referee, Consiglio Nazionale delle Ricerche.

Politecnico di Torino
May 19, 2019

I hereby declare that, the contents and organization of this dissertation constitute my own original work and does not compromise in any way the rights of third parties, including those relating to the security of personal data.

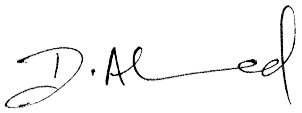

……..

Daniyal Ahmed

Turin, May 19, 2019

Summary

At present, the world in a dire need of green, renewable and sustainable energy sources. There are many reasons for this, for example, the ever-growing problem of pollution caused by fossil-fuel based energy sources, the depletion of fossil-fuel resources and the world's growing population. The main aim of my work is to investigate an upcoming source of sustainable energy – Microbial Fuel Cells (MFCs). MFCs are bio-electrochemical devices which are based on electro-active bacteria. These bacteria produce electrons in their metabolic process. The electrons produced by these bacteria can be collected on the electrode and later stored into a battery/super capacitor through a power management system.

This thesis is an in-depth explanation of the work I performed on MFCs. Initially, I worked on investigating the internal processes occurring on the anodes of MFCs, related to diffusion of substrates and the bacteria's charge transfer mechanisms. The main tool used for this study was Electrochemical Impedance Spectroscopy (EIS). EIS is a non-invasive technique used to study a variety of systems. It is performed by exciting the system under study using a small alternating voltage at different frequencies. The resulting current responses are used to calculate the impedance of the system at each frequency point. During this part of my work, we analyzed a biofilm formed by mixed community bacteria and inferred conclusions about the different processes detected by EIS.

The next part of my work was dedicated to energy harvesting from MFCs. More specifically, the work was related to a special kind of MFCs known as floating-MFCs (fMFCs). fMFCs are mostly used in aquatic/marine environments to harvest energy using seawater as the source of organic matter. An integral part of this work was to propose a setup of fMFCs which requires minimal cost and effort to start functioning as an energy harvesting device. Mostly, the MFCs used are setup in the laboratory and a considerable amount of time and effort is required in the initial acclimation period. Furthermore, different chemical compounds are also required in this phase which add to the overall cost of the device. Therefore, these methods of MFC startup impose limitations on their use. To ensure the widespread use of MFCs as devices producing sustainable energy, it is important to devise cost-effective and simple ways of setting them up. The later part of my work focused on developing an fMFC with an in-situ biofilm formation. Not only does it help reduce the cost of the fMFC's setup, but also makes its use more feasible for different applications in the marine environment.

It is important that we shift our focus towards the use of renewable and sustainable energy sources. Not only is it essential for the deteriorating environment but it also enables us to rely less on the limited fossil fuel resources. MFCs are a step in this direction. Even though, the amount of extractable energy from MFCs is low, they are still very useful in providing a continuous source of energy for low power applications based in remote environments.

Acknowledgment

I would like to take this opportunity to recognize the importance of various individuals without whose mentorship, support and guidance I would not have reached this point. First of all, I would like to thank my supervisor Dr. Marzia Quaglio for always being there for me and providing crucial guidance in both scientific and personal realms. She is not only an exceptional teacher to me but, a person who shaped me professionally. I would also like to thank Prof. Fabrizio Pirri for giving me the opportunity to work in his prestigious scientific group. I would also like to extend my gratitude to Dr. Adriano Sacco for being an excellent teacher on EIS and MFCs and an inspiration for work ethics. I also want to express my appreciation for the role Dr. Giulia Massaglia has played during these past years. She has not only been a great friend to me but also taught me a lot about MFCs. Last but not the least, I would like to thank Dr. Valeria Agostino for being a good friend and for her efforts in introducing MFCs to me. I want to once again extend my gratitude to Dr. Adriano Sacco, Dr. Giulia Massaglia and Dr. Marzia Quaglio for helping in the writeup of this thesis and for their great efforts in reviewing it. I also want to thank everyone at CSFT IIT for their kindness during this period.

Lastly, I would like to thank my family, especially Ayesha for her endless support and encouragement and my parents for their endless efforts and love throughout my life.

1 Table of Contents

List of Tables

List of Figures

2 Context of Research

Sustainable and renewable energy is one of the most crucial needs of the world at present. Not only does it solve the problem of limited fossil fuel resources, but also tackles the problem of pollution caused by energy produced using fossil fuels. Therefore, in the recent decades a lot of research is being done in the area of sustainable and renewable energy[1,2]. This need to shift to renewable and sustainable energy resources is not being stressed enough. To ensure that the world moves in this direction, many countries collectively have decided to work together towards sustainability for the first time in history. Thanks to the agreement signed in 2015 during the COP21 Conference held in Paris, the European share of renewable electricity in the overall energy production will dramatically increase over the next decades. In this scenario, production and technological processes driven by renewable electrical energy are gaining a renewed interest.

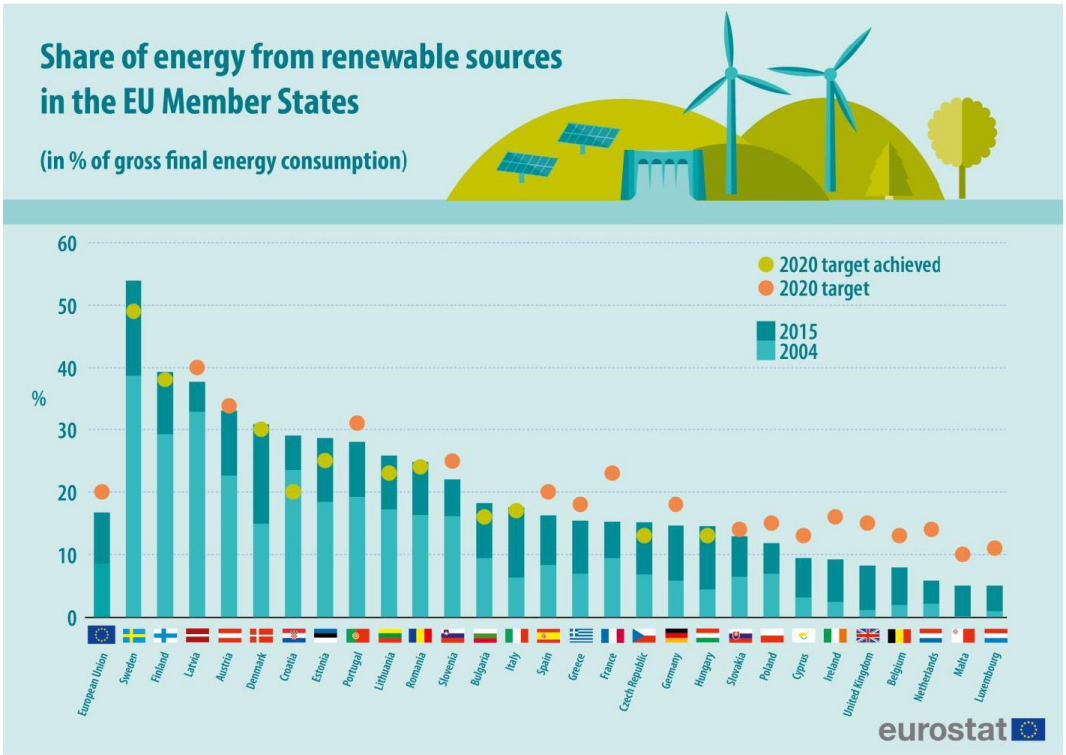

Figure 1: A comprehensive outlook on the goals and targets achieved by different European countries in terms of percentage energy consumption from renewable resources[3].

Figure 1 shows a chart of the different countries in Europe and their targets for the year 2020 in terms of percentage energy consumption using renewable energy.

The graph shows that European countries, as a whole, have set a target to use renewable energy to provide for 20% of the total energy used by the year 2020.

Another important issue being faced by the world, that needs to be addressed as soon as possible, is the unavailability of clean water to the masses and a major part of this problem stems out from the paradigm of energy expensive wastewater treatment. According to World Health Organization (WHO)/UNICEF Joint Monitoring Program (JMP) Report 2017, a total of 844 million people in the world do not have access to clean water. Another report published by WHO in 2015 stated that:

> *"Every minute a newborn dies from infection caused by lack of safe water and an unclean environment"*
>
> *(WHO, 2015)*

All these statistics point towards the dire need of not only providing clean water to people but also treating the wastewater properly.

Microbial Fuel Cells (MFCs) directly address both the issues. MFCs are bio-electrochemical devices that are based on Electroactive Bacteria (EAB). These bacteria are able to convert chemical energy stored in organic compounds to electrical energy. The sources of these organic compounds can be various but one of the most notable sources is wastewater. EABs in MFCs can break down organic compounds in wastewater and in the process produce energy. In other words, MFCs are devices able to produce energy while treating wastewater. Due to these exciting properties of MFCs, they have been studied extensively in the past few years.

The work presented in this thesis revolves around MFCs. They are described in a comprehensive manner and different techniques used to analyze their performance are also discussed. This dissertation also discusses in detail Electrochemical Impedance Spectroscopy (EIS) which is a non-invasive electrochemical technique used to analyze electrochemical systems in general and MFCs specifically. Furthermore, works that we performed on MFCs during the course of my Ph.D. are also discussed in detail. The main body of this thesis is divided into a total of 5 chapters following this chapter. The contents of these chapters are briefly described as follows:

- **Chapter 3 –**
- **Microbial Fuel** Cells, is a complete description of MFCs. It starts by giving an introduction of MFCs and the different works related to MFCs that can be found in the literature. Moving on it explains in more depth EABs and the different electron transfer mechanisms which enable the bacteria to transfer electrons from the biofilm to the anode. Furthermore, the chapter discusses the different architectures that have been used and proposed in different works. The chapter also discusses how MFCs produce energy and builds the mathematical basis to calculate voltage and power generation from MFCs. Lastly it also discusses the power management systems typically used to extract and store power from MFCs and some of the other uses of MFCs such as biosensors and their use in hydrogen production.
- **Chapter 4 – Electrochemical Impedance Spectroscopy**, is a chapter that is dedicated to the explanation of EIS. EIS was an integral part of the work I performed during my Ph.D. and an in-depth explanation, which is provided in this chapter, was necessary to understand the works presented in later chapters. This chapter introduces EIS and discusses how powerful this technique can prove to be while analyzing a variety of systems. Later, it goes into explaining the theoretical and mathematical foundations necessary to understand how EIS works. This chapter also explains the different representations and analytical techniques that are typically employed to elaborate and understand data collected through EIS. It also discusses Nyquist and Bode plots that are typically employed to represent data obtained from EIS. Lastly, this chapter discusses the use of EIS in investigating MFCs as electrochemical devices. It also explores the techniques used by different groups around the world have in order to interpret EIS data, some of which are not very suitable.
- **Chapter 5 – Characterization and analysis of MFCs based on mixed community bacteria using different enrichment methods**. This chapter is related to an experimental and analytical work that we performed as part of my Ph.D. This work mainly deals with MFCs

based on mixed communities enriched using different methods of enrichments. The main tool employed to analyze MFCs in this work was EIS but other electrochemical and biological imaging techniques were also used in order to confirm our hypothesis. The work was broken down into two sets of experiments in which the first set was related to the acclimation of biofilm while the second one was related to the analyses of different enrichment methods and their effects on MFCs' performances. This chapter discusses in detail the experimental procedures we employed and the architecture of MFCs that we used. This is followed by the results and discussions section which provides an in-depth analysis into the results we obtained and our conclusions.

- **Chapter 6 – Moving Towards an in-situ Practical Application of MFCs as Power Sources**, this chapter is related to another work that we performed during the period of my Ph.D. The main aim of this work was to develop cost effective, compact and mobile floating MFCs (fMFCs). fMFCs are a novel type of MFCs designed to operate in the marine environment. Furthermore, another important part of this work was to propose an in-situ enrichment method which would reduce the costs, time and effort required to make fMFCs operational. This work was divided into two sets of experiments, the first one was related to the comparison of a standard enrichment technique with the in-situ enrichment method that we proposed. The second part of the experiment was related to the in-situ performance monitoring of fMFCs based on the in-situ enrichment method. This second experiment was composed of two experimental campaigns – one in the summertime while the other in winter/autumn period. This was done to study the effects of seasonal changes and the robustness of the proposed systems. A complete description of the experimental techniques and methods employed has been provided in this chapter which is followed by a detailed discussion of the results obtained.
- **Chapter 7 – Conclusion**, this chapter concludes the dissertation giving a summary of all the works performed and the outcomes that we obtained from them.

3 Microbial Fuel Cells

3.1 Introduction

Microbial Fuel Cells (MFCs) are bio-electrochemical systems (BES) that can be used to drive an electrical current through an external load. These devices are based on a special type of bacteria, known as electro-active bacteria (EAB) that produce electrons during their metabolic process[4,5]. MFCs, being a type of fuel cell, are generally composed of an anode on which a substrate such as organic matter is oxidized by the EAB which form a biofilm on the electrode, and of a cathode where the oxygen reduction reaction occurs[6]. A biofilm is a layer of bacterial and/or other microorganism community that attaches itself on to a surface. In the case of MFCs, this surface is usually the anode. In the start, a biofilm is inoculated onto a material which later becomes a part of the anode. Figure 2[7] shows an image of a biofilm formed on the anode of an MFC and was obtained using scanning electron microscope (SEM). Initially, the microorganisms are attached to the surface due to a weak hydrophobic effect and due to the presences of Van der walls forces. Then, over time, these bacteria and their biofilm improve their adhesion to the surface by using pili and by producing polymeric substances which form an extracellular matrix, keeping the biofilm intact and attached to the surface.

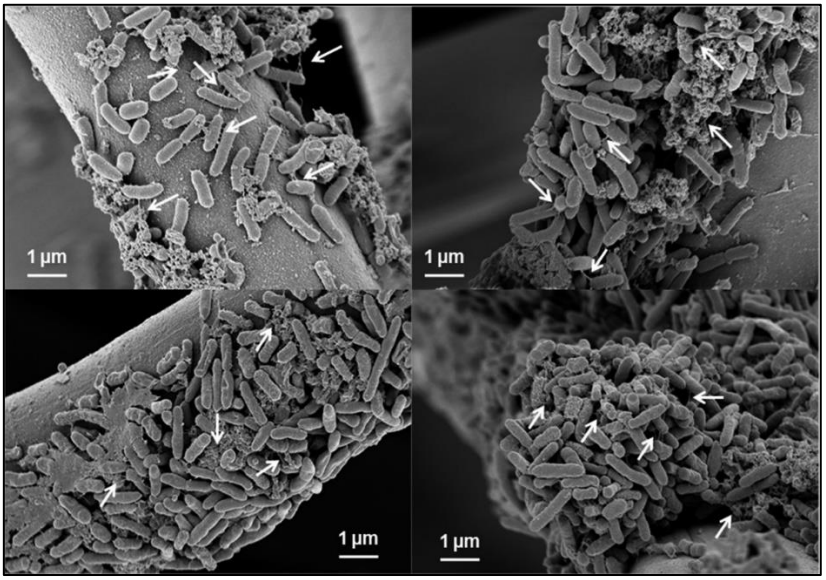

Figure 2: Biofilm formation on the anode[7]. Reprinted with permission from Environmental Science and Technology, ACS Publications.

The anode usually works in an anaerobic condition while the cathode works in an aerobic condition. Moreover, the anode and the cathode are submerged into a fluid containing nutrients for the bacteria and providing a medium for the transport of charges and molecules. Furthermore, there are specific electrochemical reactions occurring on both the anode and the cathode of an MFC. For example, typical setups of MFCs in the lab have oxidation of sodium acetate occurring on the anode while oxygen is being reduced on the cathode. There are two general types of MFCs, double chamber and single chamber. In double chamber MFCs, the anode and the cathode chambers are separated by a proton exchange membrane (PEM)[8]. While in the case of single chamber MFCs, there is no such separation between the anode and the cathode. The produced electrical current can be collected using an external load connected to the cathode and anode. Figure 3[6] shows a typical setup of an MFC. The image is not drawn to scale. It can be seen that the bacteria, which grows on the anode, consumes a substrate (glucose in this case) and in the metabolic process produces electrons. These electrons are then transferred to the anode.

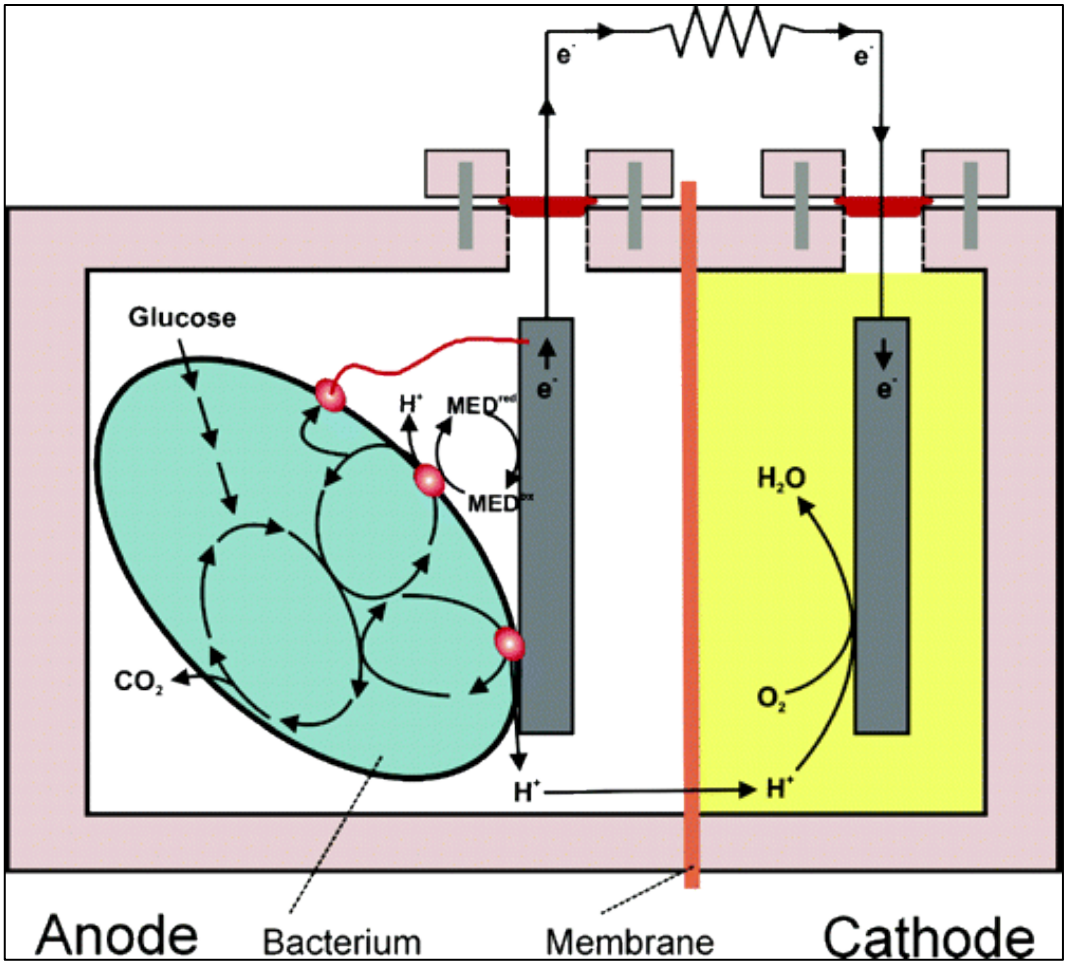

Figure 3: Setup of an MFC[6]. Reprinted with permission from Environment Science and Technology, ACS publications.

The process of an electron's transfer from the bacteria to the anode is more generally known as electron transfer mechanism. In the recent years a lot of research has been done to understand the different mechanisms by which an electron moves from the bacteria to the anode[9–11].

3.2 Electroactive Bacteria (exoelectrogens)

Electroactive Bacteria (EAB) are basically defined as bacteria able to provide conductive pathways to electrons through membranes that are biological in nature. This transport of electrons can be either to or from the bacteria's extra-cellular environment[7]. The kind of bacteria that can transfer electrons outside their cells body are known as exoelectrogens. The special feature of exoelectrogens is that they are able to transfer electrons directly outside the cell without the use of any compounds that are soluble e.g. mediators such as sulfates and nitrates etc. There are many types of exoelectrogens that have already been discovered but as research

in this field is moving on, many more bacteria have been discovered that are capable of performing exoelectrogenic activity.

Two of the most common EAB species that are used to investigate MFCs are Geobacter sulfurreducens and Shewanella oneidensis[12]. The species have particular importance in metal reduction. Nevertheless, there are studies conducted on MFCs using other types of bacteria or a mixed community[9]. In particular, Nevin et al. discovered that biofilms formed using a mixed community of bacteria performed better than a biofilm formed using Geobacter sulfurreducens[7].

3.3 Electron Transfer Mechanisms in MFCs

Exoelecrogenic bacteria uses multiple ways to transfer electrons on to an external surface and/or element. According to recent research, these electron transfer mechanisms can be categorized into three main categories[13]:

- Mediated electron transfer (MET)
- Indirect electron transfer (IET)
- Direct electron transfer (DET)

In the case of MET, molecules are present in the vicinity of the bacteria which are inert and can carry electrons through regeneration. These molecules act as shuttles for the electrons produced by the bacteria. These so-called mediator molecules, such as flavins and phenazines, are naturally produced by many microorganisms and secreted in their vicinity to help electron transfer. Such mediators are also termed as exogenous mediators since they transport the electrons from outside the bacteria's cell body to a surface such as the electrode. The middle part of Figure 4 shows a mediated electron transfer path between the microorganism and electrode surface.

Furthermore, for IET, EAB use soluble compounds that act as electron donor and acceptor pair. Examples of such compounds/molecules are formic acid and hydrogen. These molecules can either be already present in the environment or secreted by the microorganisms. This type of charge transfer usually occurs in the form of ions such as transfer of hydrogen between different species.

Lastly, DET is one of the most important and efficient electron transfer mechanism exhibited by electro-active microorganisms. This electron transfer

mechanism involves the use of specific compounds on the surface of the microorganism which enable electron transfer such as c-type cytochromes. These compounds are redox proteins, they are bounded to the bacterial cell membrane, in contact with the surface to which electrons are being transferred e.g. the anode. Furthermore, another type of DET involves the presence of wire like structures known as pili or nanowires. These nanowire structures make a physical connection between the microorganisms and the external surface to which electrons are to be transferred. The electrical behavior of such nanowires has also been studied[14] with a conclusion that these nanowires are indeed electrically conductive and can be used for the process of direct electron transfer from the bacteria to another surface e.g. anode of an MFC. The first part of Figure 4 shows a graphical representation of how direct electron transfer occurs in both the modes, through cytochromes and through pili.

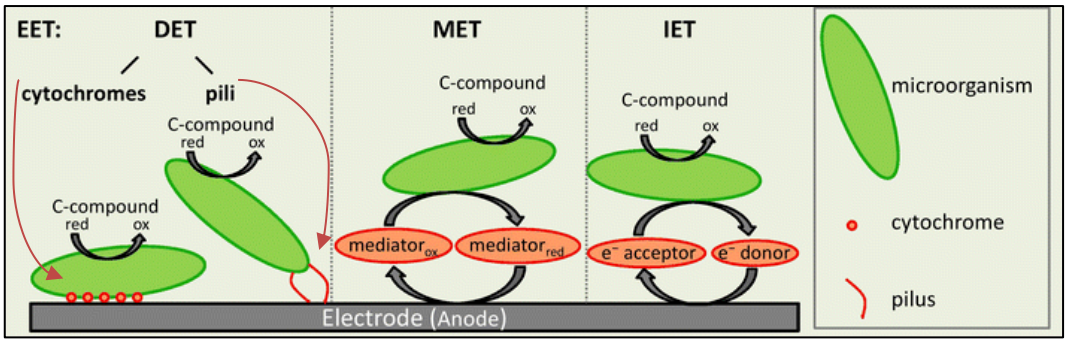

Figure 4: Electron transfer mechanisms in EAB[13]. Reprinted with permission from Applied Microbiology and Biotechnology, Springer Link.

It is interesting and useful to study how the electron transfer mechanism between bacteria and anodes is one of the limiting factors to an MFC's performance.

3.4 Energy from MFCs

The electrical energy obtained from MFCs is intrinsically a part of the energy present in the substrates that the bacteria in MFCs consume in their metabolic process. These substrates can be artificial or can be present naturally in the medium that the bacteria are inhabiting. One example of naturally occurring substrates that the bacteria can use in their metabolic process are the compounds present in wastewater. Shizas et al. found out in a study in 2004 that the waste water treated by a facility in Toronto, Canada, contained 9.3 times the energy required to treat

that water[15]. With proper research and development in this field, theoretically, wastewater treatment plants could produce energy while treating wastewater.

The total chemical energy, held in organic compounds of the substrate, that is processed by the microorganisms is partially used by them for their growth and reproduction. The remaining energy is released by the bacteria in the form of electrical energy. The following relationship in terms of Gibbs free energy of the system can hence be defined.

$$\Delta G_{MFC} = \Delta G_{total} - \Delta G_{bacteria} \quad (1)$$

Where, ΔG_{MFC}, is the energy of the system that can be theoretically delivered to other systems, ΔG_{total} is the total energy of the electrochemical process and $\Delta G_{bacteria}$is the energy required by the bacteria for its growth and reproduction. ΔG_{total}, on the other hand, can be defined using the following relationship;

$$\Delta G_{total} = -n.F.E_{cell} \quad (2)$$

Where, n is the number of electrons involved in the electrochemical reaction (the reactions involving the bacteria's metabolism), F is the Faraday's constant and E_{cell} is the total emf of the cell. Considering the laws of thermodynamics, if ΔG_{total} is negative, the electrochemical reaction under consideration will occur spontaneously while if it is positive, the reaction will not occur on its own and will require and external energy to complete the reaction. In the case of an MFC, E_{cell} can be calculated using equation (3);

$$E_{cell} = E_{cathode} - E_{anode} \quad (3)$$

The Electromotive forces (emfs) $E_{cathode}$ and E_{anode} depend on the reactions that are occurring on the respective electrode. Some examples of these reactions are given in Table 1. These examples also contain the cases where ΔG_{total} is positive and thus these reactions would require an external energy to occur.

Table 1: Different electrochemical reactions and their Gibbs free energy calculations considering standard conditions. All the voltages provided are with respect to the standard hydrogen electrode (she).

Reaction on Anode	E_{anode} (V) vs SHE	Electrons involved in reaction	Reaction on Cathode	$E_{cathode}$ (V) vs SHE	Electrons Involved in reaction	E_{cell} (V)	ΔG_{total} (kJ)
Oxidation of Acetate	-0.29	8	Reduction of O_2	0.82	4	1.1	-849
			Reduction of NO_3^- to NO_2^-	0.42	2	0.71	-548
			Reduction of Ferrycianide	0.36	1	0.65	-502
Oxidation of Water	0.82	4	H^+ reduction to H_2	-0.41	2	-1.23	475
			CO_2 reduction to acetate	-0.29	8	-1.1	849
			CO_2 reduction to CH_4	-0.24	8	-1.06	818
			SO_4^{2-} reduction to S^{2-}	-0.21	8	-1.03	795

Anode Reactions Cathode Reactions

As can be seen from Table 1, the voltages corresponding to each reaction are different. Take for example the oxidation of Acetate on the anode of an MFC. This reaction gives rise to a voltage of -0.29V on the anode with respect to the standard hydrogen electrode (SHE). If the same MFC has a cathode on which a reduction of O_2 is occurring (having a potential of 0.82V with respect to SHE), the overall potential across the MFC can achieve a theoretical value of 1.1 V, using equation (3).

MFCs provide an opportunity to obtain devices that are able to extract the energy locked in a substrate. If the function of an MFC is coupled with waste water treatment a system can be obtained which is not only useful for the treatment of waste water but also beneficial in terms of producing electrical energy[16–18]. However, there are multiple challenges that need to be tackled before these devices could be successfully used as sustainable electrical energy sources providing wastewater treatment facilities as well.

3.5 MFC Architecture

MFCs generally are based on one of the two main types of architectures – single chamber or dual chamber. In single chamber MFCs (scMFCs), the whole cell is setup in one enclosure without any partitions. The anode is kept under anaerobic conditions while the cathode is exposed to oxygen (from air) to enable the oxygen reduction reaction. Since the cell is single chamber and consequently the electrolyte is in common between anode and cathode, it is important to ensure that the anode remains in an anaerobic condition and the biofilm does not interact with oxygen. To ensure this, Cheng and co-workers added a hydrophobic layer to side of the cathode which faced the air[19]. Another key limit for scMFC performance is the oxygen reduction reaction (ORR), which occurs in the cathode compartment. To this purpose, a catalyst layer is added to the cathode to enhance the ORR. In particular, for air breathing scMFCs, that directly use oxygen from air, the cathode electrode must be modified by applying both a catalyst layer and a hydrophobic air diffusion layer, on opposite sides of the electrode. This approach avoids water leakage from the device, while permitting the diffusion of oxygen from outside, into the device. As deeply investigated in the literature[20–22], the most promising catalyst layer for ORR is Platinum, which ensures an ideal number of electrons equal to 4, guaranteeing the direct reduction of oxygen to water (H_2O) and avoiding the intermediate reaction that requires only 2 electrons with hydrogen peroxide as one of the products, which is toxic for microorganisms. Figure 5 shows a schematic of a typical setup of an air breathing scMFC, having a common medium to which both the anode and the cathode are exposed. Organic substrate is present in this medium to support bacterial metabolism on the biofilm formed on the anode. Moreover, it can be seen from the image that there is a flux of protons from the

anode to the cathode. This is due to the fact that, on the cathodic side, the electrons released from the anode have to recombine with the protons.

On the other hand, a dual chamber MFC is setup in a way that it contains two chambers – the anodic chamber and the cathodic chamber, as sketched in Figure 6. Both the chambers are separated from each other with the help of a proton exchange membrane (PEM). This membrane allows the exchange of protons from one side to the other while inhibiting other molecules to cross over. Moreover, in the case of dual chamber MFCs, the cathodic medium and anodic medium can differ from each other. Usually organic substrates are present in the anodic chamber while in the cathodic chamber solution based on chemicals such as Potassium ferricyanide are present[6]. These chemicals provide the reduction element for the cathodic reaction. In Figure 6, it can be seen that Fe^{3+} is reduced to Fe^{2+} on the cathodic side.

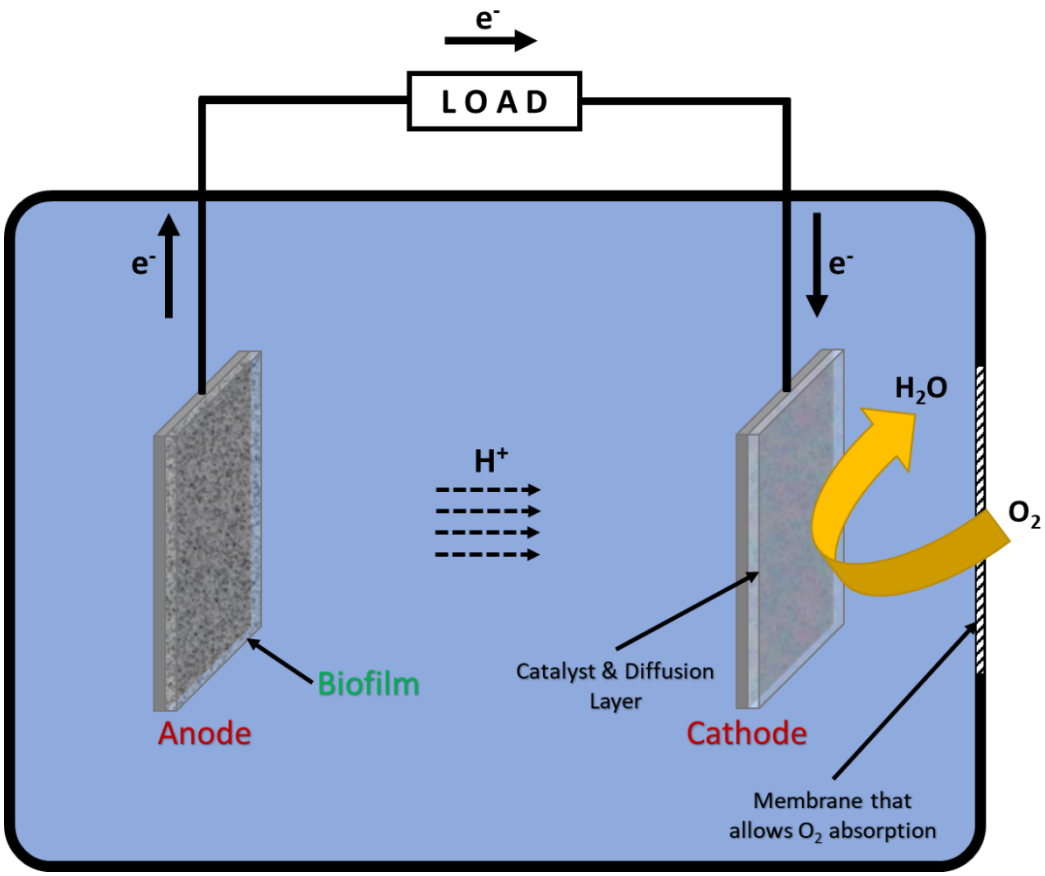

Figure 5: Schematic of a single chamber MFC.

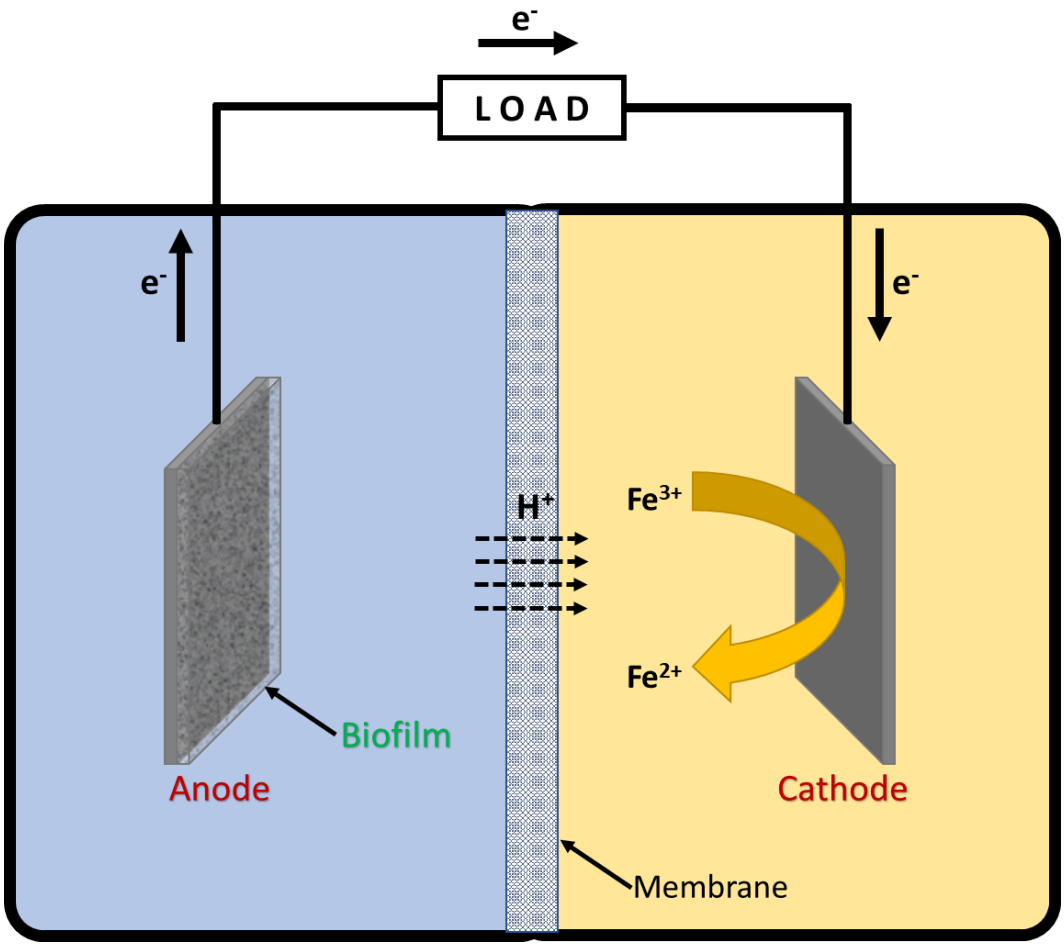

Figure 6: Schematic of a Dual chamber MFC.

A special type of single chamber MFC and one that is particularly important in my work is Sedimentary Microbial Fuel Cell (SMFC). As the name suggests, an SMFC is commonly designed to be used in the marine environment. Nevertheless, most lab experiments done on SMFC mimic the marine environment by using sediment from the sea/ocean and seawater. Figure 7 shows a representation of what the setup of an SMFC in the marine environment looks like.

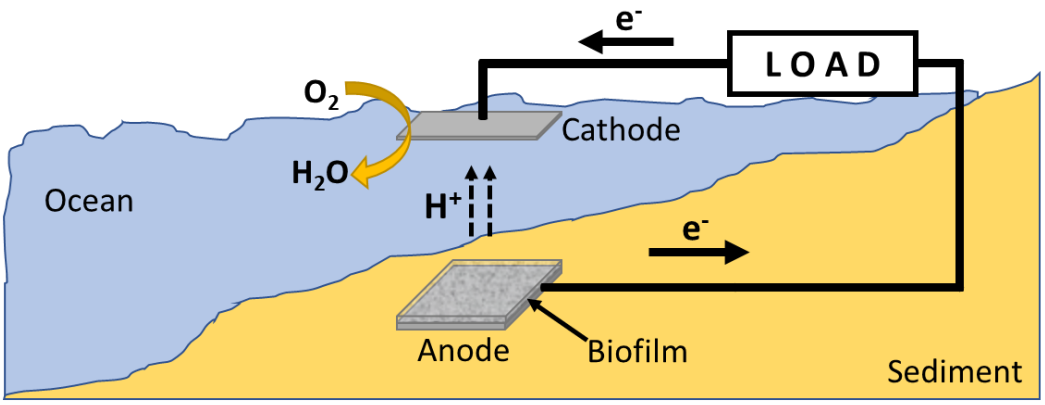

Figure 7: The setup of an SMFC in the marine environment.

In this setup of an SMFC, the anode is buried inside the sediment of the ocean/sea. This provides the anode with its required anaerobic conditions. The cathode is placed in the overlaying water. This also enables the cathode to access the dissolved oxygen in water for ORR. Since sea water is high in salinity, it provides a good conductive medium for the transfer of ions. Moreover, the organic matter present in the sediment and the seawater provide the biofilm formed on the anode with the required organic substrates to support its metabolic processes. Another advantage of SMFCs is that the microorganisms, which are required to inoculate the anode, are already present inside the sediment. Therefore, it is not required to inoculate the anode before setting up the SMFC. SMFCs, due to their ease of setup and their zero up keep, can be used in remote locations to provide energy for various applications such as remote sensing[23–25].

As discussed earlier, SMFCs can also be setup in the lab to perform experiments. An example of such a setup is shown in Figure 8.

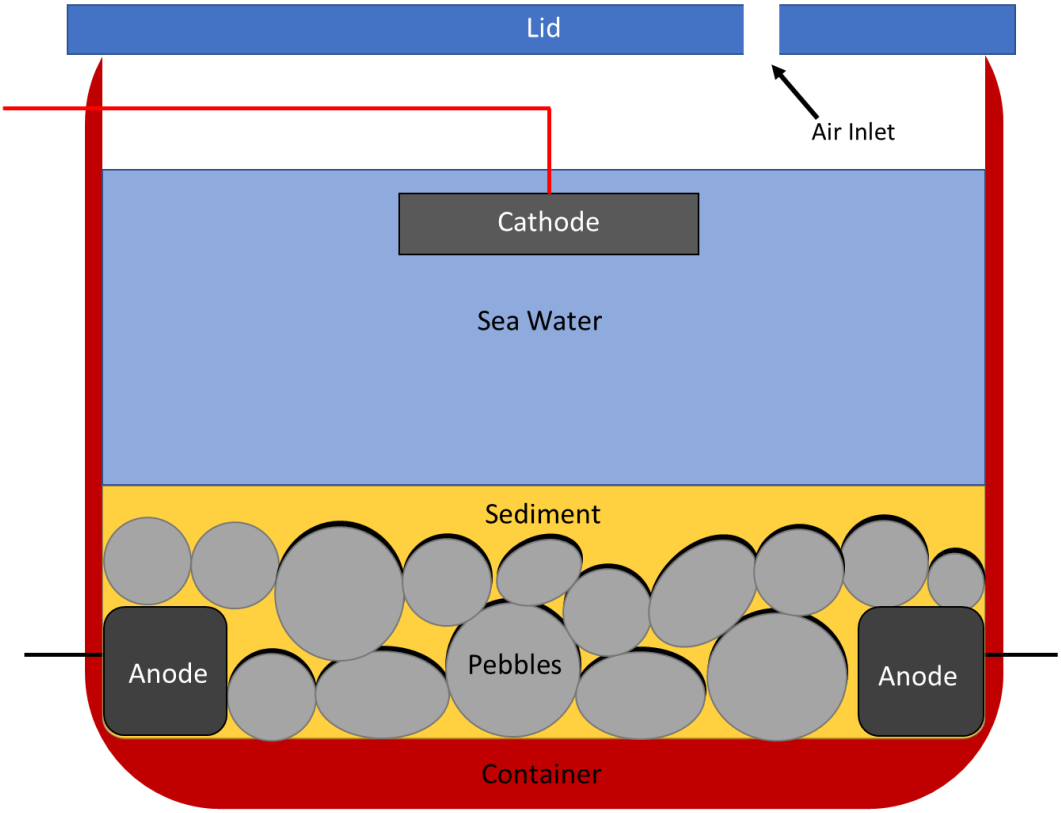

Figure 8: SMFC setup in a container.

It can be seen in Figure 8 that the SMFC is setup in a container with the anode buried inside the sediment. On the other hand, the cathode is placed near the surface of the water for better access to oxygen. Moreover, a slit is left open in the lid to provide proper aeration and absorption of oxygen into the seawater for the cathodic reaction. Several groups all around the world have conducted experiments on similar SMFC setups[26–30].

Each of these architectures have their advantages and disadvantages. Dual chamber MFCs are usually set up using water soluble electron acceptors (in the cathodic chamber) that have a quite low reduction potential with respect to SHE. This makes the reaction at the cathode quite favorable. On the other hand, the most frequently used electron acceptors (e.g. Potassium ferricyanide) are chemicals that can have implications on the environment. Moreover, these chemicals need to be renewed into the cathodic medium, therefore requiring to refresh the cathodic medium in a continuous manner or at regular intervals, consuming energy for pumping operations and needing human supervision. Furthermore, due to the low reduction potential of these chemicals, $E_{cathode}$ is low in magnitude thus reducing the overall performance of the device.

Similarly, single chamber MFCs have their own advantages and disadvantages. Single chamber MFCs typically reduce oxygen on the cathode. Therefore, they do not require any chemicals at the cathode and thus, this feature make them favorable for the environment. This also eliminates the need to continuously feed the cathode if oxygen is available at the cathode side of a single chamber MFC. Moreover, the reduction of oxygen has a potential quite high with respect to the SHE (0.82 V, see Table 1). This ensures that these cells have a better overall performance since $E_{cathode}$ is higher. One more advantage of a single chamber MFC is that it can be used in dimensions that are much smaller and having a simpler design. The smaller dimensions of this class of devices make much easier to set them up.

Despite for the all the described advantages, scMFCs also exhibit some disadvantage as well. Mainly, to support the oxygen reduction reaction, that converts oxygen directly to water a layer of catalyst is required on the cathode. Another possible path for this reaction involves the production of hydrogen peroxide in an intermediate reaction. While this reaction is more favorable even without a catalyst layer, the production of hydrogen peroxide proved to be toxic for the microorganisms. Another disadvantage of such a reaction is that hydrogen peroxide can have corroding effects on the electrodes, reducing their functional life span.

Having one of the above architectures, MFCs can take on several shapes and sizes. They can be cylindrical, cuboidal, disc-shaped or even setup in a beaker. Figure 9 shows some of the different shapes that an MFC can take.

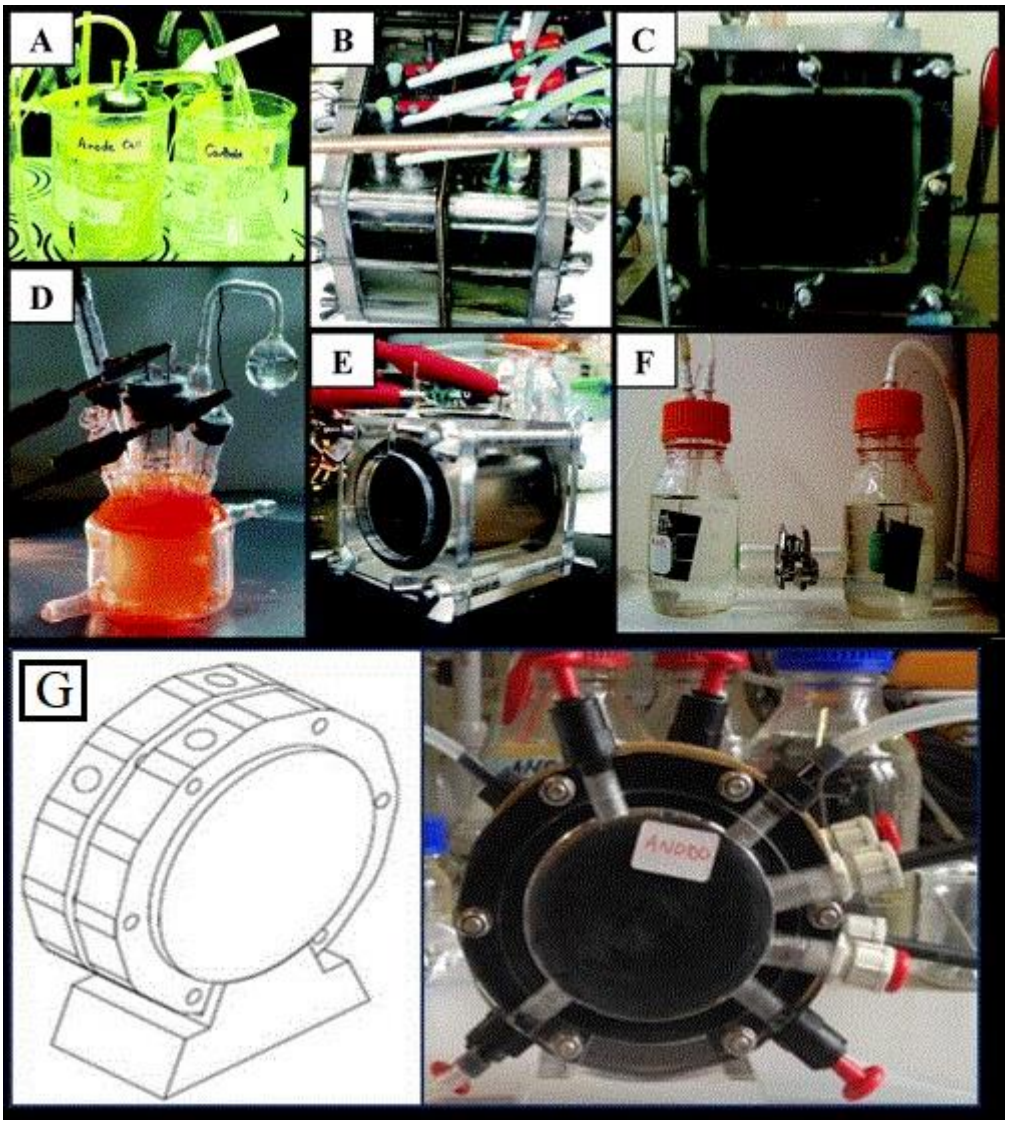

Figure 9: Different shapes and setups of MFCs. Adapted with permission from ([31]). Copyright (2018) American Chemical Society.

Moreover, MFCs can be set-up in a batch-fed or a continuous flow mode. This is basically how the medium or solution present inside the MFC is refreshed. The medium contains the substrates required for the microorganisms' metabolism. In the case of dual chamber MFCs, the cathodic medium also needs refreshing so that the chemicals required for the reduction reaction are refreshed. In batch-fed mode the medium is updated after set intervals of time while in continuous flow mode, the medium is fed at a constant rate to the MFC.

3.5.1 Anode

All MFCs have one very important component of the architecture which is the anode. Anode is the electrode on which the microbial biofilm forms. This biofilm

contains the microorganisms which metabolize different substrates, leading thus to the production of electrons. Many different types of substrates are used in MFCs such as glucose[32], alcohol[33], cellulose[34], acetate[35] and waste water[16,36,37]. For a biofilm to form, a biofilm compatible material is a pre-requisite when selecting the anode. Moreover, the material used as an anode must also be conductive with a low electrical resistance to enable efficient electron transfer from the microorganisms to the anode. Finally, the material of anode electrode must also show a high chemical resistance. Resistivity values of some materials are listed in Table 2.

Table 2: Resistivities of some materials.

Material	Resistivity (Ω/cm)
Copper	0.1
Carbon Paper	0.8
Graphite Fiber	1.6
Carbon Cloth	2.2
Conductive Polymer Sheet	130

Furthermore, the material must also have a high surface area with respect to volume. This would allow ample surface for the biofilm to grow on. Additionally, the anode material must also be porous to enable substrates and other important chemicals to easily diffuse into the full depth of the biofilm. Also, the material used as an electrode in an MFC must also be noncorroding. This is due to the fact that the electrodes are, at all times, in direct contact with water-based liquids. Lastly, the materials used for anodes must be inexpensive and scalable to ensure an MFC's cost-effectiveness.

Carbon based materials such as carbon-cloth, carbon-paper and reticulated vitreous carbon (RVC) are very commonly used as materials for the anodes. These materials fulfil most of the requirements for anodes mentioned in the previous paragraphs such as high porosity, high surface area, good conductivity and their affinity towards the growth of biofilms on them.

Furthermore, graphite-based materials are also widely used as materials for anodes in MFCs. Graphite sheets, rods, plates, felt and foams have been used by many researchers as anodes for MFCs.

3.5.2 Cathode

Another very important component of an MFC's design is the MFC cathode. At the cathode, the reduction reaction occurs in which either a chemical or oxygen is reduced. Therefore, it is important to select the cathode material and the additional layers, necessary in some cases, to provide a favorable reduction reaction.

In the case of MFCs that are not based on oxygen reduction reaction, such as dual chamber MFCs that are based on ferricyanide reduction, the same materials as anodes described in the last section are used. For example, carbon-based and graphite-based materials.

In the case of single chamber MFCs, in which an oxygen reduction reaction occurs at the cathode the most common material used is carbon paper. In these types of MFCs, one side of the cathode is usually close to air on one side for better absorption of oxygen and thus is usually referred to as 'air cathode'. This design methodology, having the advantage of better oxygen absorption, also has the disadvantages of increased oxygen flux and the loss of water due to the exposed surface.

The carbon paper used as the cathode, in the case of air cathodes, is usually supplemented with a layer of Platinum catalyst. The layer of Pt is usually facing inwards while the side of the carbon paper which is uncoated, usually faces towards the air to enable absorption of oxygen. In order to create the Pt catalyst layer, a chemical binder is also needed such as Nafion. Not only does this layer of Pt based catalyst results in better performance[38] but it also ensures that the intermediate reaction during oxygen reduction that produces hydrogen peroxide is minimized. The direct reduction of oxygen to water, which is supported by the Pt catalyst layer, is given as follows;

$$O_2 + 4H^+ + 4e^- \rightarrow 2H_2O$$

This reaction has a standard potential of 0.805 V while the other reaction which can occur during oxygen reduction is given as follows;

$$O_2 + 2H^+ + 2e^- \rightarrow H_2O_2$$

This reaction, on the other hand, has a potential of 0.38 V (this value is established through experimental results on MFCs and the standard potential of this reaction is 0.695 V) and thus is thermodynamically more favorable than the one

before without the presence of a catalyst. This can cause the production of hydrogen peroxide which is toxic in nature for microorganisms and has a corroding effect on the electrodes.

Apart from the catalyst layer, a diffusion layer is also added to the cathode on the opposite side with respect to that of the catalyst layer. This diffusion layer is made of materials such as Polytetrafluoroethylene (PTFE). There can be multiple diffusion layers on a cathode as studies have shown that they improve the performance of an MFC[19].

Even though the use of a precious metal catalyst layer increases the performance of an MFC, it also increases the cost incurred in setting up the MFC. Therefore, there is a lot of research work going on that investigates the use of novel materials and techniques that replace the Pt based catalyst on the cathode. These novel materials include pyrolysed iron(II) phthalocyanine[39], manganese dioxide[40], MnO2–graphene hybrids[41], lead dioxide[42] etc.

Another interesting area of research for MFC cathodes is the use of biocathodes. Bio-cathodes are cathodes on which a biofilm is grown and the bacteria inside the biofilm can catalyze the cathodic reactions. Bergel and co-workers used a cathode on which a sea-water biofilm had formed which helped in the catalysis of oxygen[43]. In the case of bio-cathodes, the biofilms that are formed are comprised of bacteria that are adapted to aerobic conditions and are able to donate electrons to help in the oxygen reduction reaction. Nevertheless, the use of biocathodes to catalyze the oxygen reduction reaction is an area that needs more exploration.

3.5.3 Membranes

As discussed earlier, some types of MFCs have a component known as a proton exchange membrane (PEM). More specifically, these types of MFCs are dual chamber MFCs in which the anodic chamber is separated from the cathodic chamber using this membrane. The main purpose of this membrane is to limit the cross-over of chemicals and compounds from the electrolyte in one chamber to another while allowing the transfer of protons from the anodic chamber to the cathodic chamber. It stops from chemicals such as potassium ferrycianide and also any absorbed oxygen in the cathode electrolyte to pass through to the anodic

chamber. While having these advantages, one of the disadvantages of such membranes is that they increase the internal resistance of the MFC. Moreover, these membranes are composed of expensive materials such as Nafion and thus make a considerable contribution to the expenses incurred in building an MFC.

3.6 Voltage Generation from MFCs

As discussed earlier, MFCs are devices that are capable of producing electrical energy on a low scale. To put things into perspective, the electrical devices that we use e.g. Television, Refrigerator, Computer etc., work on an electrical voltage of 220V~110V. Furthermore, handheld devices e.g. mobile phones and tablet PCs, usually work on voltage in the range of 5V~3V. While a conventional MFC is able to produce an open circuit voltage (OCV, the voltage at which the MFC does not have any load connected, therefore there is no flow of current and no energy expended) in the range of 0.3V to 0.8V. Moreover, when the MFC is connected to an external load, R_{ext}, the voltage level further decreases due to the flow of electrons through the external load. Furthermore, there is a limit to the energy that an MFC can deliver as defined by equation (2) in section 3.4.

Once a load is connected, the electrons that are collected at the anode, produced by the exoelectrogens, travel through the collector and the load towards the cathode. This produces a current. More specifically, this current, I, is related to the voltage across the MFC, V_{MFC}, and external load, R_{ext}, by the following relation;

$$I = \frac{V_{MFC}}{R_{ext}} \tag{4}$$

V_{MFC} itself is dependent on a number of factors and imposes the limit up to which energy/power can be delivered to an external load.

Since there is a current passing through the external load, power is being generated by the MFC. This power, P, produced by the MFC is given by the following relation;

$$P = V_{MFC} I \tag{5}$$

Equation (5) can be used to express power in terms of just voltage – equation (6) or just current – equation (7);

$$P = \frac{V_{MFC}^2}{R_{ext}} \tag{6}$$

$$P = I^2 R_{ext} \tag{7}$$

These relationships are related to the external parameters of an MFC such as the external load etc., but, internally, the MFCs are much more complicated than a conventional source of electrical energy such as chemical fuel cells or batteries. The way the bacteria behave and thus, produce electricity, is dependent on a variety of factors. V_{MFC} is the component of these equations which varies according to these factors such as temperature, pH, substrate concentration, internal resistance, anode overpotentials, cathode overpotentials etc. Therefore, it is extremely difficult to predict the electrical output of an MFC since it depends upon the variety of factors that affect microbial activity. A typical current density vs. voltage response of an MFC is given in the Figure 10. It is also referred to as the polarization curve.

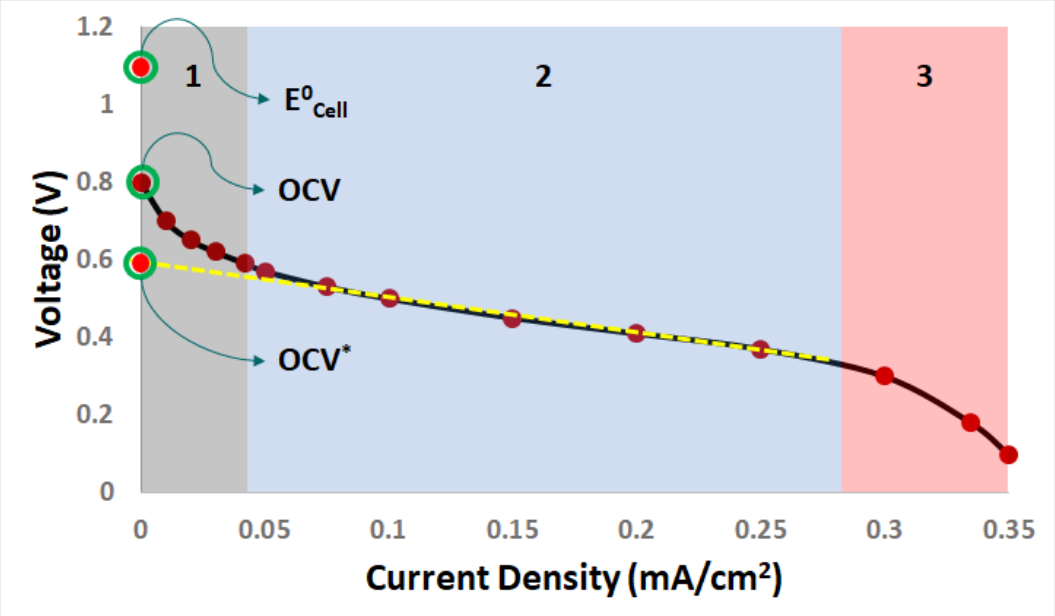

Figure 10: Polarization curve of an MFC. The figure is divided into 3 regions. Region 1 (gray color) represents the region of low current and the region in which the voltage decreases rapidly. Region 2 (light blue color) represents the region in which the MFC operates with an almost linear behavior. Region 3 (red color) represents the region in which there is again a rapid voltage drop but with a higher current.

Different regions of MFC operational behavior, in terms of voltage and current are shown in Figure 10. Moreover, if we look closely on the y-axis, we can see that different potentials relating to the MFC are marked. E^0 is the theoretical maximum potential that the cell produces. This maximum can be calculated according to the redox reactions that are occurring on the electrodes of an MFC. OCV represents the measured OCV of the device while OCV^* represents the y-intercept, if the line in the 2nd region is extended until the y-axis, as defined by the dashed yellow line.

Nevertheless, the maximum energy that can be produced have its limits based on thermodynamic principles. More specifically, on the redox reactions that are occurring inside an MFC on the anode and the cathode. The total potential difference (also known as total cell potential), E_{emf}, across any electrochemical cell is given by equation(3), $E_{Cathode}$ and E_{Anode} refer to the potentials of the different reactions occurring at the cathode and anode, respectively, of the MFC. This has already been discussed in section 3.4. Hence, the total cell potential, which is present across an MFC, depends on the reactions that are occurring on the anode and the cathode of an MFC. The factors that are directly related to the MFC, which effect the voltage of an MFC, are the anode overpotentials, the cathode overpotentials and the internal resistance. More specifically, the E_{emf} that will be present across the MFC will be given by the following relationship;

$$E_{emf} = E^0 - \left(\sum OP_{an} + \left|\sum OP_{cat}\right| + IR_{ohmic}\right) \qquad (8)$$

Where, $\sum OP_{an}$ are the total overpotentials at the anode, $|\sum OP_{cat}|$ are the total overpotentials at the cathode and IR_{ohmic} refers to losses due to the ohmic resistance in the cell. Ohmic losses are one of the most important losses that need to be dealt with when designing an MFC. These losses are dependent on the shape and architecture of an MFC. More specifically, these losses partly occur due to the resistance imposed by the solution/medium to the conduction of ions and thus is also related to the distance between the anode and the cathode. In the case of dual chamber MFC, the ohmic resistance imposed by the PEM also contributes to the ohmic losses. Therefore, it is important to select a PEM that offers minimal resistance to the protons moving across it. Moreover, it is also important to select wires and contacts, external to the cell, that offer minimum resistance.

The potential drops due to the ohmic losses that are present between a membrane and an electrode (reference) due to the electrolyte can be quantified using the following relationship;

$$\Delta V_{\Omega} = \frac{\delta_w J}{\sigma} \tag{9}$$

Where, δ_w is the distance between the test points in water in cm, J is the current density with units A/cm^2 and σ represents the conductivity of the solution with units S/cm.

Overpotential, is the difference in the theoretical potential of a redox reaction and the actual experimental potential at which the redox reaction is occurring. This difference in the potential can occur due to a number of reasons such as:

i. *Activation losses*. A part of activation losses occurs due to the unavoidable energy loss whenever a redox reaction is initiated. This loss is usually in the form of heat and occurs at both the cathode or the anode. Moreover, this loss also encompasses the losses due to the transfer of electrons from the bacteria to the anode. This involves all the different electron transfer mechanisms that are discussed in section 3.3. To reduce activation losses, it is advisable to use catalysts at the cathode and try out different types of bacteria that exhibit more efficient electron transfer mechanisms. These losses cause the voltage drop in the 1st region of Figure 10.

ii. *Bacterial metabolism*. When a bacterial metabolizes any substrate, there are voltage losses that occur in its metabolic process. Basically, bacteria need to expend energy when they metabolize a substrate. For example, a part of this energy is spent to pump a proton across a bacteria's membrane to facilitate the metabolic process.

iii. *Mass transfer losses*. The redox reactions occurring inside an MFC, that enable it to produce a voltage have certain limitations. As the reactions are occurring at the electrodes, it is not always the case that the reactants necessary for the redox reactions are present in the electrode vicinity or being transported efficiently to the electrode's vicinity. Moreover, it can also happen that the products of these reactions are not efficiently

transported away from the electrode to give way for more reactants. Both these factors combined, impose a limit on the reaction's rate. Which in turn limits the power produced by the MFC.

In region 2 of Figure 10, which represents the linear behaviour of an MFC, it can be seen that the E_{emf} produced by the cell is related linearly to the internal resistance and the current flowing through an MFC if the y-intercept of this region (obtained by extended the line up till the y-axis) is taken as the y-intercept of the relationship. This relationship is given by equation (10).

$$E_{emf} = OCV^* - IR_{internal} \quad (10)$$

It is important to notice here that $R_{internal}$ comprises of both the ohmic resistance that the cell exhibits and the losses due to the over potentials of both the cathode and the anode. This internal resistance can be measured, or approximated using different techniques, some of these techniques are mentioned below:

i. Slope of the Polarization curve in the linear region can be used with equation (10) to approximate the internal resistance.
ii. Peak of the power density curve (Section 3.7.3) can be used to approximate the internal resistance. As explained in section 3.7 equation (18), the maximum power is obtained if the external resistance is equal to the internal resistance. In this way, the resistance calculated at the peak power (using the values of voltage and current at the peak power point and the ohm's law) is estimated as the internal resistance of an MFC.
iii. Electrochemical impedance spectroscopy is a technique that is widely used to investigate the internal resistance of an MFC. It is a very useful technique gives more insight into the internal resistance of an MFC than other methods. In particular, this technique is important for the work I have performed in my Ph.D. and thus a whole chapter is dedicated to it – Chapter 4.

The different components of the MFC's internal resistance of an MFC are explored in section 3.7.1.

3.7 Power Generation from MFCs

One of the main highlights of research on MFCs has been the ability to extract power from them. The level of power obtained from an MFCs is low (<2000 mW/m^2)[44] and practically, this level of power and the level of output voltage from an MFC, as discussed in the previous section, is not very useful for direct use. But research has shown that with proper techniques and external components, MFCs can have useful applications as energy resources. For example, an MFC can be used to power a remote sensor[45].

Power generated from the MFC can be calculated using equations (5), (6) and (7). This power can be normalized according to different factors relating to the MFC such as the volume of its chamber, the area of its anode, the area of its cathode etc. Studies have shown a relationship between these factors and the power produced[46].

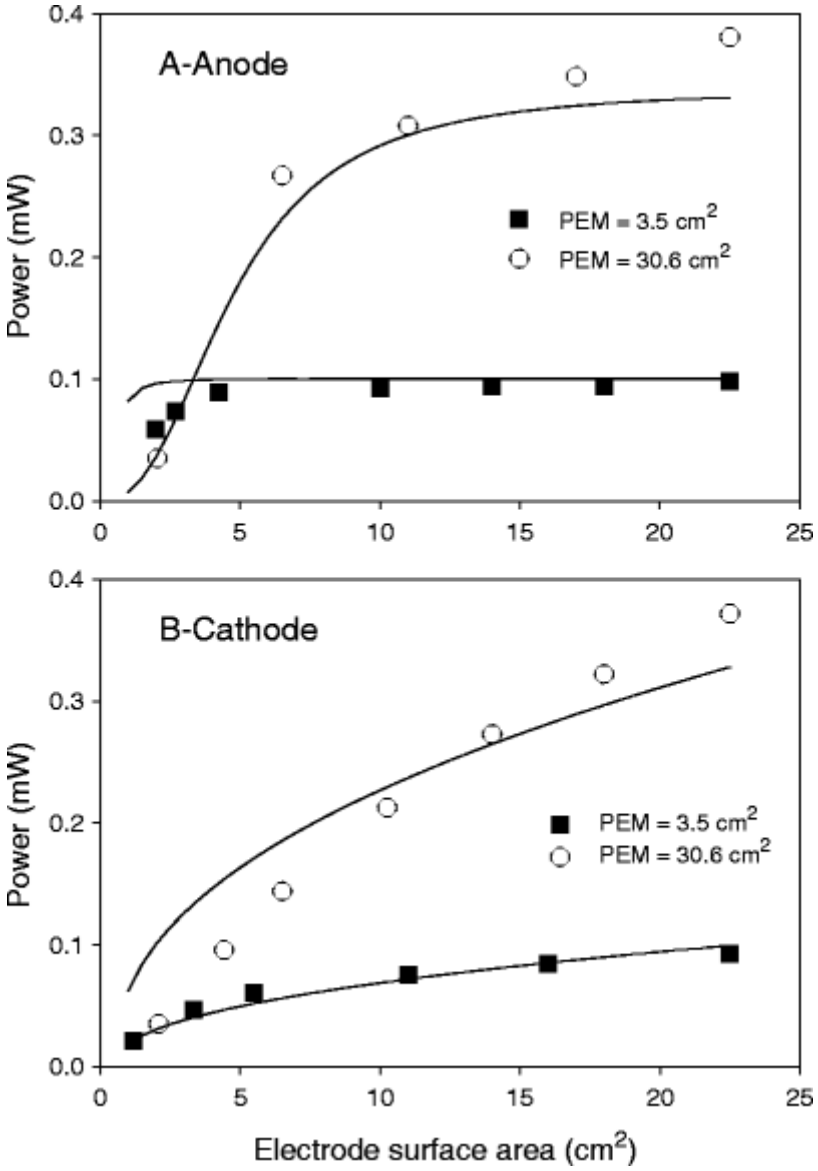

Figure 11: Relationship between produced power and Anode area (a) and Cathode area (b)[46] (PEM refers to the Proton Exchange Membrane). Reprinted with permission from Applied Microbiology and Biotechnology, Springer Link.

To calculate the normalized power of an MFC with respect to the area of its anode, it is required to calculate the active or accessible area of the anode. If the anode is not pressed against a surface than both the sides of the anode will contribute to its area. In this case, to calculate the anode area, A_{an}, the following relationship can be used;

$$A_{an} = 2 \times L_{an} W_{an} \tag{11}$$

Where, L_{an} is the length of the anode and W_{an} is the width of the anode. The factor of 2 is present to consider both sides of the anode. In the case that the anode is pressed against a surface, such as a support or an electron collector, the factor of

2 must be ignored. Moreover, in this case, the anode is considered to be of a rectangular shape. If the shape of anode is different e.g. if it is of a circular shape, the respective formula to calculate the area of the anode must be used.

Once the area of the anode is calculated, the normalized power produced, with respect to the anode area can be calculated using the following relationship;

$$P_{an} = \frac{V_{MFC}^2}{A_{an} R_{ext}} \tag{12}$$

Furthermore, as discussed earlier, the power can also be normalized to the chamber/reactor volume. In order to calculate the power of an MFC normalized to its reactor volume, the following relationship can be used;

$$P_{reactor} = \frac{V_{MFC}^2}{V_{reactor} R_{ext}} \tag{13}$$

Where, $V_{reactor}$ is the volume of the reactor and $P_{reactor}$ is the volumetric power of the MFC. To calculate the volume, the volume of the medium/electrolyte can be used, or the volume of the reactor can also be calculated using proper dimensions.

Power generation in MFCs can be optimized through proper design of the system, which involves proper selection of all its components. Moreover, external circuitry and power management systems need to be used to properly extract the energy generated by MFCs. These components will be discussed in detail in section 3.8.

MFCs are systems that produce electrical energy. Nevertheless, these systems exhibit an internal resistance, R_{int} which affects the overall behavior and the power output of the device.

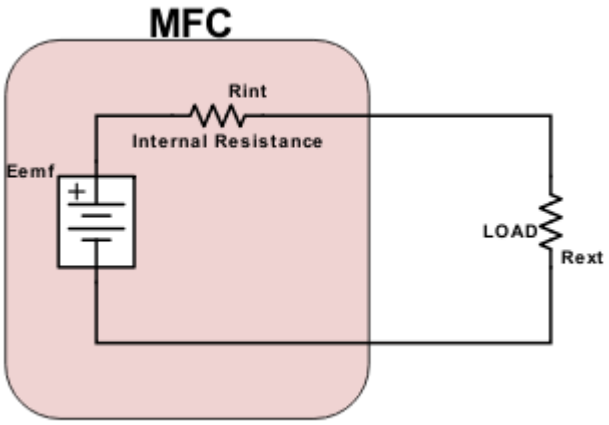

Figure 12: MFC with the potential difference produced, E_{emf}, internal resistance, R_{int} and load, R_{ext}.

Figure 12 shows how the resistances are imposed on the system once a current flow through the device. E_{emf}, is the total potential difference between produced by the MFC. As shown in the earlier sections, E_{emf} is dependent on both the anode reactions and the cathode reactions. This is equal to the voltage recorded on the terminals of an MFC when it is not loaded, in other words, the voltage is Open Circuit Voltage (OCV), V_{ocv}. OCV is equal to E_{emf} because when the MFC does not have a load connected to it, no current flows. Consequently, there is no potential drop across the internal resistance, R_{int}. Therefore, whenever there is an external load connected, there will always be a potential drop (and energy lost) across the internal resistance, V_{int}. This value would be deducted from the E_{emf} to give the voltage across the load, V_{mfc}.

$$V_{mfc} = \frac{E_{emf} \times R_{ext}}{(R_{int} + R_{ext})} \tag{14}$$

Thus, there is a difference between the total power generated by the MFC and the total power that is delivered to the external load. The total power produced by an MFC can be calculated, using equation(6), by equation(15).

$$P_{total} = \frac{E_{emf}^2}{R_{int} + R_{ext}} \tag{15}$$

On the other hand, the power delivered to the external load is given by equation(16), using equation(6) and equation(14).

$$P_{delivered} = \frac{E_{emf}^2 \times R_{ext}}{(R_{int} + R_{ext})^2} \quad (16)$$

Since, E_{emf} is equal to V_{ocv}, we can re-write equation(16) as follows,

$$P_{delivered} = \frac{V_{ocv}^2 \times R_{ext}}{(R_{int} + R_{ext})^2} \quad (17)$$

It is evident from equation(17) that the power which is delivered to an external load by an MFC is inversely related to the internal resistance. Therefore, it is very important to study in detail and minimize the internal resistance of an MFC. Furthermore, it can be seen that if $R_{int} = R_{ext}$, equation (17) will reduce to equation (18).

$$P_{delivered} = \frac{V_{OCV}^2}{4R_{int}} \quad (18)$$

3.7.1 Internal Resistance of an MFC

Since the power that can be extracted from an MFC depends on its internal resistance, it is important to explore what factors contribute to the internal resistance of an MFC. Equation(19) represents the factors that contribute to the internal resistance of an MFC;

$$R_{int} = R_{an} + R_{cat} + R_{mem} + R_{electrolyte} \quad (19)$$

Where, R_{an} is the resistance related to its anode. Typically, this involves the resistance of the material used as the anode as any material that is used as the anode will exhibit its own resistance. Table 2 lists some resistivities associated to different materials. Similarly, R_{cat} is the resistance related to its cathode. As for the anode, the cathode will be made out of a specific material e.g. carbon paper. This material will have its own resistive effect which will contribute to the overall internal resistance. R_{mem} is the resistance related to the exchange membrane which is usually found in dual chamber MFCs. This membrane acts as a barrier for the different chemicals and compounds present in the cathodic and anodic chamber of an MFC and offers an additional resistance to the internal electrical path of ions in

an MFC. Lastly, $R_{electrolyte}$ refers to the resistance related to the electrolyte present inside an MFC[47]. All of these resistive elements limit the power production of an MFC. Moreover, resistive elements such as R_{an} and R_{cat} also exhibit complex parts, therefore, in reality, they are impedances. These complex parts are related to the capacitive effects of the different layers present on these elements and the different reactions and processes occurring on them. A more detailed study of these resistive elements can be performed using Electrochemical Impedance Spectroscopy (EIS) which is discussed in detail in chapter 4. Further research on the internal resistance of an MFC can help improve their performance and hence, their practical application as renewable energy resources.

3.7.2 Columbic Efficiency

MFCs generate power by unlocking the electrons stored inside a biomass. This is done by the EAB which form a biofilm on the anode of an MFC. The EAB metabolize biomass (e.g. biomass present in wastewater) and in the process produce electrons. The degree by which the MFCs are able to extract/recover electrons from the biomass is a measure known as columbic efficiency. It is defined as the ratio between the charge recovered and the total charge present inside the organic matter. Columbic efficiency, C_e, in terms of the current measured through an external load, I, over a time period, T, is given by the following relationship;

$$C_e = \frac{M_s \int_0^T I \, dt}{F b_{es} v_{anode} \Delta C} \tag{20}$$

Where, M_s is the molecular mass of substrate, F is the Faraday's constant, b_{es} are the moles of electrons that can be extracted from the substrate, v_{anode} is the volume of liquid present inside the anode compartment of an MFC and ΔC is the change in the concentration of the substrate.

3.7.3 Polarization Curve and Power Density Plot

Polarization curves are plots obtained by recording the value of current produced over a wide range of operating voltage of a particular device. The range of voltage is usually from OCV (or very high resistance) to short circuit (SC, or very low resistance) condition. Polarization can be performed using a series of

external resistances connected one after another, starting from the highest value. Furthermore, it can also be performed using Linear Sweep Voltammetry (LSV) technique. In LSV, a device varies the voltage from OCV to SC at a fixed rate (e.g. 1 mV/s) and measures the current produced at each voltage step. These plots are used to characterize the performance of an MFC and therefore, it is necessary to introduce them. Figure 10 in section 3.6 explains the different regions of a polarization curve and the reasons behind this particular behavior. From the data obtained, the power density related to the voltage/current density values can also be calculated. These power density and current density values can then be used to plot the power density curve. Power density curves also carry significance when it comes to evaluating an MFCs performance.

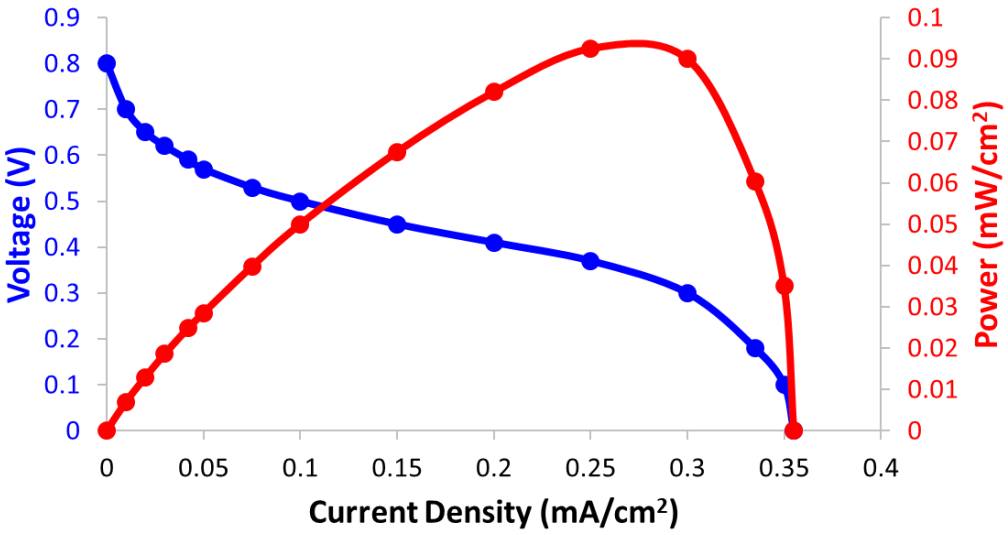

Figure 13: Typical polarization curve and power density plot related to an MFC.

Figure 13 shows a polarization curve plotted with the power density curve of the same MFC. Polarization curve shows the behavior of an MFC in the different voltage regions. On the other hand, power density plot shows how the output power changes with respect to the operating voltage and current density. It is useful in order to find out the optimal operating point which gives the maximum power output. Figure 14 shows the points related to the Maximum Power Point (MPP) marked on the graph. I_{MPP}, V_{MPP} and P_{MPP} represent the current density at the MPP, voltage at the MPP and power density at the MPP respectively.

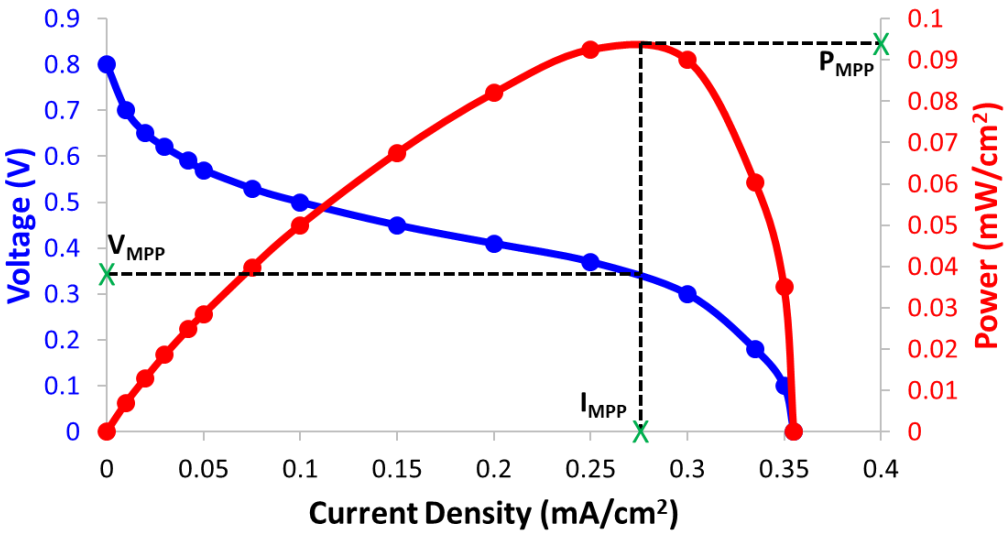

Figure 14: Polarization curve and power density plot with the MPP marked.

It is evident from Figure 14 that this particular MFC has an optimal operational point, in terms of voltage, in between the range 0.3V to 0.4V. Moreover, this MPP corresponds to a produced power density of about 95 $\mu W/cm^2$. To enforce the MFC to work within these operational parameters, power management systems are used which are discussed in detail in section 3.8. Due to the important information they present, both of these graphs are very important and are often displayed in the same image.

3.8 Power Management Systems

Most of the research that has been done in the past two decades on MFCs has been regarding their use as a sustainable energy source which is beneficial to the environment. An important aspect of making MFCs useful as energy sources is the development of efficient Power Management Systems (PMSs).

MFCs produce energy in the low voltage range (< 1 V) and the electrical energy produced in this voltage range is not very useful. To power even the simplest and least demanding (in terms of voltage and power) electrical device, voltage higher than 1.8 V is required. Special electrical circuits and components are used to build a PMS to step up voltage, store and properly use the electrical energy that is extracted from an MFC. Figure 15 shows a typical setup of an MFC with a PMS used to power a load and store any excess energy, for use later.

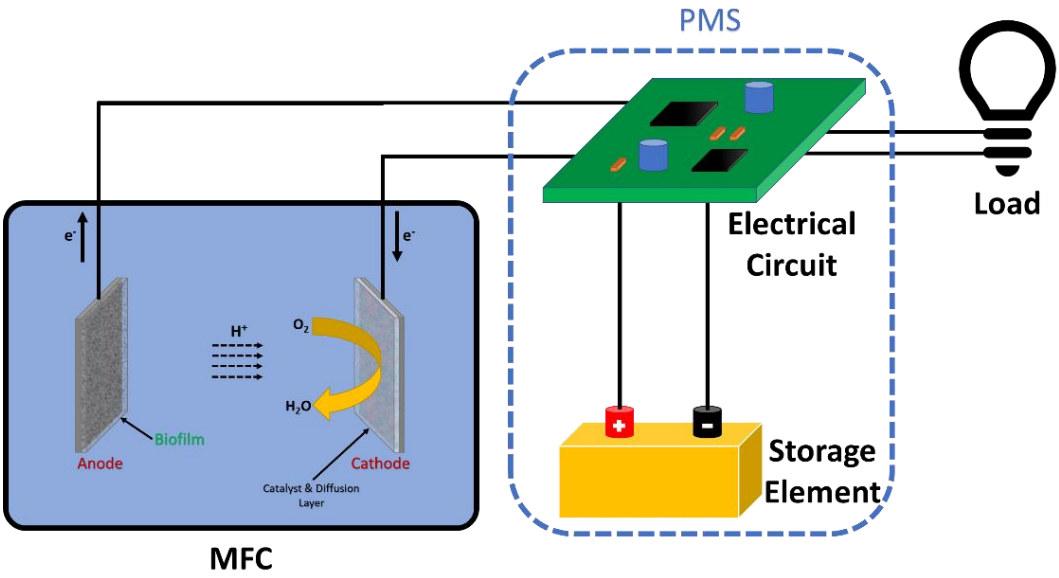

Figure 15: MFC connected to a PMS for efficient energy extraction, energy storage and its use.

PMS comprises of two main components, an electrical circuit and a storage element. The electrical circuit has the main function of capturing the electrical energy coming from an MFC and conditioning it for storage. Furthermore, it also boosts the voltage level so that it is compliant to be used with other devices such as sensors etc. On the other hand, the storage element is used to store this energy for use whenever needed. This storage element could be a battery similar to the ones found in our smart phones[48] or it can also be a supercapacitor[49].

Not only do the PMS extract energy from the MFCs, but, with recent developments, they can also set an operational voltage for the MFCs. This way the power extracted from the MFCs is the maximum power possible from these devices as discussed in section 3.7.3. PMS technology at present employs different techniques to also track the MPP of an MFC. The popular techniques that are used to extract energy from an MFC are the following:

i. PMS based on capacitors[50–52]. These are the simplest power extracting circuits in which the MFC is directly connected to a capacitor. As the capacitor gets connected to the MFC, charge flows from the MFC and gets stored on the capacitor. The total energy, E, that gets stored on the capacitor is dependent on its initial and final voltage and its capacitance, C, according to the following equation;

$$E = \frac{1}{2}(V_{final}^2 - V_{initial}^2)C \qquad (21)$$

A PMS based on capacitor might simply have many parallel capacitors, storing energy. When they are required to output the energy, they can be connected in parallel to provide a higher voltage and sustainable current. Different versions of capacitor-based PMS use different methods and connections to enhance the output according to the requirements.

ii. PMS based on charge pumps[53–55]. Charge pumps are devices that are commercially available which are able to store and transfer energy at a voltage level higher or lower than the inputs. These devices use capacitors as temporary charge storing elements and with the help of internal switches, are able to output higher voltages which are directly compliant with other electrical devices.

iii. PMS based on boost convertors[56–58]. Boost convertors have a similar functionality to that of charge convertors since they also increase the level of voltages. These devices use not only capacitors but also inductors and diodes as external components. Moreover, similar to charge pumps, boost convertors are also widely available as commercial devices. In some PMSs, charge pumps and boost convertors are also used together.

Figure 16 shows how the above devices can be used in the form of a schematic to build a PMS[44]. As shown in the figure, there are several ways in which these components can be arranged to design a PMS.

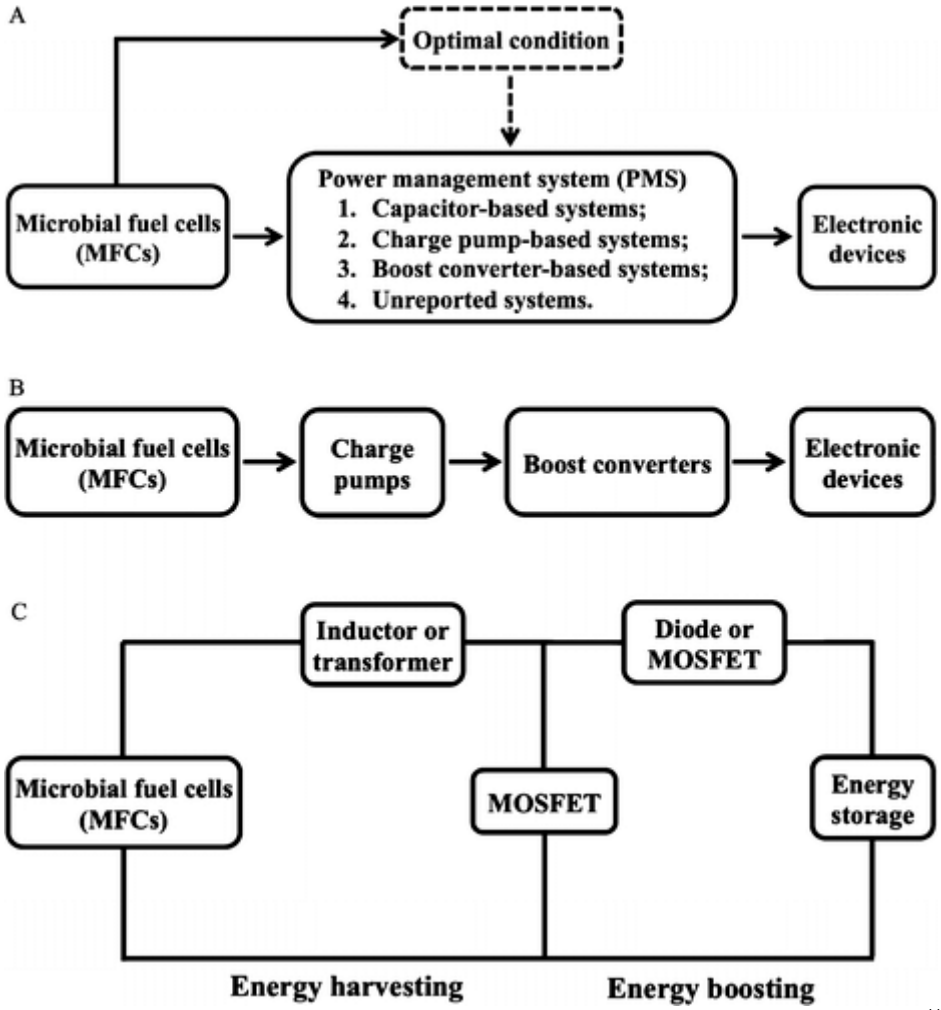

Figure 16: Different topologies used in energy harvesting. Reprinted with permission from ([44]). Copyright (2018) American Chemical Society.

The three techniques/devices explained above can be used independently to extract energy from an MFC or can be used with more circuit components to implement the MPP Tracking (MPPT) technique[44]. A PMS that operates an MFC at MPP basically extracts energy intermittently from the MFC. When such a circuit initially starts extracting energy from the MFC, the voltage of the MFC drops (since the MFC is taken out of the OCV condition). This is represented by the red line that starts at T=0 in Figure 17.

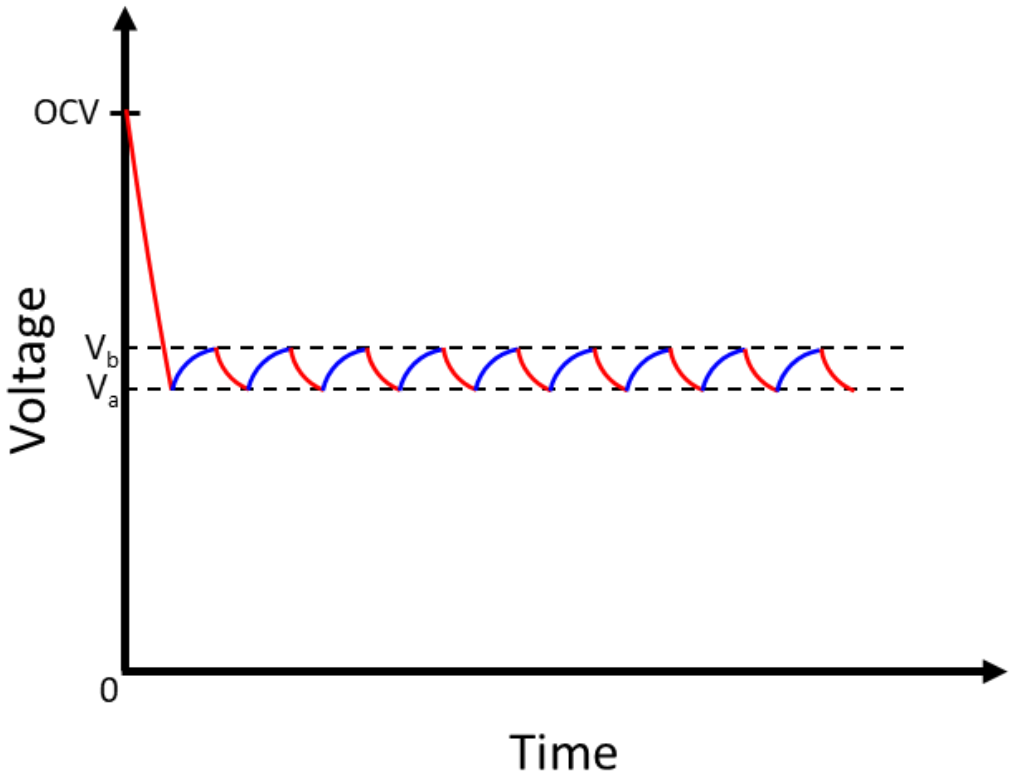

Figure 17: Voltage curve of an MFC operating with a PMS that operates the MFC within a voltage range corresponding to the MPP. The red curves indicate when the device is in a loaded condition. Blue curves indicate that the device is in open circuit condition

Once the voltage reaches a certain threshold, V_a, the PMS stops extracting energy from the MFC and thus the MFC goes again into open circuit condition with the voltage starting to rise, represented by blue lines in Figure 17. V_b is another threshold of the PMS which is very close to V_a but greater than it. When the MFC, now in open circuit, reaches V_b, the PMS again closes the circuit and starts to extract energy from the MFC. This cycle of opening and closing the circuit goes on until the PMS is in operation. This way the operational voltage of the MFC is restricted in between V_a and V_b. At present, there are several PMS systems that are commercially available, which have both the energy harvesting systems (comprising of charge pumps/boost converters) and MPPT circuitry. Most of these commercially available also have the option to set externally the MPP voltage thresholds.

To make the MFC's energy harvesting capabilities matter at a practical level, it is not only important to optimize the MFC's internal design, but it is also important to develop novel and efficient ways of extracting and using an MFC's energy. Moreover, the PMSs used must be developed in a way that they are

inexpensive and energy efficient. Furthermore, these PMSs should also be able to incorporate the MPPT circuitry.

3.9 Applications of MFCs

MFCs have a variety of applications in the real world. Therefore, a lot of research has been done on MFCs in the past decade. This section will discuss the main uses of an MFC.

3.9.1 Electricity generation

MFCs can generate electrical current. This current can either be stored in an external element such as a battery[36]/supercapacitor[55] or it can be used directly to power an external load such as a resistor[59] for the purpose of power generation calculations.

To calculate the power produced by an MFC, a known resistance can be connected to the terminals of an MFC (anode and cathode) and the voltage can be measured using a voltmeter. The current is obtained using equation(45) and the power is obtained from equation(5), it can be normalized according to the cathode are or the anode area. In some cases, the power value is also normalized according to the MFC volume[59].

Although the power generated by an MFC is low and not constant, it can still prove to be useful when it comes to powering sensors in remote locations. A lot of research has been done on sMFCs for their use as power sources[25,51,54,60,61] especially in remote marine locations.

One very important factor in energy generation applications of MFCs is the use of a proper power management system. The use of a system that can efficiently extract energy from an MFC makes it possible for MFCs to be used as power sources.

3.9.2 Wastewater treatment

Another important use of the MFCs is their ability to treat wastewater. Wastewater has several compounds and molecules inside it that need to be treated. The way MFCs can help treat wastewater is by consuming organic matter present

inside wastewater. Not only does this reduce the chemical oxygen demand (COD) of the waste water but, in the meanwhile, also produces energy[62]. In simpler terms, the EAB in MFCs would be feeding on the organic waste present in the wastewater and in the process, cleaning it.

This dual functionality of MFCs of producing energy while treating wastewater makes them ideal candidates for an increased research in this field. For applications of MFCs as wastewater treatment devices, single chamber and continuous flow modes have been found to be more useful[63–65].

At present, the wastewater treatment facilities use up a lot of energy. In 2017 alone, the United States spent nearly $40 billion on water and wastewater infrastructure[66]. With more developments in the MFC wastewater treatment technology, this number could reduce dramatically. Recent studies have shown that MFCs also have the potential to reduce sulphides and not just organic compounds. Rabaey et al. showed a removal of up to 98% of sulphides using MFCs[67]. MFCs hold a lot of potential to be used as wastewater treatment devices that also produce energy.

3.9.3 Hydrogen Production

Hydrogen production is important in present day world. The present production of hydrogen occurs from several sources as described in Figure 18.

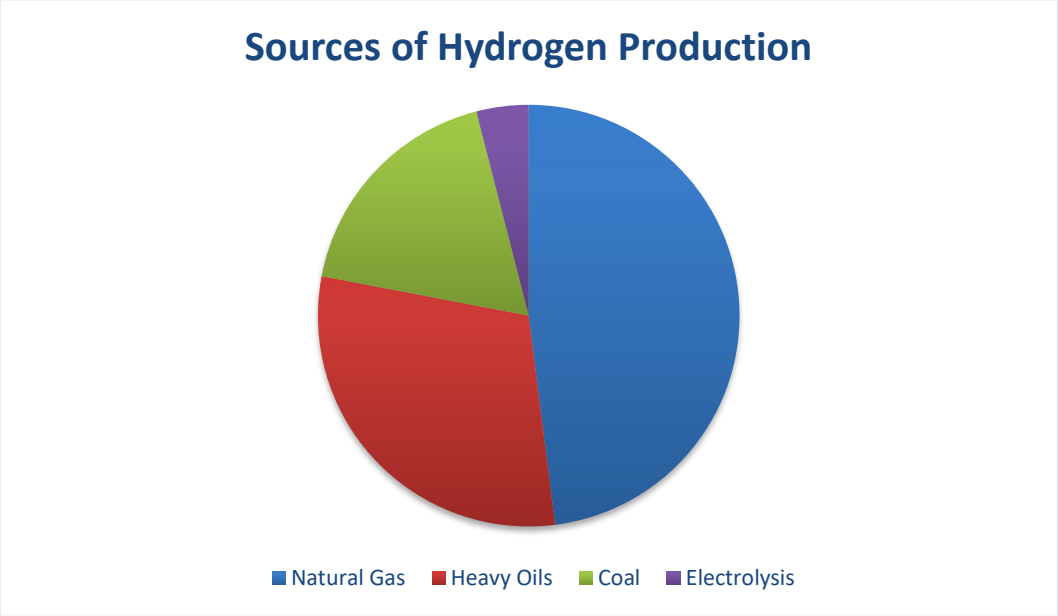

Figure 18: Sources of hydrogen production in the world.

Considering that most of the hydrogen produced in the world is produced by burning fossil fuels, it is important to consider alternative sources of hydrogen production. More importantly, sources have to be identified that are environment friendly. One such source could be the use of MFCs for the production of hydrogen.

A small external potential is applied, in this case, to the MFCs to overcome the electrochemical limitations to allow the Hydrogen evolution reaction (HER) for production of Hydrogen in MFCs[68]. Moreover, the cathode in this case is kept under anaerobic conditions. The chemical reactions that take place in the MFC are explained by the following equations;

$$C_2H_4O_2 + 2H_2O \rightarrow 2CO_2 + 8e^- + 8H^+ \quad (22)$$

$$8H^+ + 8e^- \rightarrow 4H_2 \quad (23)$$

Where, equation (22) belongs to the reaction occurring at the anode. On the other hand, equation (23) belongs to the reaction occurring at the cathode.

3.9.4 MFC based biosensors

Another very important and upcoming feature of MFCs is their use as biosensors. MFCs are based on EAB, which are biological organisms. Like all other living organisms, EAB have a response to an external stimulus. Conditions like temperature[69–71], salinity[72,73] and pH[74–76] can have substantial effect on the performance, more specifically the power and voltage production, of an MFC.

Moreover, another important use of the MFCs' sensitivity to external stimuli is their use as sensors for toxicity detection. Not only the processing of wastewater is an issue but also the detection of toxicants present in the waste water is an important issue. Furthermore, toxicants that are introduced into the environment and the river stream through industrial waste can be hazardous for the marine life and the general well-being of the society. MFCs are biological devices which are based on EAB. EAB use the organic matter present in water bodies to feed themselves and while doing so, produce electrons (building a potential difference across its electrodes). This production of electrons is somewhat proportional to the EAB's metabolic activities. If, toxicants are introduced to the MFCs, they can inhibit bacteria's

metabolic activity, and this can result in a dramatic decrease of potential difference across the MFC's electrodes. Intelligent systems can be designed and developed to detect these voltage patterns across an MFC and in turn, predict if a toxicant has been introduced into the MFC. A lot of research is being performed at present to develop reliable and quick MFC based toxicity sensors[77–79]. The presence of these systems in river streams and other water bodies can help us detect toxicants and enable us to act in time to reverse damage caused by toxicants.

4 Electrochemical Impedance Spectroscopy

4.1 Introduction

Electrochemical Impedance Spectroscopy (EIS) is a technique that is widely used to obtain the impedance response of a variety of systems. It is a useful non-invasive technique that can be used to understand the different processes occurring inside an electrochemical system. These processes can be occurring at the interface between an electrode and the electrolyte. Moreover, they can be related to the diffusion of substrates and ions within the electrolyte and can also be related to the presence of different membranes. The systems which are investigated using EIS are the ones in which, primarily, the main conduction is through ions and not through electronically conducting elements such as di-electrics.

In the past few decades, EIS has been widely used to study a variety of systems[80–85]. This includes batteries[76–84], solar cells[94–100], fuel cells in general[101,102], studies related to materials prone to corrosion[84,103–107] etc. EIS has also been found helpful in the detection of antibodies[108–110], DNA[111–113] and cancer cells[114–116]. The variety of fields in which EIS can be applied signifies its importance, reliability and robustness as a technique to investigate a system.

More related to my Ph.D. thesis, EIS has also been widely used to investigate the processes and reactions occurring inside an MFC and the different materials used as anodes and cathodes in an MFC[9,117–121]. EIS is also used to calculate the overall internal resistance of an MFC, different components of which are introduced in section 3.7.1. Once the EIS is performed, most of the components of internal resistance can be assigned respective values by analyzing the EIS results.

EIS is performed using specialized devices known as Potentiostats. The specific device that I have used during the course of my Ph.D. is a potentiostat by Biologic. Once the EIS results are obtained there are a range of software and techniques that are used to analyze the results. One of the most common technique

is the fitting of EIS data using equivalent electrical circuits (EECs). This technique will be discussed in detail in the following sections.

4.2 Fundamentals of EIS

EIS is performed by applying a small AC signal on the electrodes of the system under study. EIS can be performed in 2-electrode and 3-electrode configurations. In the case of 2-electrode configuration, EIS is simply performed on the primary electrodes of the system. In the case of a traditional MFC, these are the cathode and the anode. As for the 3-electrode configuration, the architecture of an MFC (or the device under study) must be modified to add an additional electrode, known as the reference electrode.

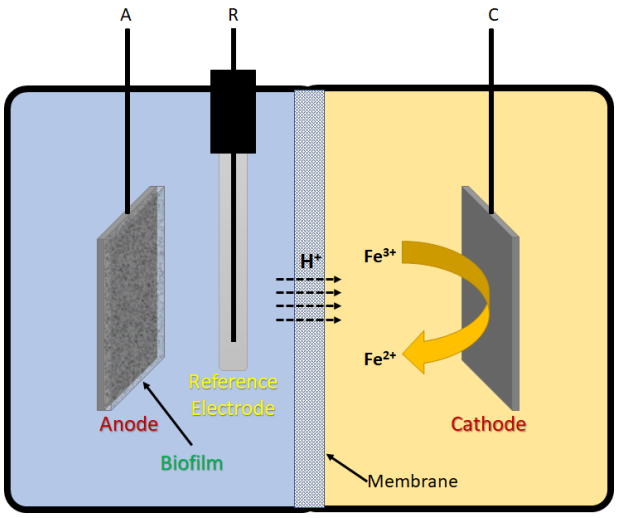

Figure 19: A dual chamber MFC with a reference electrode.

Figure 19 shows a dual chamber MFC with a reference electrode. The architecture of any type of MFC can be modified to include reference electrode if the physical dimensions do not introduce any complications. The reference electrode has a known potential that is fixed. An example of a possible reference electrode could be one based on Ag/AgCl which has a potential of 0.23 V ± 10 mV with respect to the standard hydrogen electrode. With the help of a reference electrode, EIS can be used to investigate the processes occurring on any one of the two primary electrodes i.e. cathode or anode. In addition to the reference electrode, anode and cathode need to be connected as the working and counter electrodes. This role of a working or a counter electrode can be inter-changed depending on the requirements. This is discussed in section 4.5.

In contrast, a 2-electrode configuration is only able to investigate the total cell. The use of a reference electrode is not restricted to EIS but can also be used for other characterization techniques such as the polarization curve and power density plots which are discussed in section 3.7.3.

The AC signal, which is applied to perform EIS, is usually a voltage signal but can also be imposed as a current signal to the concerned system (in this case it is known as galvanostatic EIS). The signal imposed on the system must have a small amplitude, relative to the operational voltage of the system, to make sure that the steady state response of the device under study is not disturbed. This amplitude is usually within the range of 5 mV to 50 mV. The AC signal is applied over a range of frequencies with fixed frequency steps. This frequency range can be in between very low frequencies to very high frequencies, e.g. from 1 mHz to 1 MHz. Moreover, a DC bias can also be added to the AC signal that is applied to the system. A DC bias is when a constant DC voltage is added to the signal throughout the experiment.

After the voltage signal is imposed, at a specific frequency, on to the system, the current response is recorded and used to calculate the impedance of the system at the respective frequency point. In this way, impedance of the system is recorded at different frequencies within the defined frequency range at fixed frequency intervals. Hence, an impedance spectrum is obtained which is inherent to the system on which EIS was performed.

Figure 20 shows an example of an applied voltage and the respective current response from the system. The frequency of the applied voltage in this case is 500 Hz and the voltage has an amplitude of 50 mV.

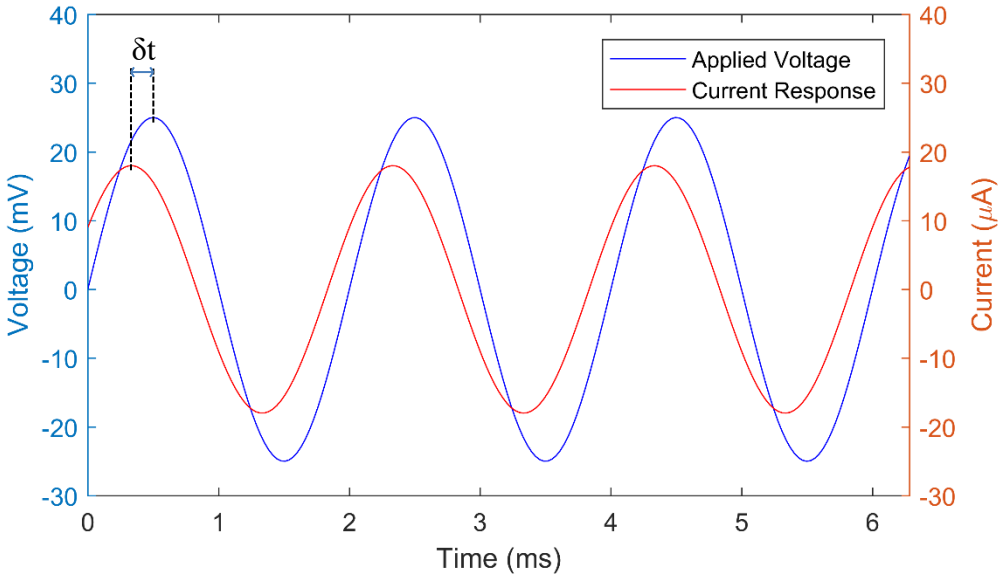

Figure 20: Imposed voltage on a system and the current response.

It can be seen from Figure 20 that the current response of the applied voltage has the same frequency but is shifted, on the time axis, by a certain amount, δt, towards the left side of the graph. This kind of behavior occurs if the system under study has a capacitive behavior which causes a certain phase difference between the voltage and the current. A shift towards the right would correspond to an inductive behavior of the system. Moreover, the current signal is also different in terms of amplitude from the applied voltage signal. Both, the phase difference and the change in magnitude are related to the impedance exhibited by the system at the specific frequency.

The impedance of any system at a frequency, f, is given by equation (24);

$$Z(f,t) = \frac{V(f,t)}{I(f,t)} \tag{24}$$

The functions of voltage and current are given by equation (25) and equation (26), respectively;

$$V(f,t) = V_0 sin(2\pi f t) \tag{25}$$

$$I(f,t) = I_0 sin(2\pi f t - \theta) \tag{26}$$

In equation (26), θ is the phase difference between the current and the voltage due to the impedace imposed by the system. Equations (25) and (26) can be re-written as follows;

$$V(\omega, t) = V_0 e^{(j\omega t)} \tag{27}$$

$$I(\omega, t) = I_0 e^{j(\omega t - \theta)} \tag{28}$$

where, $\omega = 2\pi f$ and $j = \sqrt{-1}$ (the imaginary unit). Using equations (27) and (28), equation (24) can be rewritten as follows;

$$Z(\omega, t) = \frac{V(\omega, t)}{I(\omega, t)} = \frac{V_0}{I_0} e^{j\theta} = |Z(\omega)| e^{j\theta} \tag{29}$$

Therefore, it can be seen that the impedance, at a given frequency, is directly related to the ratio of the amplitudes of the voltage and current and to the phase difference between the voltage and current. Equation (29) can be further modified using Euler's formula to obtain the following relationship;

$$\begin{aligned} Z(\omega, t) &= |Z(\omega)| \left(\cos(\theta) + j sin(\theta)\right) \\ &= \underbrace{|Z(\omega)| \cos(\theta)}_{\text{Real, } Z_r} + \underbrace{j|Z(\omega)| sin(\theta)}_{\text{Imaginary, } Z_i} \end{aligned} \tag{30}$$

Equation (30) provides two different parts that comprise the total impedance – real and imaginary. In electrical systems, imaginary part of the impedance, reactance (X), is present due to capacitive or inductive effects. If a system only comprises of resistances, the total impedance has no imaginary part.

Mathematically, to have a zero imaginary part in the impedance calculated in equation (30), θ must be equal to zero. Consequently, there would be no phase difference between the current response and the applied voltage. Moreover, what is referred to as the total internal resistance of an MFC in chapter □ is actually the total internal impedance of an MFC.

There are certain important conditions that need to be fulfilled to obtain reliable and robust EIS data:

i. *Linearity*. It is important that the system under study behaves linearly while the EIS signal is imposed. This would allow us to develop linear models which help interpret the data obtained through EIS. Linearity puts the limit on the amplitude of the imposed AC signal. If a system has a fairly linear behavior, a relatively large AC signal can also be imposed to perform EIS. But, since MFCs do not have an ideally linear behavior, especially in certain regions (Figure 9, regions 1 and 3), it is important to keep the amplitude of applied AC signal low. In the end, it becomes a trade-off between keeping linearity (which requires a low amplitude signal) and reducing noise (which requires a signal with high amplitude).

ii. *Causality*. The current response that is received is primarily due to the imposed voltage, but there are other factors that can interfere with the current response. Causality imposes the limitation that the current response should only be due to the imposed voltage and thus other factors that can interfere with the current response should remain minimal.

iii. *Stability*. The system should remain stable throughout the extent of the EIS measurement. An EIS measurement can take from 2 minutes to up to several hours to finish. The time for an EIS measurement depends on the range of frequency and the experimental points per decade, in terms of frequency. The clause of stability says that we have to ensure that system remains stable during this period and does not drift in terms of voltage. Moreover, once the perturbation i.e. imposed externally ends, the system should return to the same state as before the perturbation starts.

4.3 Representation of EIS data

The data obtained through EIS is a collection of the values of impedance at different frequencies. These values of impedance can be perceived in two different

ways. The first way to look at it is as the sum of its real and imaginary parts. The second way is to consider it as a magnitude and phase combination. Both of these representations are visualized in separate plots.

First, let's have a look at the plot which presents the real and imaginary parts of impedance on the x and y axis, respectively. This plot is called a Nyquist plot and is shown in Figure 21.

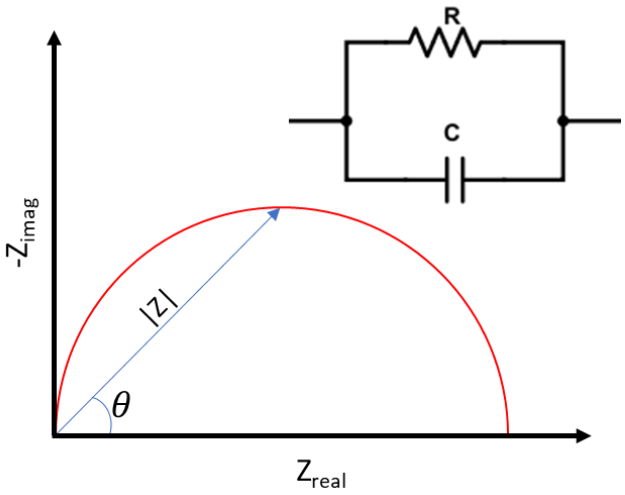

Figure 21: Nyquist plot of the EIS performed on a simple RC circuit.

This Nyquist plot is obtained by performing EIS on a simple RC circuit similar to the one shown in Figure 21. If you look closely, the y-axis is the negative of imaginary value of impedance. This is done to make the representation more intuitive and so that the data is plotted in the first quadrant. One drawback of a Nyquist plot is that the frequency at which a particular point of impedance was obtained cannot be inferred from the graph. The blue arrow points to a certain impedance at a frequency. The length of this arrow represents the magnitude of the impedance at this point and the angle this arrow imposes on the x-axis represents the phase of the impedance at this point.

The plot of Figure 21 belongs to the RC circuit shown in the image. Since there is only one resistor and one capacitor present, there is only one time constant related to the capacitor. The semicircle contained in the Nyquist plot is the characteristic of such a setup where there is only a single time constant. Other systems, such as MFCs, are much more complicated than a simple RC circuit. Therefore, they might have several time constants related to their EIS. Thus, they may have multiple partial semi circles in the plot. Figure 22 shows the Nyquist plots of data obtained

by performing EIS on MFCs under different operational conditions. As it can be seen from the images, one Nyquist plot may have more than one semicircular arc.

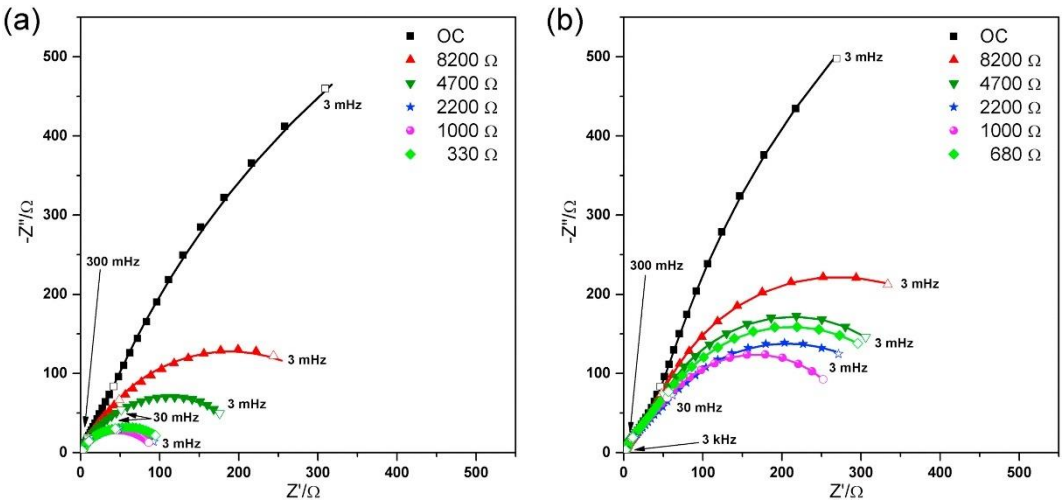

Figure 22: (a) and (b) Nyquist plots pertaining to EIS measurements performed on MFCs under different conditions[9]. Reprinted with permission from Electrochimica Acta, Elsevier.

Impedance of a system can also be written in terms of its magnitude and phase (the quantities that represent the blue arrow in Figure 21). To calculate the magnitude and phase, following equations can be used;

$$|Z| = \sqrt{Z_r^2 + Z_i^2} \tag{31}$$

$$\theta = \arctan\left(\frac{Z_i}{Z_r}\right) \tag{32}$$

Where $|Z|$ is the magnitude of the impedance of the system and θ is the phase of the impedance of the system. $|Z|$ and θ can be used to plot another representation of the EIS data known as the Bode plots. Both the components are plotted on separately, on the y-axis, with the frequency (or log of frequency) as the variable on the x-axis. A typical bode plot, of a simple RC circuit is shown in Figure 23.

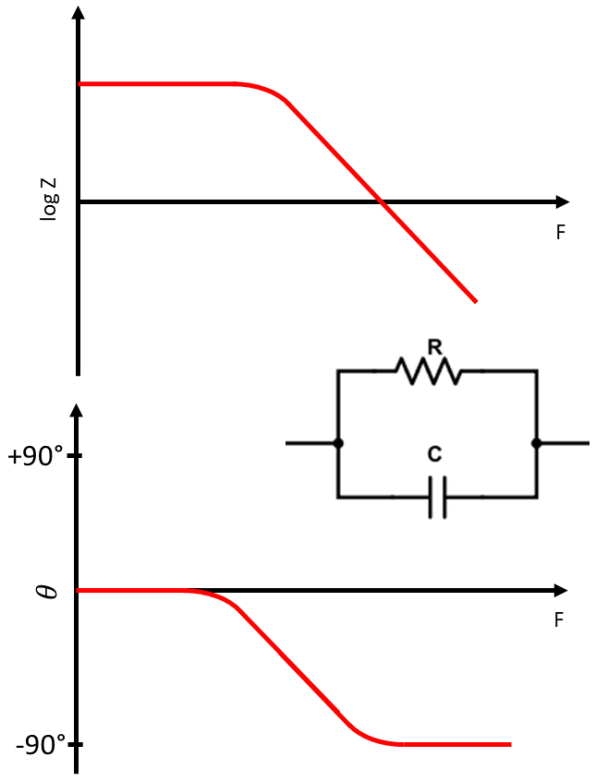

Figure 23: Bode plot representation of EIS data of a simple RC circuit.

An important feature of the bode plot is that it shows the frequency data as well as the impedance data. Typically, $|Z|$ and θ curves are plotted on the same graph with the proper color coding and a dual y-axis setup. The representation shown in Figure 23 is for a simple circuit and is quiet straight forward. There is a change in the magnitude and a change in phase of 90° due to the capacitor and resistor. The frequencies around which these changes occur are dependent on the values of R and C.

In real systems such as MFCs, these plots can be much more complicated since there are multiple capacitance, resistances and processes that contribute to the whole impedance spectrum. Figure 24 shows a bode plot representation of EIS data which was performed on an MFC under different operational conditions.

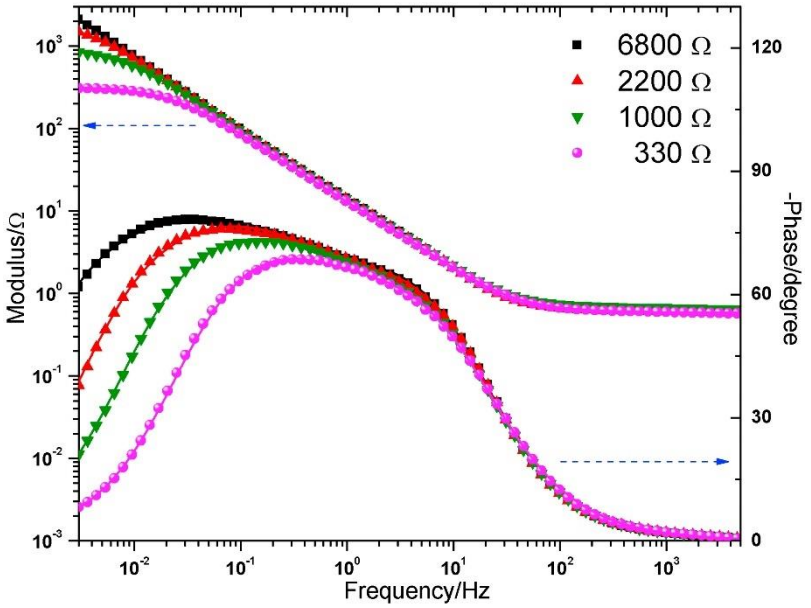

Figure 24: Bode plot of EIS measurement performed on an MFC[9]. Reprinted with permission from Electrochimica Acta, Elsevier.

4.4 Analysis of EIS data

It is important to analyze the EIS data and obtain meaningful parameters which carry information about the system under study. Using EIS data, the system under study can be modelled as a series of electrical components, connected in specific arrangements. For example, if EIS data is used to fit an EEC model of an MFC, there are several parameters, related to the MFC's internal impedance, that can be quantified. Figure 25 shows an example of the possible impedance elements present on the anode side of an MFC. As it can be seen, the total impedance related to the anode side can be broken down into several elements. Each of these elements play its own role in the overall impedance. Furthermore, each of these elements can be co-related to the different biological, interfacial and chemical processes occurring on the anode of an MFC.

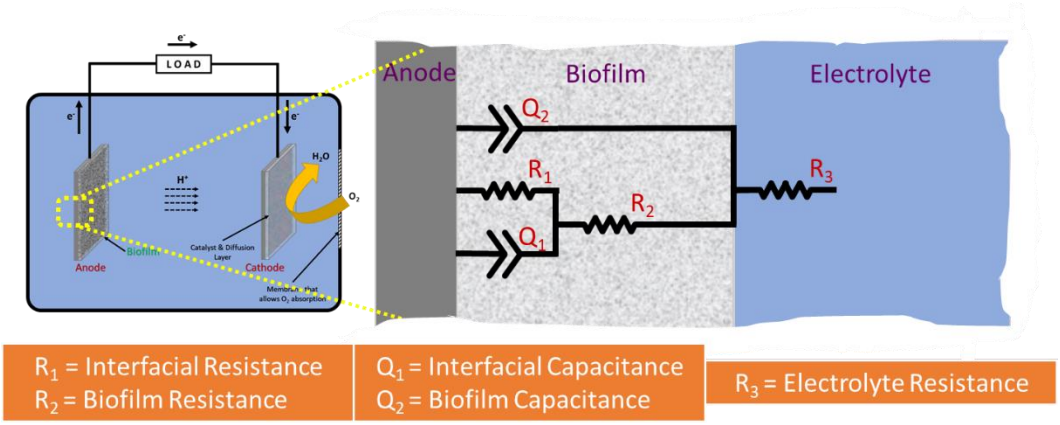

Figure 25: A possible EEC model of an MFC's anode.

In Figure 25, the capacitances, both interfacial and biofilm, are denoted by the letter 'Q' instead of the more common symbol for a capacitor 'C'. Moreover, the symbols are also slightly different. This is because the element shown in the image is a Constant Phase Element (CPE). CPEs are discussed in mores details later in this section.

To delve deeper into the analysis of EIS data, let us first consider the simplest form of an electrical system – a system that just contains a resistance. In this case, the impedance of the system will be given directly by using Ohm's law and using the amplitudes of the applied voltage and the current response;

$$Z = \frac{V_0}{I_0} \tag{33}$$

This is due to the fact that a resistor does not introduce any kind of phase different between the applied voltage and the current response. Moving on, let us consider a capacitor. The current response of capacitor, if a voltage $v(\omega, t) = V_0 \sin(\omega t)$ is applied is given as follows;

$$i(\omega, t) = C\frac{dv(\omega, t)}{dt} = CV_0\omega\cos(\omega t) = CV_0\omega\sin(\omega t + \frac{\pi}{2}) \tag{34}$$

Where C is the capacitance of the capacitor. It is evident from equation (34) that the waveform of the current is different only in terms of magnitude and is shifted in the time axis. This shift in the time axis is known as a phase difference and this case, the phase difference is π/2. To summarise, the current is leading the

voltage by a value of -π/2. This phase difference is also seen when plotting the bode plot of an RC circuit, which introduces a phase change of 90°, see Figure 23. The introduction of a -π/2 phase difference indicates the characteristics of a component that is purely imaginary. To calculate the impedance of the capacitor we can use the ohms law as follows;

$$Z_C(\omega,t) = \frac{V(\omega,t)}{I(\omega,t)} = \frac{V_0}{I_0}e^{j\theta} = \frac{1}{\omega C}e^{-j\frac{\pi}{2}} = \frac{1}{j\omega C} \tag{35}$$

Similarly, if we consider an inductor instead of a capacitor, we can calculate the current response of an applied voltage, $v(\omega,t) = V_0\sin(\omega t)$ of the inductor. The relation between the current and voltage of a capacitor is given by equation (36).

$$v(\omega,t) = L\frac{di(\omega,t)}{dt} \tag{36}$$

Consequently, using equation (36), we can calculate the impedance using equation (37).

$$Z_L(\omega,t) = \frac{V_0}{I_0}e^{j\theta} = \omega L e^{j\frac{\pi}{2}} = j\omega L \tag{37}$$

It can also be seen from equation (37) that, for an inductor, the current lags the voltage by 90°. The magnitude of phase change is the same as that of a capacitor but in the case of a capacitor, current leads the voltage by 90°. Moreover, it is important to notice that if a system has an inductive behaviour, the imaginary part of equation (30) will be positive. On the contrary, if a system has a capacitive behavior, the imaginary part of equation (30) will be negative. Furthermore, MFCs mostly have a capacitive behavior and only very rarely show inductive elements. This is the reason why the Nyquist plot of Figure 21 has a y-axis which is $-Z_{imag}$ rather than Z_{imag} for a more convenient visual representation.

To obtain the EEC model of the internal resistance of an MFC, ideal behavior of a capacitor as defined by equations (34) and (35) is not always sufficient. Therefore, additional components which are not mainstream electrical components, are used to assist in the proper modelling of EIS data. These elements are:

i. *Constant Phase Element (CPE)*. CPE is a more general form of a capacitor. In other words, it can be thought of as an imperfect capacitor. It is mostly used as an element for modeling equivalent circuits. More specifically, it plays an important role in modelling double layers. In the case of a CPE, the impedance is given by equation (38).

$$Z_{CPE}(\omega, t) = \frac{1}{Q(j\omega)^n} \tag{38}$$

Where, Q is referred to as the CPE's pre-factor and n is the CPE's index (0<n<1). It can be noticed here that the capacitor is a special case of a CPE in which n = 1. Moreover, if n = 0, the CPE becomes a resistor. The phase difference that a CPE introduces is given by $-n\frac{\pi}{2}$ (- n . 90°) CPE is usually denoted by the letter 'Q' and has a symbol like the one shown in Figure 26.

Figure 26: Symbol of CPE.

ii. *Warburg Element*. Warburg impedance element is related to the impedance caused by the diffusion process. It is also known as the Warburg diffusion element. The Warburg element comes in handy when modelling is required for a process related to linear diffusion that is semi-infinite. To elaborate, the process is an unhindered diffusion towards a planar surface, which in our case is the electrode. When considering diffusion processes, this is the simplest case in which the only factor that matters is the linear distance to the electrode. Moreover, Warburg is again a simplification of the CPE in which the CPE index, n, is equal to $\frac{1}{2}$ and the CPE factor, Q, is equal to $\frac{1}{W}$ (where W is the Warburg constant). Therefore, the impedance related to a Warburg element can be simplified to equation (39).

$$Z_W(\omega, t) = \frac{W}{\sqrt{j\omega}} \tag{39}$$

Warburg element is denoted by W. Since, in the case of Warburg element, n = $\frac{1}{2}$, the value of phase introduced by a Warburg element is $-\frac{\pi}{4}$ (- 45°). The symbol used for a Warburg element is given in Figure 27.

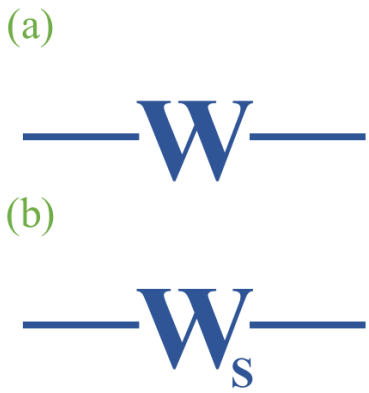

Figure 27: Symbol of (a) Warburg element and (b) Warburg short element.

A more specialized case of the Warburg element is known as the Warburg short element, W_s. This element is used to model a process in which the diffusion is occurring at length which is finite. In the case of W_s the impedance is given by equation (40).

$$Z_{W_S}(\omega, t) = R_d \sqrt{\frac{\omega_d}{j\omega}} \tan^{-1}\left(\sqrt{\frac{j\omega}{\omega_d}}\right) \tag{40}$$

Where ω_d is known the frequency related to the diffusion process and R_d is known as the diffusion resistance.

All the elements that are introduced in this section are summarized in Table 3.

Table 3: Impedance elements used for EEC models. Adapted with permission from Renewable and Sustainable Energy Reviews, Elsevier.[122]

Impedance Element	Letter Representation	Impedance Equation	Electrical Circuit Symbol
Resistor	R	$Z_R = R$	
Capacitor	C	$Z_C(\omega, t) = \frac{1}{j\omega C}$	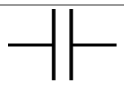
Inductor	L	$Z_L = j\omega L$	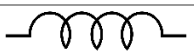
Constant Phase Element	Q	$Z_{CPE} = \frac{1}{Q(j\omega)^n}$	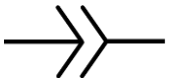
Warburg	W	$Z_W = \frac{W}{\sqrt{j\omega}}$	
Warburg Short	W_s	$Z_{W_S} = R_d \sqrt{\frac{\omega_d}{j\omega}} \tanh^{-1}\left(\sqrt{\frac{j\omega}{\omega_d}}\right)$	

Using the parameters and elements explained in this section and summarized in Table 3, EIS data, from a variety of systems, can be used to give meaningful information and insight into the systems. The systems that are more relevant to my thesis are MFCs. Therefore, the use of EIS to investigate MFCs only will be discussed in the following section.

4.5 EIS and MFCs

It is important to minimize the MFCs' internal impedance to improve their power production. There are several phenomena, surfaces and processes that are occurring inside an MFC which contribute to the MFC's overall internal impedance. Therefore, it is not only important to calculate the overall impedance of an MFC but, it is also essential to get knowledge about the contributions of the different resistive elements present inside an MFC. This way more targeted approaches can be formalized to reduce the internal impedance of an MFC, resulting in an improved power performance.

Initially, EIS was adopted by Min and co-workers to evaluate the internal resistance of an MFC[123]. Later, studies using EIS began to investigate the

impedance contribution of different membranes, usually found in a dual chamber MFC, on the overall power production of an MFC[47,124–129]. A large number of studies also investigated the effect of electrode spacing and different substrates/electrolytes, along with the PEM, on the internal impedance of an MFC in different setups and configurations[46,130–138]. Most of these studies found that reducing the inter-electrode spacing increases the power density due to a decreased internal resistance of the MFC. In addition, Cheng and co-workers found that the OCV is increased by reducing the electrode spacing[138]. Studies cited above, and more similar ones were the reason for employing MFCs with reduced electrode spacing such as air-cathode MFCs. Furthermore, it was discovered that a larger area of anode with respect to the area of cathode resulted in a reduced internal impedance of an MFC[139].

When considering impedance analysis and EEC modelling, the internal impedance of an MFC can be summed up into three main components – the ohmic resistance, R_{ohm}, the charge transfer resistance, R_{ct} and the diffusion resistance, R_d[119]. Therefore, the internal resistance of an MFC can be written as equation (41).

$$R_{int} = R_{ohm} + R_{ct} + R_d \tag{41}$$

The sum $R_{ct} + R_d$ is also referred to as the polarization resistance[137]. Polarization resistance is related to the interface between an electrode and the electrolyte. Moreover, polarization resistance is also related to the diffusion of substrate or other chemical species in the vicinity of an electrode. Both, anode and cathode, possess a polarization resistance. Therefore, equation (41) can be further extended to include all the components related to the total cell. Moreover, the resistance due to the membrane can also be included to give it a more complete form. This extended version is given in equation (42).

$$R_{int} = R_{mem} + R_{ohm} + R_{ct}^{anode} + R_{ct}^{cathode} + R_d^{anode} + R_d^{cathode} \tag{42}$$

Since R_{int} is obtained through the data collected by EIS and it embodies all the different components mentioned in equation (42), it is important to fit the overall internal impedance of an MFC to quantify, if not all, at least most of the elements

defined by equation (42). At the same time, it is also very important to properly understand and assign the results obtained from fitting. This is because the results gathered by performing EIS on an MFC are obtained by applying a voltage in a wide frequency range. The resulting current response in not governed by a few ideal components e.g. resistors and/or capacitors. Instead, the current response is a result of the cumulative impedance effect of several non-ideal equivalent electrical elements present within the MFC. This type of quantification from fitting has been performed by several works in literature[9,47,140].

A typical simple circuit that can be used to define the interface between an electrode, e.g. the anode, and the electrolyte is shown in Figure 28.

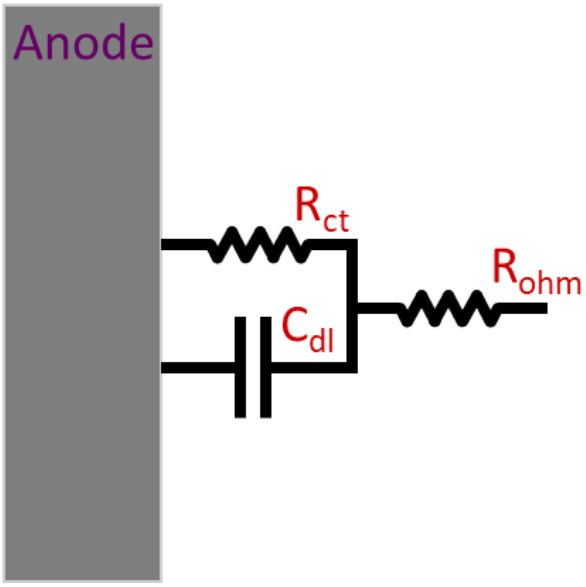

Figure 28: EEC of an anode-electrolyte interface.

Where, C_{dl} is known as the double layer capacitance. A double layer capacitance is the capacitance resulting from an electrical double layer effect. More specifically, it is the behavior which is seen at the boundary of an electrode (in the case of Figure 28 an anode), and a liquid medium such as the electrolyte. Basically, the charges present on the ions in the electrolyte are separated from the charges present inside the electrode by a finite distance (of the order of nm). Such interaction between the two types of charges, which happens at the interface between the electrode and the electrolyte, causes this capacitive effect. C_{dl} has a behavior similar to that of a capacitor.

Additional elements might also be observed in a bio-anode that is modeled using this technique. These elements are related to the biofilm that is formed on the

anode, due to which additional charge transfer process occurs. Moreover, the thickness of the biofilm also effects the double layer capacitance. Furthermore, an element that is related to the diffusion of substrate is also present. The most typical element that is introduced due to the diffusion is the Warburg element. Figure 29 shows the EEC of a bio anode with the Warburg element which represents the substrate diffusion.

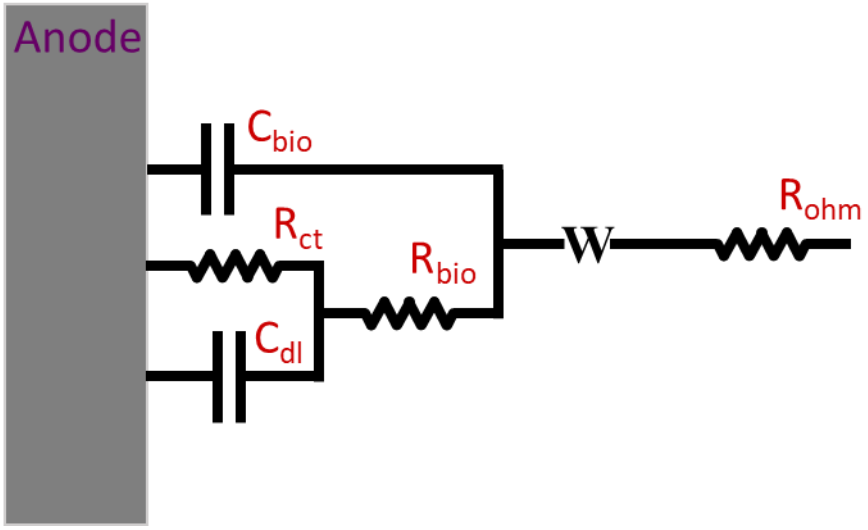

Figure 29: EEC of a bioanode with the diffusion element.

Similar to Figure 28 and Figure 29, the EEC of cathodes can also be obtained. In fact, to obtain parameters that are specific to either the anode or the cathode, it is important to perform EIS in a 3-electrode configuration which was discussed in section 4.2. In this case, where we need to calculate the impedance parameters specific to the anode, it is required that we connect the anode as the working electrode and cathode as the counter electrode. The third node, which is referred to as the reference electrode, will be connected to the reference electrode we have selected. On the other hand, if we need to calculate the parameters specific to the cathode, we need to connect the cathode as the working electrode, anode as the counter electrode. The third node will again be connected to the reference we have chosen. A 3-electrode experimental is used to investigate half cells – either the anode half or the cathode half.

In the case of a 2-electrode setup, the data we obtain through EIS will contain the information about the total cell. This includes the polarization resistances of both the anode and the cathode, the series resistance due to the electrolyte and the resistance due to the membrane, if any. It will also contain information about the

diffusion resistance. Moreover, if a biocathode is also present, the EIS data will also contain information about it. Therefore, in a 2-electrode setup, it will be more difficult to extract results that give precise information about the different elements of the internal impedance. In fact, many studies performed in the past incorrectly interpret the data obtained through EIS. This has been discussed in detail by Benetton et al. in their comprehensive review on the use of EIS to investigate MFCs[119].

5 Characterization and analysis of MFCs based on mixed community bacteria using different enrichment methods

MFCs can offer a sustainable source of clean energy, but at the present scale their exploitation is still limited. Moreover, MFCs also have a potential as biosensor. To make these use-cases possible, it is very important to increase their efficiency and performance. In addition, it is important to understand their sensitivity towards toxicants introduced in the MFCs medium. Hence, it is essential to understand how the biofilm present on the bio anode performs all the necessary electrochemical processes. For this purpose, many techniques and methods have been employed in the past to study bio anodes. We chose the use of EIS along with other characterization techniques to study the biofilm formed using bacteria from a mixed community. Another important part of this study was to properly analyze and interpret the data obtained through the characterization since many studies in the past, using EIS have not properly explained the results. Part of this chapter, relating to the experiments, results and discussions are also issued in an article published in Electrochimica Acta:

Agostino, V., Ahmed, D., Sacco, A., Margaria, V., Armato, C., & Quaglio, M. (2017). Electrochemical analysis of microbial fuel cells based on enriched biofilm communities from freshwater sediment. Electrochimica Acta, 237, 133-143.

5.1 Introduction

As the use of MFCs as bio sensors and electricity generating devices is increasing, the investigation into how the bio anodes work is becoming increasingly important. The interest not only lies in the functioning of the biofilm but also in how the biofilm is formed. The majority of the research performed on biofilm formed in an MFC, designed to perform biosensing, uses specific type of bacteria[78,141-145]. Therefore, MFCs pertaining to these studies are based on exoelectrogens belonging to a pure culture. These pure cultures of bacteria usually belong to one of the two strains:

- Geobacter sulfurreducens
- Shewanella oneidensis

Moreover, mixed cultures were also used in studies which were taken from already operating MFCs and thus the start-up period, referring to the bio-anode formation, was investigated[79,143–147]. Consequently, there are only few studies that discuss the use of mixed culture bacteria in biofilm formation and MFC operation[148,149]. For practical applications of MFC, it is important to investigate MFCs based on a mixed consortium. For the latter purpose, a mixed consortium, which comes directly from the environment, results to be more adapt to the conditions that prevail in a real environment where MFCs based on these consortia could be used as sensors. Such real environment bacterial consortia have already been used to implement MFCs used as power sources for applications such as wireless sensing. The sources of these consortia are mostly sediments belonging to seawater and freshwater. Both these resources inhabit bacteria that are active electrochemically.

An important step in any MFC setup is the biofilm formation and acclimation. Moreover, the future performance of an MFC depends on this phase of its life. For the formation of a biofilm, a source of the bacteria is required. This can be taken as pure culture, mixed culture direct from the environment or mixed culture from already running MFCs. The consortia from already running MFC has an advantage as it takes lesser time for the acclimation. Furthermore, specific enrichment methods in the start-up phase of an MFC have been proposed to reduce the time

taken. For example, Pierra and co-workers used iron-enrichment method which resulted in reducing the time required for the MFC start-up[150]. A method based on Iron enrichment enables selective growth of bacteria in the mixed consortia. Apart from the bacterial sample and enrichment methods, another factor that plays an important role in the biofilm formation is the potential at which the anode is kept with respect to the cathode. This potential inherently decides the amount of energy that is used for the growth of the biofilm. Theoretically, to reduce the time required for the formation of biofilm, it is important to have the anode at a potential which is higher with respect to the reaction potential of the redox compound. This would effectively provide an increased amount of energy to the bacteria for the growth of the biofilm. Nevertheless, having a lower anode potential (resulting in a higher overall potential difference between anode and cathode) results in a biofilm which is better in terms of current density. Therefore, the potential selected is a tradeoff between the required time and the current density produced. Moreover, the chosen potential, for the biofilm formation, also depends on factors such as the substrate (carbon source) and medium employed.

5.2 Experiment structure

The main purpose of this experiment was to study the complete setup of an MFC which includes the acclimation phase, the enrichment phase and electrochemical characterizations on a functional bioanode. Different investigation techniques were used to understand better the formed biofilms under different enrichment strategies. For the purpose of this experiment, we used a disc shaped dual chamber MFC[76] which is shown in Figure 30. Moreover, the MFC system used here is a continuous flow one, in which, the cathodic and anodic chamber medium are constantly injected into the MFC using a syringe pump system – NE1600, New Era Instrument, USA. This syringe pump system, working with the MFCs, is also shown in Figure 30.

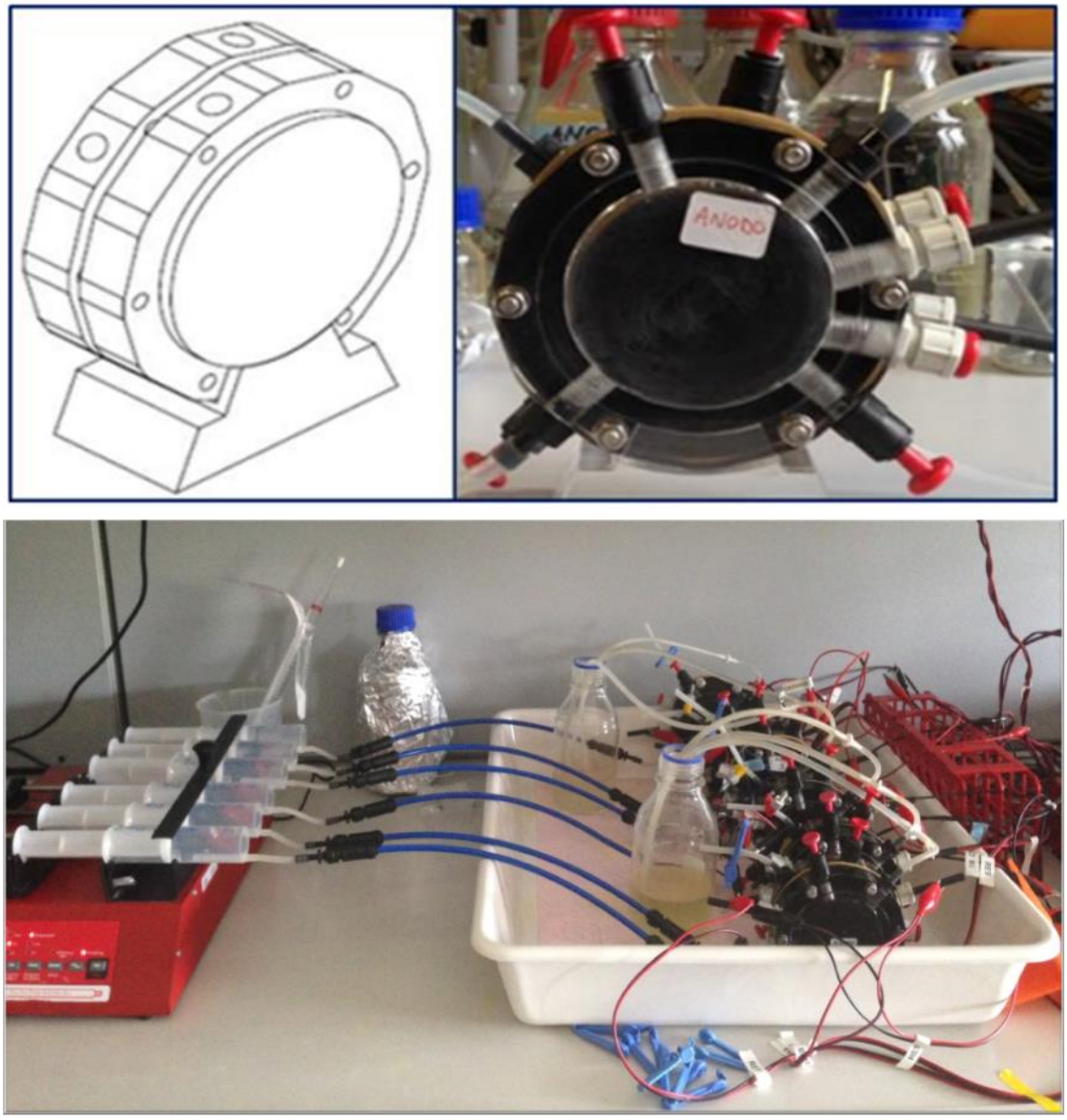

Figure 30: Architecture and setup of the MFC systems used.

5.2.1 Acclimation Experiment

In the start, for the acclimation of the biofilm, it is necessary to set a potential across the cathode and anode as discussed in the previous section. One way to do this is to use a resistor connected to the anode and the cathode. To test the influence of value of the external resistor and hence the potential difference across the anode and cathode, we used 3 different values of resistances, 47 Ω[151–153], 470 Ω and 1 kΩ. For each value of the resistance, a duplicate of MFCs was used to improve the robustness of the results. Therefore, a total of 6 MFCs were used for this part of the experiment. The syringe volumes used to pump the anodic and cathodic medium were 60 mL and the retention rate selected was 0.5 mL/h[76]. The length for which

this experiment was conducted was 3 weeks. Furthermore, the experiments were conducted at room temperature i.e. 21 ± 2° C. After this initial phase, polarization tests on the MFCs were started from the 5th week to analyze the difference in performance of MFCs based on the three initial resistances. During the experiment, the anodic voltages with respect to a reference electrode Ag/AgCl were also recorded.

5.2.2 Enrichment Experiment

The enrichment method affects the MFCs performance. In our experiment we used two different enrichment methods to study their effect on the MFCs power production. These two enrichment methods are:

i. *General Enrichment (GE)*. The chemicals and nutrients added are given in Table 4.

Table 4: Composition of the General Enrichment.

Name	Chemical Formula	Amount
Potassium chloride	KCl	0.10 g/L
Ammonium chloride	NH_4Cl	1.5 g/L
Sodium hydrogen phosphate	Na_2HPO_4	4.28 g/L
Sodium dihydrogen phosphate	NaH_2PO_4	2.45 g/L
Sodium acetate	$C_2H_3NaO_2$	2.5 g/L
Wolfe's Vitamin solution (ATCC)	-	10 mL/L
Wolfe's trace mineral solution (ATCC)	-	10 mL/L

ii. *Ferric Citrate Enrichment (FeC)*. In the FeC enrichment, a high concentration (13.70 g/L) of Ferric Citrate (formula: $FeC_6H_5O_7$) was added to the electrolyte composed by all chemical compounds summarized in Table 4. Therefore, the only difference between the two enrichments was that of Ferric Citrate. FeC enrichment was used in

order to create an environment that favors the growth of Dissimilatory metal-reducing bacteria (DMRB)[150,154]. DRMB is the same group of bacteria that contains Geobacter sulfurreducens and Shewanella oneidensis, which are the preferred types of EABs in the field of MFCs.

Before the use of both these mediums, in order to ensure anaerobic conditions, enhancing then the microorganisms' proliferation, nitrogen gas was used to remove any oxygen present. The volume of inoculum was 40 mL which contained both the freshwater and sediment. Furthermore, the volume of enrichment medium added was 40 ml. Thus, the total volume was 80 ml. The total enrichment time was 3 weeks and the experimental was carried out under room temperature i.e. 21 ± 2° C.

After this enrichment phase, double chamber MFCs, as shown in Figure 30, were used for the inoculation. Similarly to the acclimation phase, the experiments were conducted in a duplicate. Therefore, two MFCs were derived from GE enriched inoculum and two MFCs were derived from the FeC enriched inoculum. For all the inoculations, 10 % inoculum volume with respect to the total anodic chamber volume was used. Moreover, during the acclimation phase, the cells were put under a load of 47 Ω, based on the result of acclimation experiment (see Section 5.3.1). As explained above, the acclimation phase is defined as the start-up period, during which the EAB properly proliferated on the anode surface, leading thus to the formation of biofilm. Since, these experiments were also setup in a continuous flow mode, the cathodic and anodic medium were pumped in using a syringe pump system – NE1600, New Era Instrument, USA. The rate of medium injection was 0.5 mL/h.

After the initial acclimation phase, a series of electrochemical characterizations were performed on the MFCs to analyze the effects of the two different enrichment methods. These characterizations included EIS, Cyclic Voltammetry (CV) and Polarization. Moreover, the voltage of the MFCs were monitored throughout the experiment. Electrochemical characterizations were also performed on identical MFCs which were abiotic, i.e. without any biofilm. This was done for greater depth in the analysis of the data obtained from the various electrochemical characterizations, which included:

i. *Polarization Test*. Polarization tests were performed by varying the external resistance applied to the MFCs. Initially, the cells were set to open circuit and the voltage value was recorded. Then, resistances were varied using the following values: 8.2 kΩ, 6.8 kΩ, 4.7 kΩ, 2.2 kΩ,1.5 kΩ, 1 kΩ, 0.68 kΩ and 0.33 kΩ. The cells were allowed to stabilize each time the value of a resistance was changed, before recording the values. Current and power densities were calculated using the values of voltage obtained and the resistance values.

ii. *EIS*. EIS was performed at each point in the polarization test. Therefore, impedance data of all the cells were collected in all the different stages of polarization. The parameters used for EIS are listed in Table 5.

Table 5: EIS Parameters.

EIS Parameters	
Frequency Range	3 Khz – 3 mHz
Signal Amplitude	25 mV
Configuration	3-electrode (Anode – Working Electrode, Cathode – Counter Electrode and Ag/AgCl – Reference Electrode)

VSP potentiostat by BioLogic was used to perform the EIS measurements. Moreover, EIS measurements were also performed in non-turnover condition and on identical MFCs in which the anodes were abiotic. Non-turnover conditions refer to the situation in which an anodic substrate is not present. In our case, the anodic substrate is sodium acetate.

iii. *CV*. Lastly, after the polarization tests and EIS were finished CV was performed on the MFCs[155,156]. The selected scan rate was 1 mV/s and the potential range, vs. Ag/AgCl, selected was -0.6 V to +0.2 V. After polarization test and EIS, the MFCs were left to stabilize under a load of 1 kΩ for 1 week during which the values of voltages were recorded. CV is important in characterizing the reactions that are occurring the

electrodes and the microorganisms which cause electron transfer. In the experiments, we collected CV data to further affirm the hypothesis we developed using EIS, which deduces that the GE enrichment performed better than the FeC based enrichment. CV was performed in both turnover and non-turnover conditions

Once the electrochemical characterizations were completed, a biological study of the bio anodes was also performed. This was performed using the technique known as fluorescence microscopy. The device used for fluorescence microscopy was the Nikon ECLIPSE Ni. The main purpose was to analyze the distribution of the biofilm within the anode. As a precursor to this analysis, LIVE/DEAD BacLight Bacterial Viability Kit by Invitrogen was used to stain the anodes. For this purpose, carbon felt from the anodes were washed using sterile PBS. This was done to remove any medium from the original MFC setup. Afterwards, the carbon felt was stained using the dye for 20 minutes. Then, the anodes were re-washed using PBS to remove the excess of dye that is not bounded with microorganisms. Lastly, the software NIS Elements Image Software was used to analyze the images and to approximate the count of living and dead microorganisms.

5.3 Results and Discussion

5.3.1 Acclimation Experiment

The main purpose of this experiment was to assess the difference in the performance and hence, the acclimation of a mixed community biofilm that was formed under different load conditions. For this purpose, duplicate MFCs were loaded with different values of external resistances (47 Ω, 470 Ω and 1 kΩ).

Figure 31 displays the results of anodic performance in terms of the anode voltage with respect to a reference (Ag/AgCl).

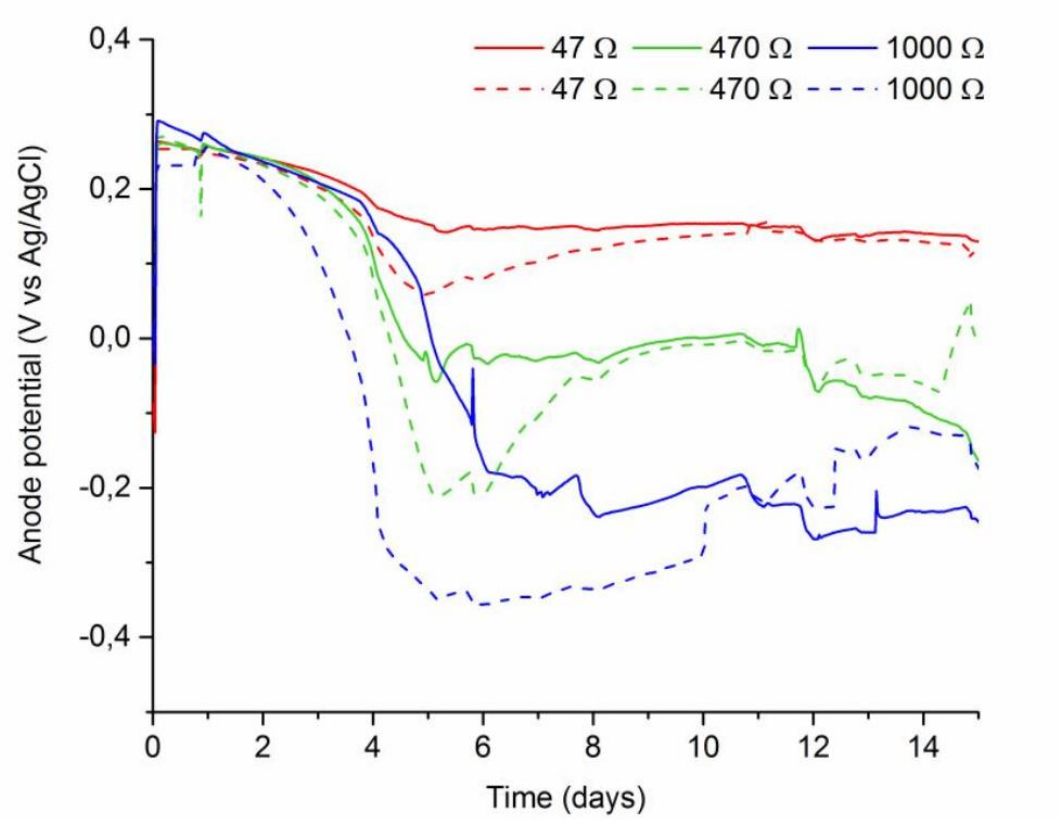

Figure 31: Anode potential vs. Ag/AgCl reference of MFCs in acclimation phase under different load conditions.

It is evident from Figure 31 that all the different resistances had a different effect on the acclimation phase. Furthermore, for MFCs47 (MFCs connected to 47 Ω) and MFCs470 (MFCs connected to 470 Ω) the duplicates had a similar response to each other. On the other hand, for MFCs1k (MFCs connected to 1 kΩ) the duplicates had a slightly different response to each other especially in the first few days, which can also be referred to as the lag phase. Moreover, it is important to highlight how MFC47 duplicate was the one which performed better than the rest, in terms of a stable voltage production. The average values anodic voltage with respect to Ag/AgCl is given in Table 7. It is important to notice that the values presented in Table 7 and Figure 31 are the anode half-cell voltages i.e. the voltage of the anode with respect to the reference. Therefore, some of the values are also negative.

Table 6: Average anodic voltages of the three duplicates with respect to the reference (Ag/AgCl).

Duplicate Name	Average Anodic Voltage vs. Ag/AgCl (V)
MFCs47	0.134 ± 0.013
MFCs470	-0.050 ± 0.015
MFCs1k	-0.238 ± 0.025

Furthermore, all the cells showed a current production over the period of this experiment. The maximum current densities produced by each duplicate is shown in Table 7.

Table 7: Maximum current densities produced by the 3 duplicates.

Duplicate Name	Maximum Current Density Produced (mA/m^2)
MFCs47	241 ± 106
MFCs470	198 ± 18
MFCs1k	130 ± 12

Following this initial phase of voltage monitoring, polarization tests were conducted on the MFCs in the third week. As discussed in section 3.7.3, polarization tests enable us to obtain important information about the performance of an MFC. The results of the polarization test are shown in Figure 32 and Figure 33.

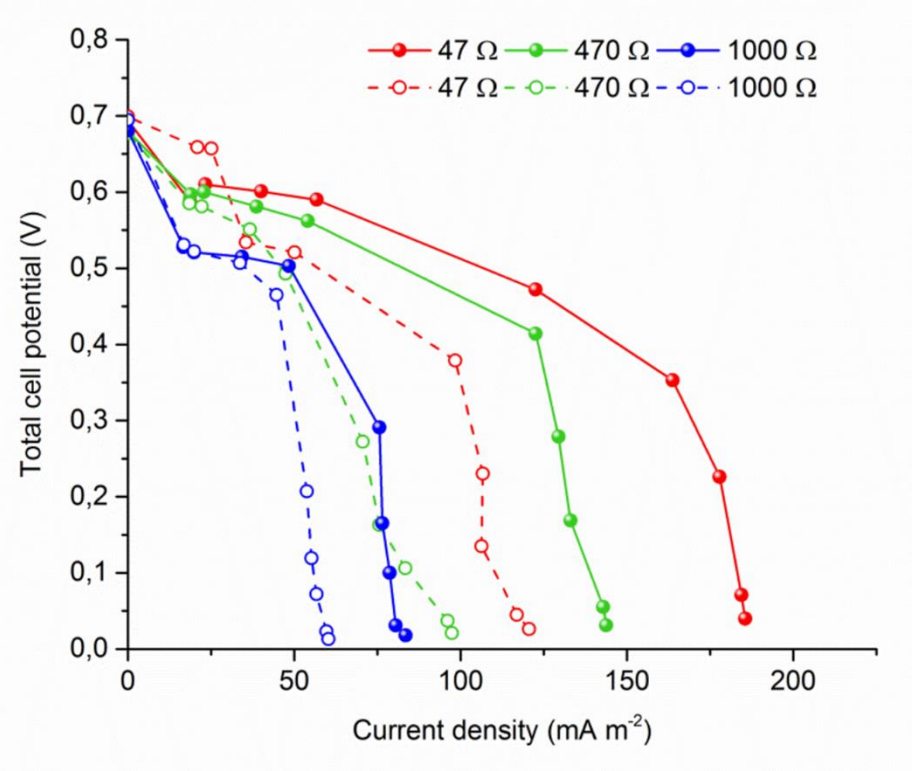

Figure 32: Polarization Plot.

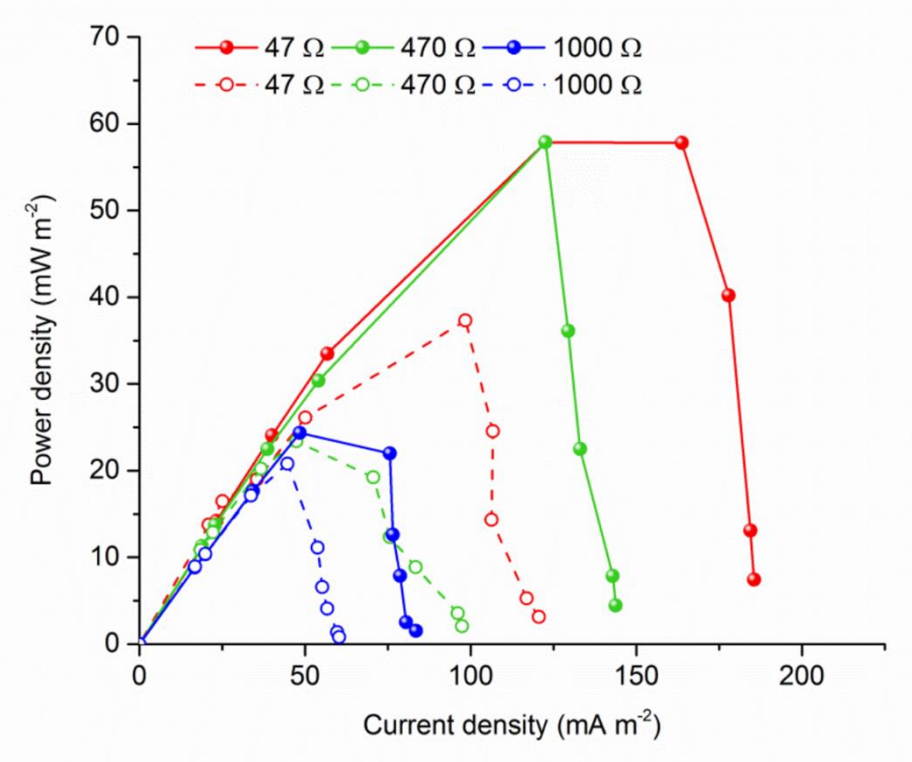

Figure 33: Power density plot.

In terms of performance related to current density and power density produced by an MFC, it is clear from Figure 32 and Figure 33 that the MFC under the lowest

external resistance (47 Ω) performed better than the rest. On the other hand, the MFC under the highest external resistance (1 kΩ) resulted in the worst performing MFC. This can be seen in both the polarization and power density plots. Moreover, the MFCs connected to the intermediate resistance, i.e. 470 Ω, exhibited performances in between the best and the worst cases.

Therefore, it can be concluded from the results that a lower external resistance, in the acclimation phase, enabled the MFCs to perform well in terms of the MPP and the maximum current density.

5.3.2 Enrichment Experiment

This part of the overall experiment dealt with the study on two different types of enrichment used i.e. GE and FeC. As discussed earlier, FeC enrichment was used to favor the selective growth of Dissimilatory metal-reducing bacteria (DMRB)[150,154]. Furthermore, Geobacter sulfurreducens and Shewanella oneidensis, which are the most widely used EABs in the field of MFCs, both are members of the DRMB group.

This part of the experiment was divided into a series of electrochemical characterizations. After the initial phase of sub-culturing, the GE and FeC enrichments were inoculated in MFCs. Since the MFCs used were double chamber, the inoculation was done in the anodic chamber. In this initial phase, the technique used to monitor the growth and development of the biofilm was the voltage monitoring. For this biofilm acclimation phase, the external resistance used was 47 Ω, which was chosen based on the results from section 5.3.1. Biofilms acclimated at lower resistances become robust in terms of current density and can maintain a good current generation even at higher voltages.

5.3.2.1 Voltage monitoring in the inoculation phase

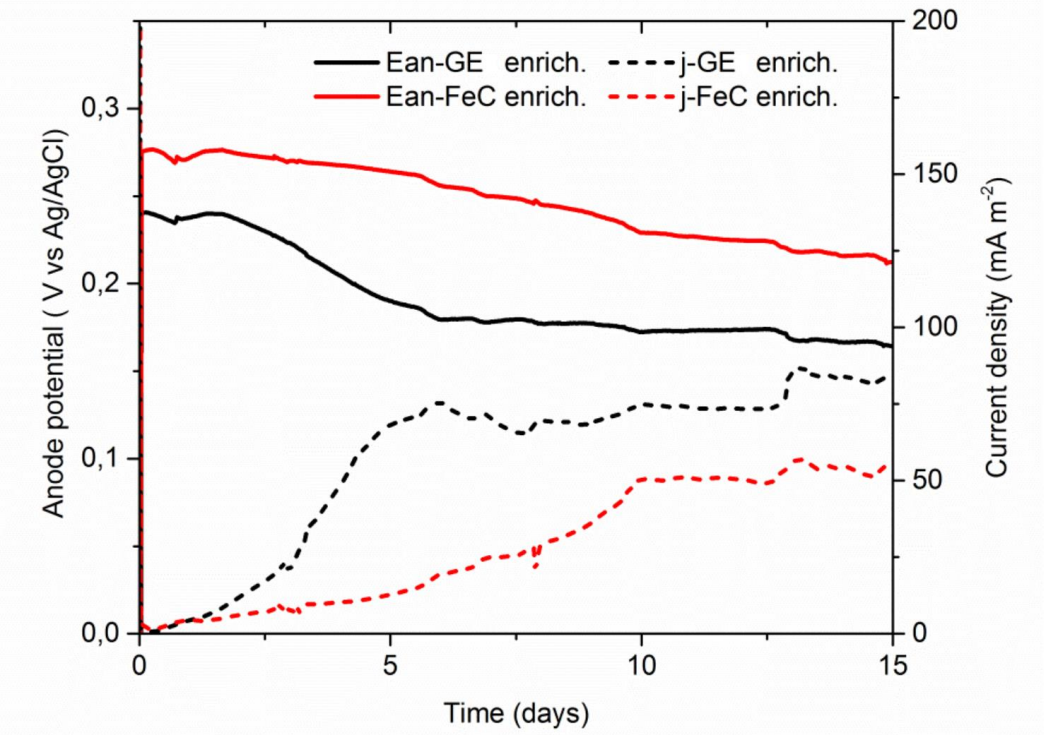

Figure 34: Voltage monitoring of the MFC inoculation phase of the two enrichments.

Figure 34 shows the results of voltage monitoring of the inoculation phase of the MFCs belonging to the two enrichments. The voltage results are again related to the half-cell voltage i.e. the voltage of the anode with respect to the reference. As it can be seen in, the low acclimation resistance produced an anode voltage that was positive. Furthermore, it can be noticed in Figure 34 that the time required, for startup, was larger for FeC enriched MFCs when compared to the GE enriched MFCs.

Table 8: Important parameters obtained through voltage monitoring in the inoculation phase.

Type of Enrichment	Start Up Time (Days)	Anode Voltage (V)	Steady State Current Density (mA/m²)
GE	5	0.173 ± 0.012	74 ± 4
FeC	10	0.224 ± 0.015	50 ± 3

FeC enriched MFC exhibited a lower current density in comparison with GE enriched MFC. This, in addition to the fact that the FeC enriched MFCs took a

longer time to startup, points to the relatively poor performance of the FeC enriched MFC in this initial phase of the experiment. One reason for this could be the fact that there might still be present a trace amount of Ferric citrate from the enrichment phase. The presence of Ferric citrate would introduce a competition between the anode and the Ferric citrate as electron acceptors form the bacterial metabolism and thus would reduce the number of electrons travelling to the anode and through the external load.

5.3.2.2 Polarization Test

After the MFCs completed the inoculation phase and were producing a stable current, the polarization tests were conducted. These tests were conducted by varying the value of the external resistance, moving from a high resistance towards a lower resistance. Every time a new resistance was imposed, each cell was allowed to stabilize before recording the value of voltage.

The results from the polarization tests are shown in Figure 35. It can be seen from the results that the GE-MFCs outperformed the FeC-MFCs. It can be seen from Figure 35 (a) that the MPP achieved by GE enrichment MFCs is almost twice as large as the MPP reached by FeC enrichment MFCs, as reported in Table 9. The MPPs, for both types of enrichment, corresponded to an external load of 1 kΩ. Furthermore, the current density plot in Figure 35 (a) shows a higher current density produced by GE enrichment MFCs relative to the FeC enrichment MFCs at low voltage.

Table 9: MPP parameters obtained.

Enrichment Type	MPP (mW/m^2)	Anode Voltage at MPP (V)
GE	79 ±12	-0.4 V
FeC	38 ± 2	-0.3 V

Moreover, it is important to underline that the MPP for FeC enriched MFCs and GE enriched MFCs did not occur at the same voltage, as represented in Figure 34 (b).

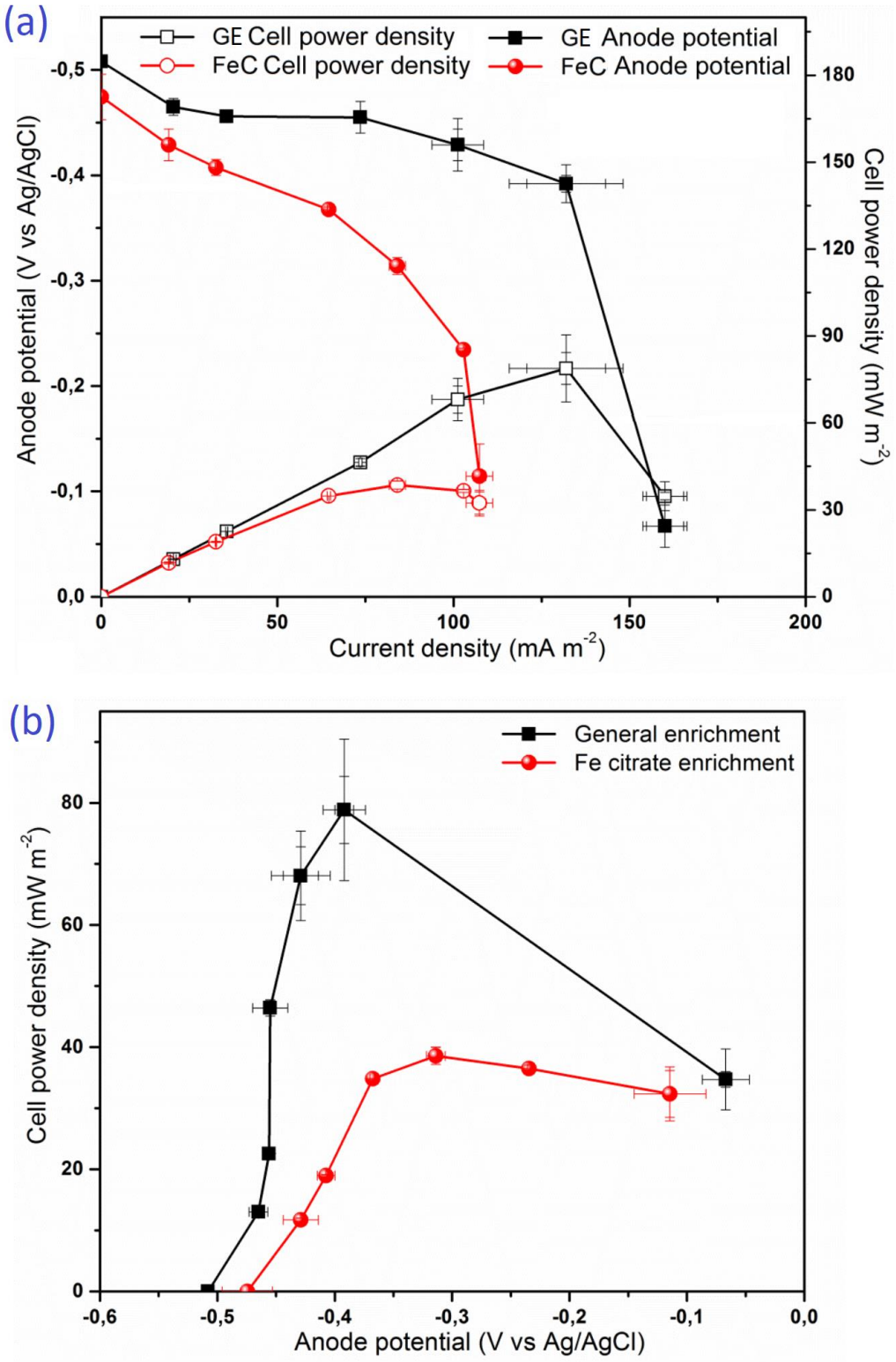

Figure 35: (a) Polarization plot with power density vs. current density. (b) Power density vs. anode voltage. Both plots represent the half cell anode voltage. The valuues that are ploted here are the mean values from dupliate MFCs with error bars shown.

Considering the results we obtained, the hypothesis of the work[154] performed by Sathish-Kumar and co-workers, which suggests that an iron based enrichment improves MFCs' performance, is negated. On the other hand, our results are in line

with those of Kim et al. and Pierra et al. where an inoculum enrichment with ferric citrate resulted in a relatively poor performing MFC when compared to an MFC enriched with the general procedure for anaerobic bacteria[157,150]. There can be multiple reasons for this result:

i. *Diversity of DMRB*. There are many different bacteria that are present in the DMRB group and not all of them have the ability to transport electrons to the extracellular matrix.
ii. *Inoculum Source Composition*. It is also possible that the source of our inoculum i.e. fresh water, did not present the possibility of a selective growth of DRMB group through iron-based enrichment.

Nevertheless, it is evident from the data collected during the polarization and voltage monitoring tests that the MFCs based on GE enrichment method performed better.

5.3.2.3 EIS

EIS was performed on the MFCs of both enrichments to understand better the different processes occurring on the anode electrode. Moreover, the scheme chosen for these experiments was to perform EIS on each of the polarization points. In this way, we also studied the impact of the polarization on the processes occurring inside the MFC. Therefore, for each MFC, EIS was performed at a total of 9 points in the polarization curve – OCV, 8.2 kΩ, 6.8 kΩ, 4.7 kΩ, 2.2 kΩ,1.5 kΩ, 1 kΩ, 0.68 kΩ and 0.33 kΩ. Another important fact to notice here is that the polarization was not performed through Linear Sweep Voltammetry (LSV) which uses a potentiostat to impose a potential across the cell. On the other hand, fixed loads were applied and the MFCs were left to stabilize on each potential before performing further characterizations. This approach minimizes external perturbations and improves EIS results as discussed in section 4.2. Figure 36 shows the Nyquist plots plotted using the EIS results.

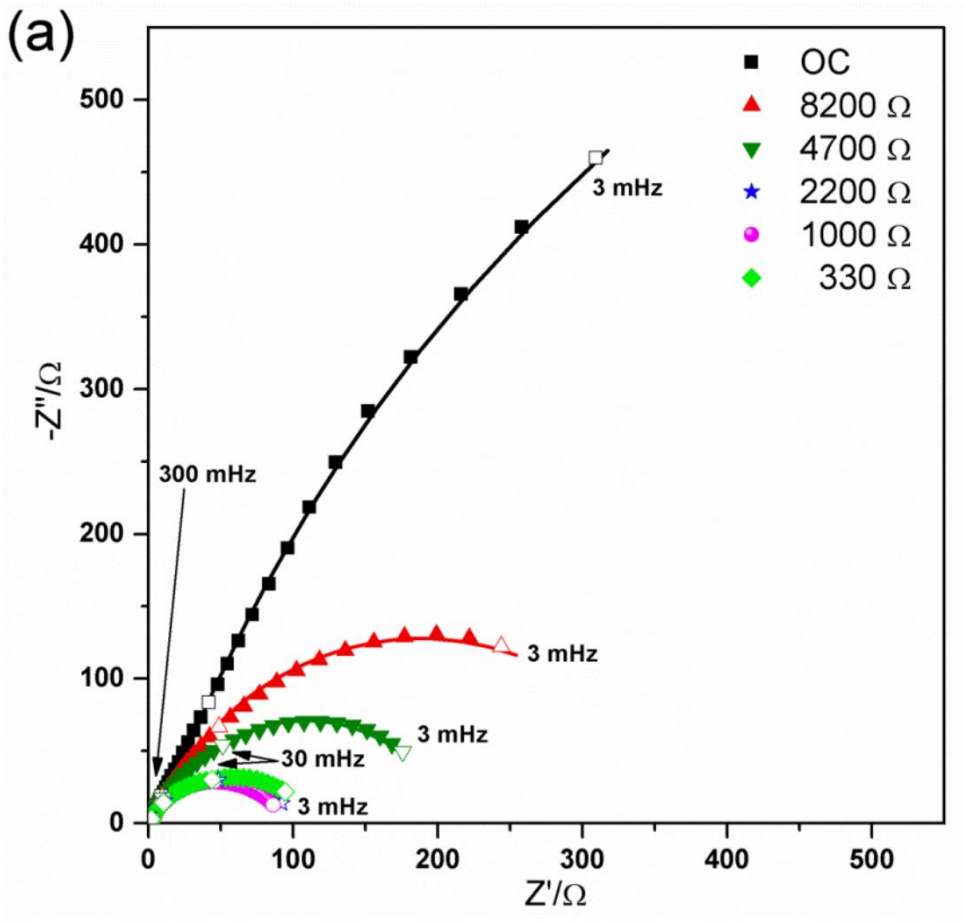
(a)
OC
8200 Ω
4700 Ω
2200 Ω
1000 Ω
330 Ω
3 mHz
300 mHz
3 mHz
3 mHz
30 mHz
3 mHz
-Z''/Ω
Z'/Ω
0
100
200
300
400
500

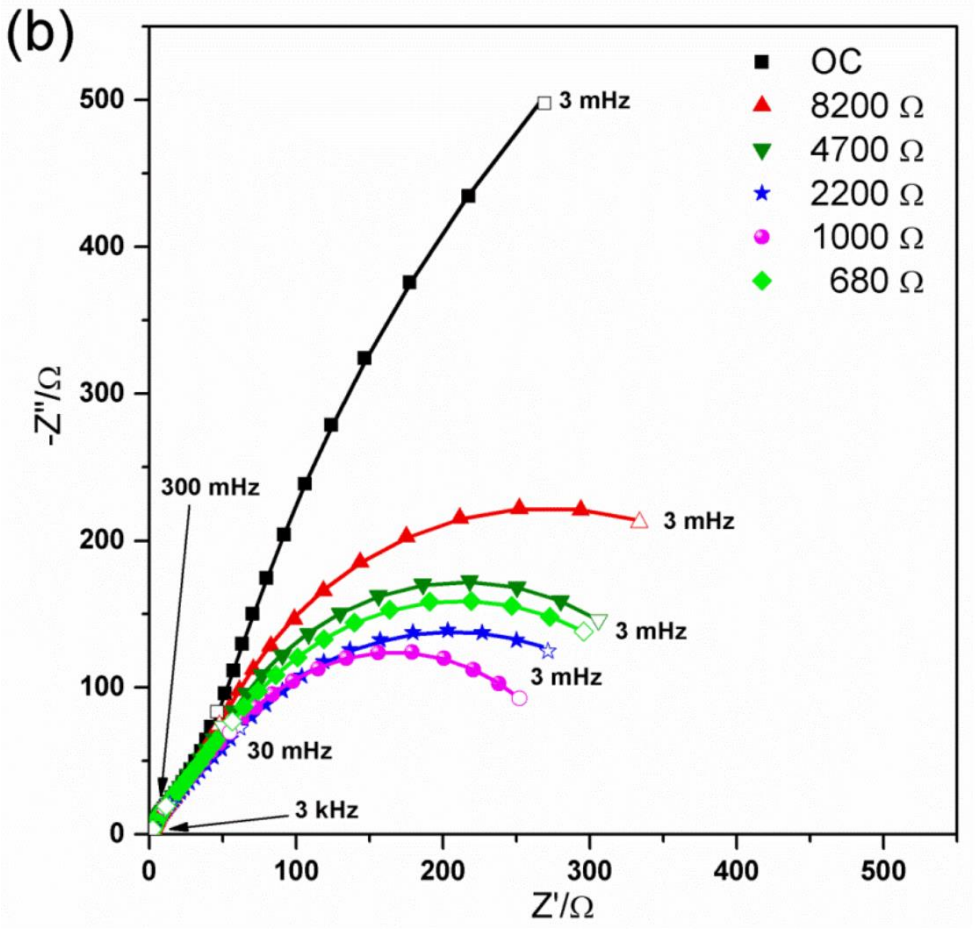
(b)
OC
8200 Ω
4700 Ω
2200 Ω
1000 Ω
680 Ω
3 mHz
300 mHz
3 mHz
3 mHz
3 mHz
30 mHz
3 kHz
-Z''/Ω
Z'/Ω
0
100
200
300
400
500

Figure 36: Nyquist plots: (a) GE enrichment based MFCs. (b) FeC enrichment based MFCs.

It is evident from Figure 36 that the polarization has a considerable impact on the impedance of an MFC. Even though, the impedance is measured between the anode and the reference, it has an impact on the overall cell. It is very interesting to notice that the impedance for MFCs from both types of enrichments decreases until 1 kΩ and then starts to increase again. This is the same point of the power density curve (1 kΩ) at which both the types of MFCs reached the MPP (Figure 35 (b)). The values of resistances calculated from the impedance data do not match the value of resistance connected externally to the MFCs. Therefore, the MPP achieved by these MFCs is not due to a matching of the internal and external resistance. On the other hand, we believe that the MPP is achieved due to the minimal internal resistance experienced by the anode side at this specific polarization. In other words, the polarization condition is optimal for the biofilm, which produces the electrical energy extracted from MFCs. It is important to understand that MFCs are based on biological microorganisms and are different from conventional fuel cells, for which the MPP is governed by the internal and external matching of resistance. On the contrary, for MFCs, it is more important to create optimal conditions for the biofilm so that they perform at their best.

Figure 36 (a) shows the results obtained for the GE enrichment based MFCs while Figure 36 (b) shows the results obtained from the FeC enrichment based MFCs. A clear difference, in the impedance, between the two types of cell is visible. GE enrichment based MFCs showed an impedance lower than the FeC enrichment based MFCs. This is in line with the results obtained from the polarization tests in which it was seen that the GE enrichment based MFCs outperformed FeC enrichment based MFCs. Furthermore, despite the fact that the maximum impedance (which is observed for the open circuit condition) is similar for both the types of MFCs, the minimum impedance observed for both the MFCs is quite different. For GE enrichment MFCs, it is quite lower relative to that of FeC enrichment based MFCs.

In the Nyquist plots shown in Figure 36, the points marked by different shapes are the experimental data obtained. On the other hand, the lines are plotted using the fitting results. Nyquist plots give information regarding the impedance spectra (about the imaginary and real parts of the impedance) but do not provide information about the frequencies at which these impedances were calculated. Due

to this reason, some frequencies such as the minimum and maximum frequencies are marked on the images for reference. But to better understand the relation of impedance with the frequency of applied signal, it is important to visualize the results using the Bode plots.

Figure 37 shows the Bode plot representation of the EIS data. The data plotted is for some selected points of the polarization. This is necessary to visualize and analyze the graphs properly without over-crowding them. Moreover, similar to Nyquist plots, the points represent the experimental data while the lines are obtained by fitting the EIS results.

It can be noticed that the data related to the frequency and magnitude are plotted using a logarithmic scale. The plot related to the phase of the system is of particular importance in a Bode plot. This is because, whenever a peak (or a change in the trend) is encountered in a Bode plot's phase part, it corresponds to the impedance due to a process occurring inside the system under study or is related to an impedance due to a particular interface. Furthermore, it can also be related to diffusion process. The frequency corresponding to this peak/change in phase trend gives the information about the time constant corresponding to the particular process or interface. From here on, a process and an interface are collectively referred to as 'process'. Moreover, if within this range more than one processes are contributing to the overall impedance, it is possible that one of the processes overshadows the effect of the rest and therefore hides the change related to them in the Bode plot.

The peaks related the processes occurring in the MFCs are visible in Figure 37. In particular there are two that can be noticed, one that is occurring around 1 Hz and the other occurring below 100 mHz. Moreover, the peaks are separated better in the open circuit condition for GE enrichment based MFCs (Figure 37 (a)) and overall in the FeC enrichment based MFCs (Figure 37 (b)). More information that can be extract just by looking at the Bode plots is knowing how 'fast' or 'slow' a process is in terms of its time constant. The peaks occurring towards lower frequencies corresponds to processes that are slower. Generally, the slower process is related to the diffusion process discussed in section 4.4. It can also be seen that the peak related to the slower process has a slight dependence on the polarization. On the contrary, the peak related to the faster process is not dependent on the polarization.

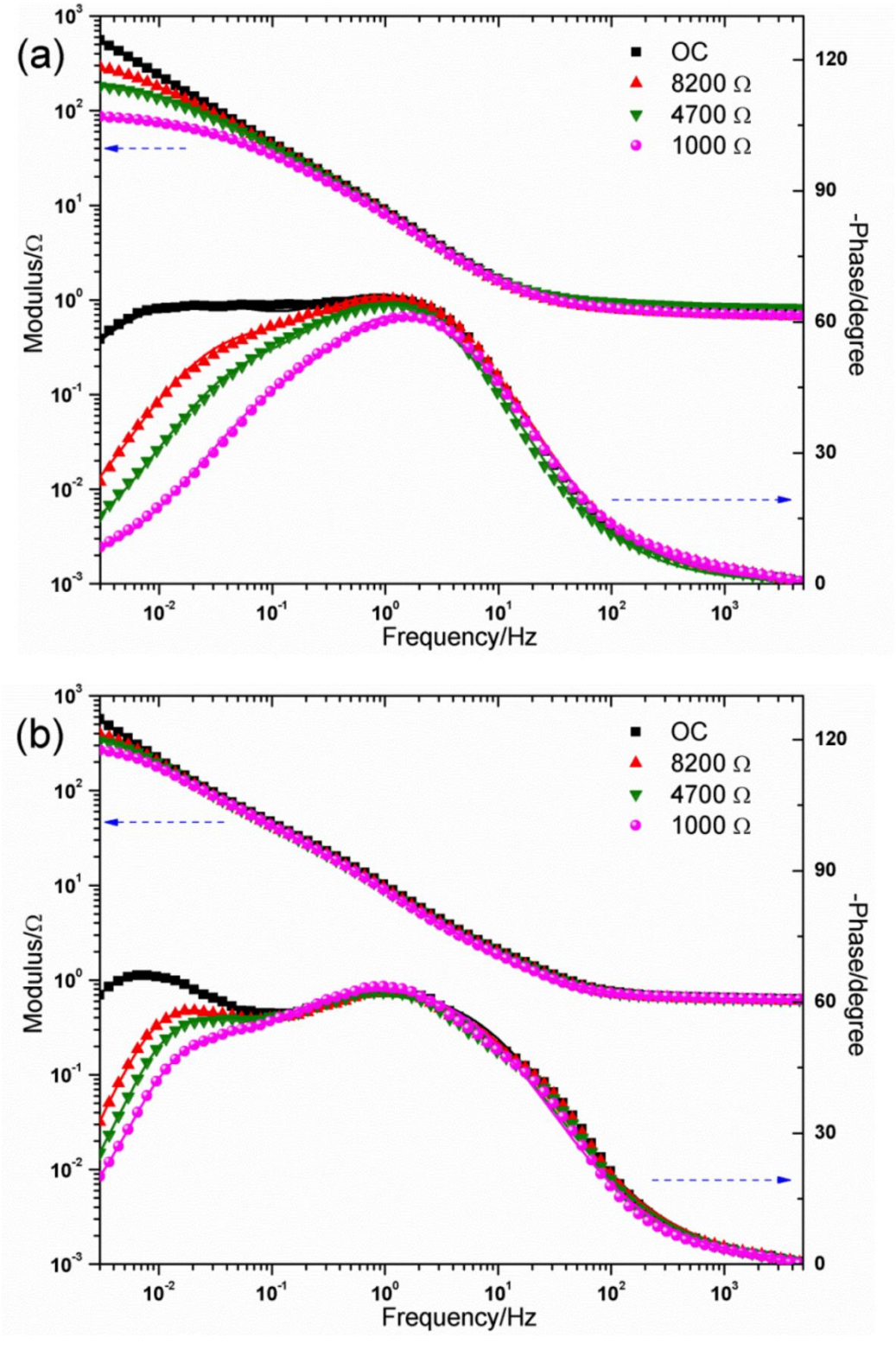

Figure 37: Bode plots: (a) GE enrichment based MFCs. (b) FeC enrichment based MFCs.

Impedance data were also collected for MFCs in non-turnover condition and with abiotic anodes. The results for the abiotic anode are shown in Figure 38.

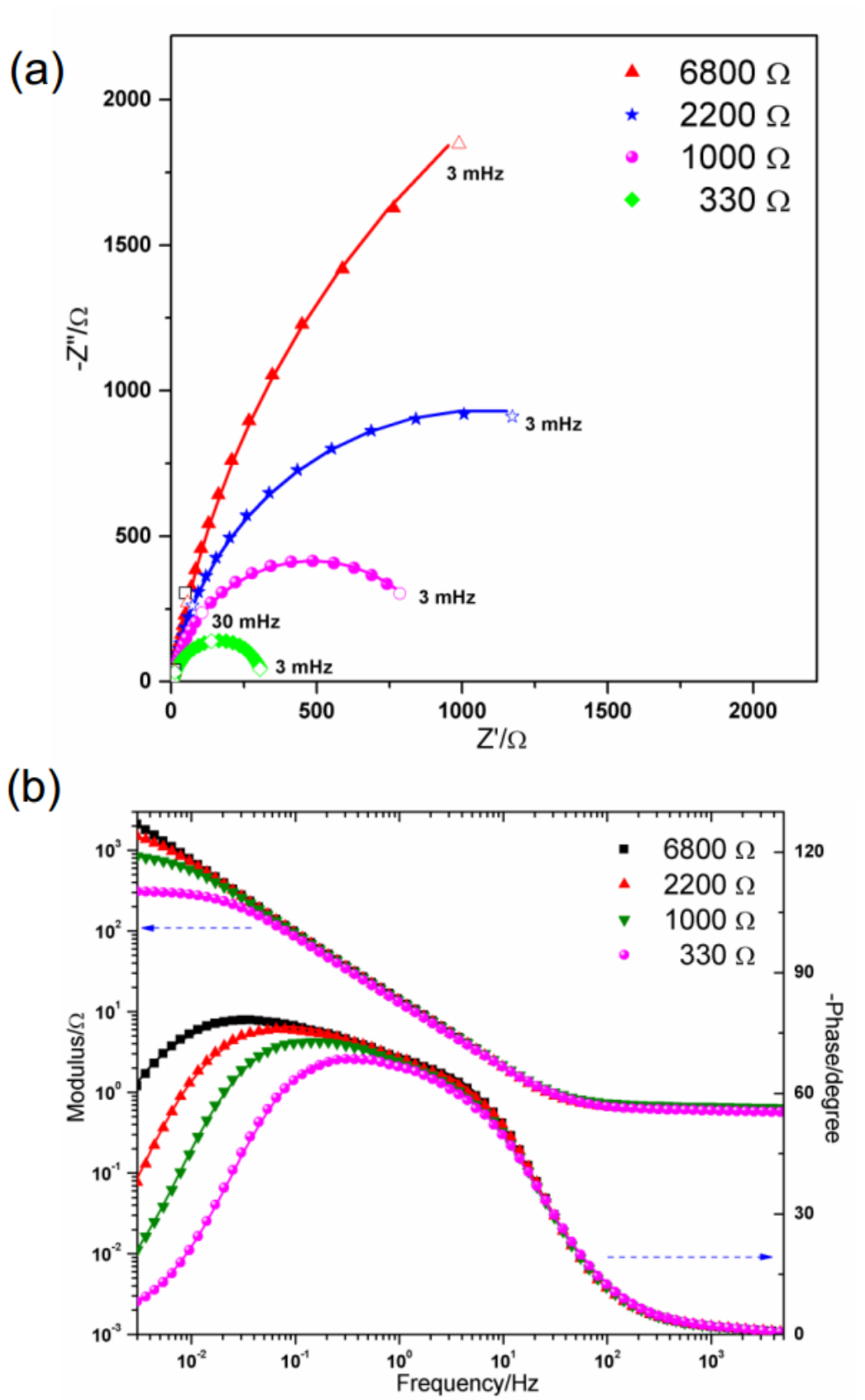

Figure 38: EIS results relating to the abiotic anode MFC: (a) Nyquist plot, (b) Bode plot.

It can be seen from Figure 38 (b) that the dependence of the slower process, on the polarization is stronger while the first process remains unaffected by the polarization

The two processes that are visible in the Bode plots refer to the charge transfer process and the diffusion process. Charge transfer process is the faster of the two process and refers to the charge transfer that is happening at the anode – electrolyte interface. It is important to keep in mind that all these tests were performed in a three-electrode configuration with the anode as the working electrode. Therefore, the results discuss the processes occurring at the anode side of the MFC. Moving on, the slower process represents the diffusion process, of the ionic species present in the electrolyte, that is occurring at the anode side. This also explains the dependence of the slower process on the polarization. A certain polarization that favors diffusion will result in a relatively faster diffusion process and vice versa. On the contrary, the charge transfer process at the anode – electrolyte interface is independent of the polarization since it is occurring in the vicinity of the anode electrode (in the nm scale) and takes no effect from the spatial polarization.

Bode plot and Nyquist plots are the graphical methods used to plot and visualize the impedance data. To extract more quantitative data related to the time constants and the values of equivalent electrical components that model the system, it is important to fit the EIS data.

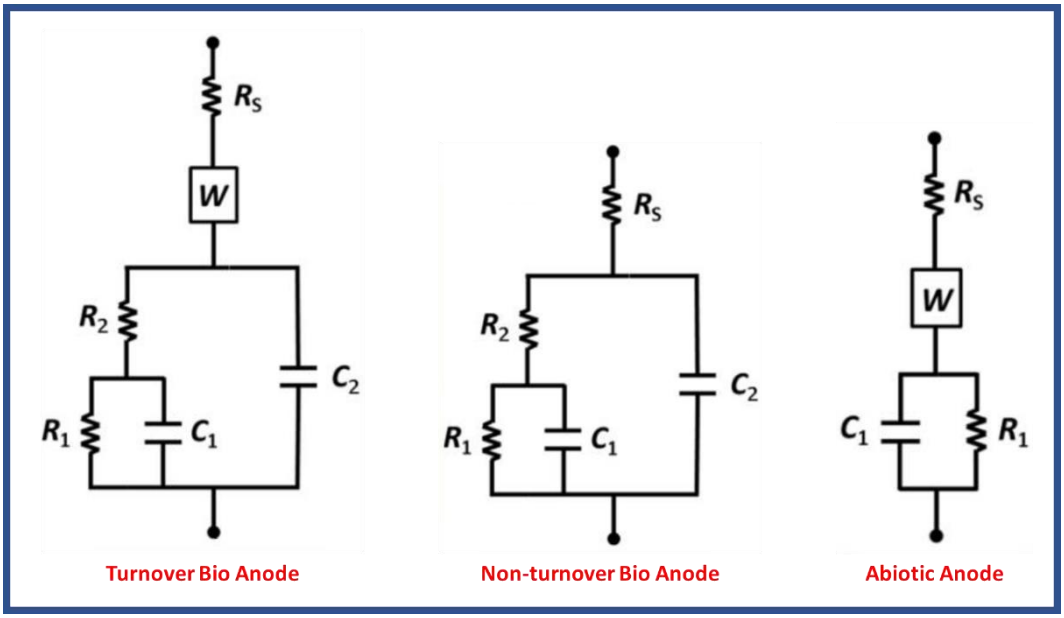

Figure 39: Fitting results.

Figure 39 shows the results that we obtained from fitting our EIS results in obtained under different conditions. It is important that the fitting results are carefully analyzed, and the elements present in the EEC model are properly associated with the underlying processes occurring in the MFC. Since this study is focused on the bioanode, the results all refer to the anodic side of the cell. Table 10 shows the proper interpretation of the elements obtained through fitting.

Table 10: EEC elements' association to Anodic half-cell processes.

Process	Element(s) related to the process
Series Resistance	R_S
Substrate Diffusion	W
Anode – Electrolyte Interface	R_1
	C_1
Biofilm	R_2
	C_2

It can be seen in Figure 39 that all the EEC models contain a resistance R_S, which is more commonly known as the series resistance. This resistance is due to the electrolyte solution and wired connections. Furthermore, the element W refers to the Warburg diffusion discussed in section 4.4. This is related to the diffusion of the substrate within the anodic half-cell. It is important to appreciate that the Warburg diffusion element is not present only in the non-turnover condition. This further strengthens the claim that it is related to the diffusion of the substrate. Moving on, the elements R_1 and C_1 are related to the charge transfer on anode – electrolyte interface. As evidence, it can be seen that these components are present in all different conditions of Figure 39, since in all of them this interface is present. Lastly, the elements R_2 and C_2 are related to the process introduced due to the presence of a biofilm. When a biofilm forms on the surface of the carbon felt which is used as the anode electron collector, it introduces a new interface which is in between the electrolyte and the electrode. This layer introduces capacitive effects due to the charge transfer between biofilm and the electrode. Moreover, it also introduces a double layer capacitance due to the charge accumulation. These two impedances cumulatively introduce the R_2 and C_2 elements in the EEC.

Confirmation of this hypothesis is given by the fact that the R_2 and C_2 elements are missing from the abiotic anode EEC.

Now that the processes related to the elements present in the EEC are appropriately associated, it is important to have a quantitative analysis of the values of these elements.

Table 11: Parameters obtained by fitting the EIS results of the GE enrichment based MFCs.

Polarization resistance (Ω)	GE enrichment Based MFCs								
	Anode – Electrolyte Process			*Biofilm Process*			*Diffusion of Substrate*		*Goodness of Fit*
	$R_1(\Omega)$	C_1(mF)	τ_1(s)	R_2 (Ω)	C_2(mF)	τ_2 (s)	$R_d(\Omega)$	τ_d(s)	$\chi^2(\cdot 10^{-5})$
OC	16.2	18.7	0.30	2861.0	128.7	368.34	8.1	3.88	6.03
8200	16.5	20.4	0.34	357.1	61.9	22.10	7.3	3.26	14.12
4700	13.9	20.2	0.28	177.0	62.2	11.01	7.1	3.22	2.93
2200	12.8	20.0	0.26	80.5	63.2	5.09	7.0	2.99	5.51
1000	11.0	20.6	0.23	75.7	63.0	4.76	6.8	2.77	5.90
330	9.9	21.3	0.21	100.2	98.8	9.88	7.9	3.39	3.70

Table 12: Parameters obtained by fitting the EIS results of the FeC enrichment based MFCs.

Polarization resistance (Ω)	FeC enrichment Based MFCs								
	Anode – Electrolyte Process			*Biofilm Process*			*Diffusion of Substrate*		*Goodness of Fit*
	$R_1(\Omega)$	C_1(mF)	τ_1(s)	R_2 (Ω)	C_2(mF)	τ_2 (s)	$R_d(\Omega)$	τ_d (s)	$\chi^2(\cdot 10^{-5})$
OC	46.3	26.1	1.21	3106.2	36.5	113.45	16.1	16.36	5.86
8200	40.9	27.4	1.12	500.9	28.4	14.25	15.5	15.95	8.88
4700	42.4	26.3	1.11	335.8	36.2	12.14	15.2	14.75	5.87
2200	45.9	25.0	1.15	295.0	46.4	13.67	14.4	12.56	2.66
1000	40.0	25.9	1.03	240.5	44.3	10.67	13.3	12.16	4.84
680	41.2	23.6	0.97	317.3	39.3	12.47	15.0	14.23	4.13

Table 13: Parameters obtained by fitting the EIS results of the MFCs with abiotic anode.

Polarization resistance (Ω)	MFC with Abiotic Anode					
	Anode – Electrolyte Process			*Diffusion of Substrate*		*Goodness of Fit*
	$R_1(\Omega)$	C_1(mF)	τ_1(s)	$R_d(\Omega)$	τ_d (s)	$\chi^2(\cdot 10^{-5})$
6800	19.37	11	0.22	9800	16.10	2.54
2200	19.33	11	0.22	2404	11.74	2.18
1000	20.81	11	0.22	1007	7.82	1.15
330	18.94	12	0.23	323	4.07	2.45

Table 11 and Table 12 present the parameters that were calculated using the EIS data's fitting results for the GE enrichment based MFCs and the FeC enrichment based MFCs, respectively. Furthermore, Table 13 displays the results obtained from EIS data's fitting of the MFC with an abiotic anode. These tables

show the values for capacitance and resistance for different processes and calculates the time constants as well. In reality, the EEC were not obtained through capacitors but through CPEs[118,158]. CPEs are discussed in section 4.4. To obtain the equivalent values of capacitance form the CPE's parameters, equation (43)[159] can be used.

$$C = Q^{\frac{1}{n}} \times R^{\frac{1}{n}-1} \tag{43}$$

Where Q is the CPE's pre-factor and n is the index of CPE. Furthermore, to obtain the time constant τ, the following equation can be used:

$$\tau = R \times C = (R \times Q)^{\frac{1}{n}} \tag{44}$$

In the case of Table 13, which represents the fitting results of an abiotic MFC, it can be seen that the anode – electrolyte interface is not dependent on the polarization. Both the values of capacitance and resistance remain consistent. On the other hand, the diffusion process reported in Table 13, which is represented by the parameters R_d and τ_d is has a significant amount of dependence on the value of the external resistance. Table 11 and Table 12 represent the parameters calculated from the EEC of MFCs based on GE enrichment and FeC enrichment, respectively. It is evident from looking at the tables that the fastest process for the MFC anodes is the process pertaining to anode – electrolyte interface. Moreover, the values of the time constants do not change as the polarization changes. Furthermore, the values of this first process remain almost the same in all conditions i.e. abiotic, non-turnover and turnover conditions. To confirm this visually, a Bode plot of the EIS was constructed at 1 kΩ (which refers to the MPP). This plot is presented in Figure 40.

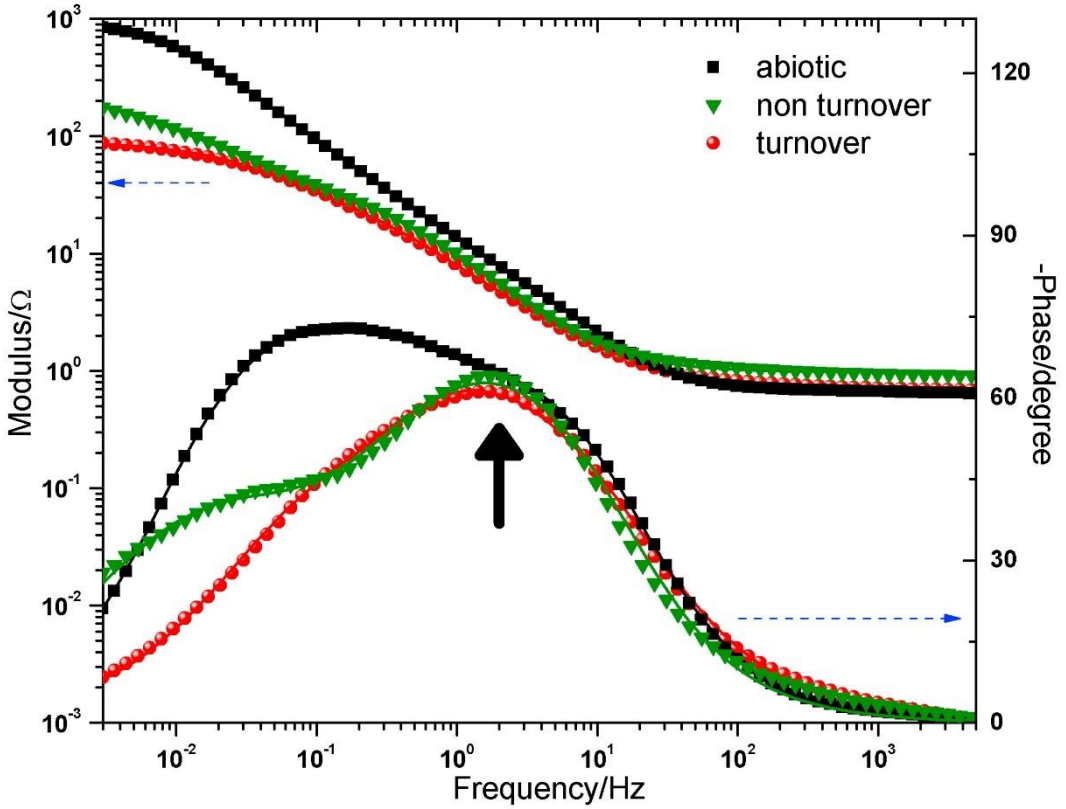

Figure 40: A comparison of the first process seen under 3 different conditions - abiotic, non-turnover and turnover. The arrow points to the peak which is related to the first process.

In Figure 40, the arrow points to the peak that is related to the anode – electrolyte interface process. This process is comprised of a double layer capacitance and the charge transfer resistance. The double layer capacitance is in the order of tens of millifarads, which is quite high. This is due to the fact that we used carbon felt as the electrode which a highly porous material thus resulting in a large double layer capacitance[159,160].

Moving on with the analyses of the parameters obtained, the slower charge transfer process represented in both Table 11 and Table 12 is the process due to the biofilm. As it can be seen from Figure 39, a new process is introduced in all the EECs related to MFCs with a bio anode. This is due to the fact that an additional interface – the biofilm, has formed on the carbon felt. The parameters calculated, relating to this process are also listed in Table 11 and Table 12. Apart from the fact that this is the slower amongst the two charge transfer processes, it is also dependent on the polarization of the MFC. Especially, the charge transfer resistances of this process are dependent on the polarization while the dual layer capacitance associated with this process remains more or less the same for all values of polarization and in both types of enrichments. Furthermore, another interesting fact

to notice here is that the change transfer resistances, R_2, for this process kept decreasing until the polarization at which the MPP occurred (1 kΩ) and increased again when the external resistance was reduced further. Therefore, it confirms the hypothesis that the MPP is achieved due to an optimally functioning biofilm rather than a matching of the external and internal resistance. Furthermore, similar to the faster charge transfer process, this slower charge transfer process also exhibited relatively large double layer capacitances. This again is due to the fact that the biofilm grew on the porous carbon felt.

Lastly, the process related to the diffusion of substrate is also listed in Table 11 and Table 12. The parameters of this process are extracted from the Warburg element shown in the EECs of Figure 39. This process is related to the diffusion of sodium acetate towards the biofilm and of the products of the metabolic process (HCO^{3-} and H^{+}) away from the biofilm. A further confirmation of this hypothesis is the absence of this process in the EEC of non-turnover condition in Figure 39, for which there is no substrate present in the MFC. The time constant related to the diffusion process falls in the same range of the charge transfer of the biofilm which has a large capacitance. It is due to this that the effect of the diffusion process is not visually apparent as a third process in the bode plots of Figure 37. The biofilm charge transfer process has 'masked' the diffusion process in the graphical representations. Nonetheless, with the help of fitting, we were able to extract important data relating to the diffusion process. Moreover, the diffusion process of Table 11 and Table 12 show no co-relation with the polarization condition of the MFCs. It is also important to compare the two enrichment types that were used for this experiment – GE and FeC in terms of the parameters obtained through EIS and fitting (Table 11 and Table 12). It is evident from the data that GE enrichment based MFCs performed better than FeC enrichment based MFCs having lower resistances for all the respective processes. Furthermore, GE enrichment based MFCs also exhibited faster processes than those of FeC enrichment based MFCs. Quantitatively, the diffusion time constants for GE enrichment based MFCs were 4 times smaller those of FeC enrichment based MFCs. This can be explained by the fact that the two enrichments produced biofilms that were different in terms of population, composition and structure. Since GE enrichment based MFCs performed better, it can be inferred that they had a more active biofilm which therefore created a stronger diffusion gradient for the substrate. This resulted in a

faster diffusion process of the substrate in the case of GE enrichment based MFCs. Similarly, for the biofilm charge transfer process, GE enrichment based MFCs exhibited a time constant which was faster than that of FeC enrichment based MFCs. Especially, the biofilm process time constant at MPP for GE enrichment based MFCs was about two times faster than that of FeC enrichment based MFCs. This superior performance in terms of the time constant, related to the biofilm process, at MPP is in line with the relative superior performance of GE enrichment based MFCs shown in the results of polarization tests (section 5.3.2.2). Furthermore, the dual layer capacitance values related to the biofilm charge transfer process are also quite different. For GE enrichment based MFCs they fall in the range of 1.6 – 3.3 mF/cm^2 while in the case of FeC enrichment based MFCs, they are in the range 0.7 – 1.2 mF/cm^2. This confirms the hypothesis that the biofilms formed as a result of the two enrichments were different in terms of structure and electrical performance. Lastly, as expected, the dual layer capacitance related to the anode – electrolyte interface remained more or less the same for MFCs of both enrichments. This is because this interface is very similar for both the MFCs i.e. the interface between the anodic medium and the carbon felt (anode). On the other hand, the charge transfer resistance for this process was lower for GE enrichment based MFCs than the FeC enrichment based MFCs.

5.3.2.4 CV

Figure 41 shows the voltammograms that were obtained through CV of MFC based on both the enrichments. Part (a) of the figure, relating to the GE enrichment based MFCs, shows a shape that is sigmoidal catalytic. This usually belongs to the acetate oxidation by bacteria in which electrons are transferred in a conduction-based manner[161–164]. The figure also shows sigmoidal function's first derivative. This first derivative is a curve that has peak which can be used to detect a mechanism of charge transfer involved in the production of current. Looking at the insert of Figure 41 (a) it can be noticed that the site responsible for the putative electron transfer has a center at -0.4V versus Ag/AgCl which is very close to the potential of G. sulfurreducens' cytochromes of the outer membrane (0.190 V vs SHE equivalent to −0.387 V vs Ag/AgCl)[165].

As for the FeC enrichment based MFCs, the voltammograms are shown in Figure 41. These voltammograms demonstrate the occurrence of a redox system

which has an oxidation peak centered at -0.115 V versus Ag/AgCl and a reduction peak centered at -0.315 V versus Ag/AgCl having a midpoint potential, E^f which is equal to -0.215 V versus Ag/AgCl. This E^f is the same as what is found for phenazines which act as shuttles carrying charges and are produced by a variety of microorganisms[165]. Pyocyanin is one of the most popular phenazine in research and is produced by Pseudomonas spp. In previous studies, Pyocyanin has been identified on carbon electrodes which are submerged in aqueous solutions[166,167]. These results that point towards a condition which is not in steady-state in terms of the rates of the two processes – electron transfer and diffusion. These results comply with the results obtained through the analysis of EIS data, i.e. for FeC enrichment based MFCs the time constant for the charge transfer process related to the biofilm was smaller than the constant of the diffusion process. In contrast, GE enrichment based MFCs exhibited a slower charge transfer process related to the biofilm with respect to the time constant for the diffusion process which allowed a steady state condition. Therefore, resulting in a voltammogram that is shaped like a sigmoid. The non-turnover voltammogram of the MFCs from both the types of enrichment are also plotted in Figure 41. It is evident from these voltammograms that in the condition when there is an absence of the substrate, the catalytic wave is not present. This further confirms that the catalytic wave in turnover condition belongs to the metabolism of acetate that the microorganisms perform.

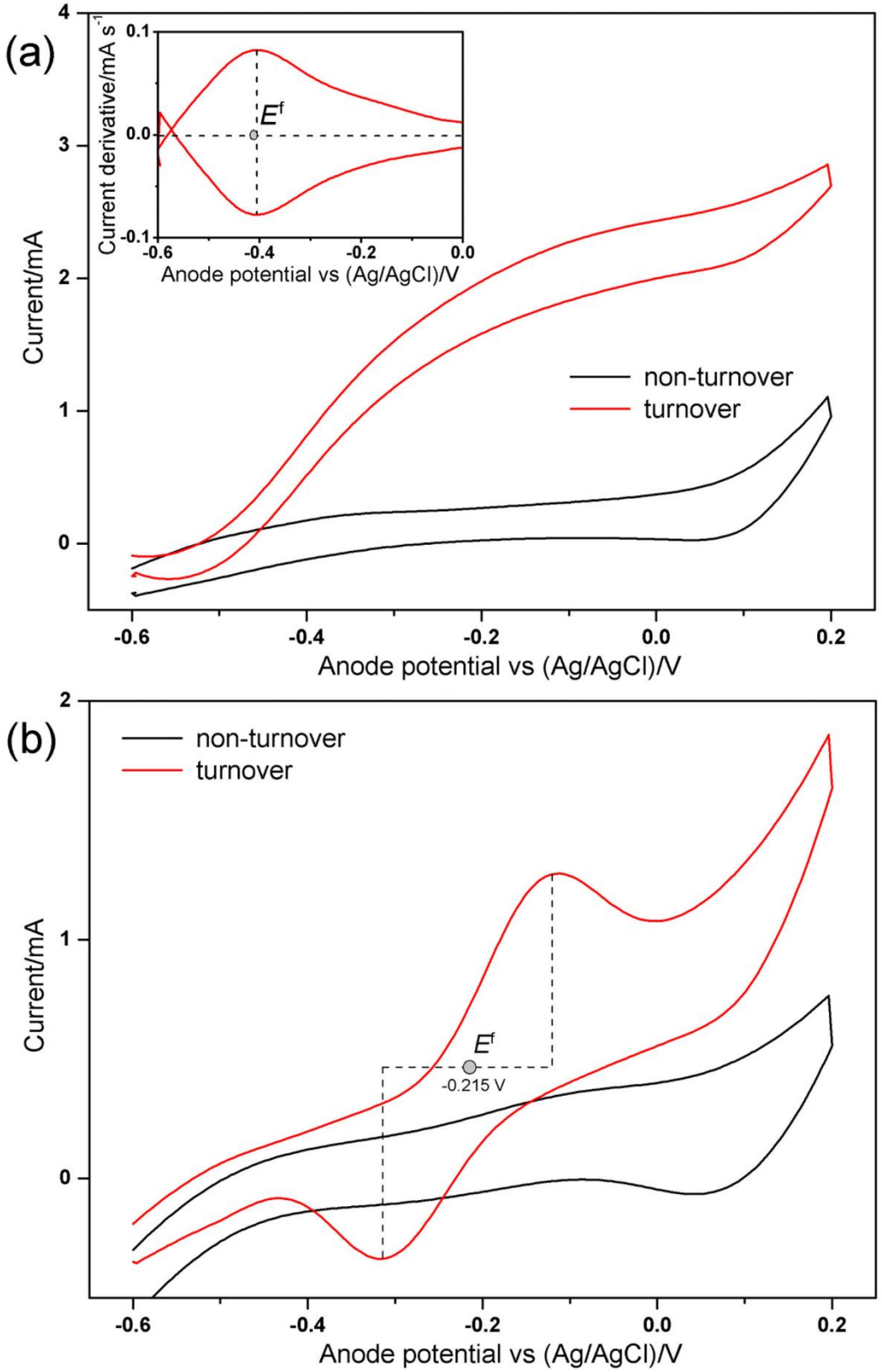

Figure 41: Cyclic voltammograms (both turnover and non-turnover): (a) General-enriched biofilm. First derivative of the turnover CV is also shown, where E^f indicates the putative electron transfer site centered at −0.4 V. (b) FeC-enriched biofilm. E^f centered at −0.215 V indicates the arithmetic average of the oxidation and reduction peaks.

5.3.2.5 The use of Butler-Volmer-Monod model in the analysis of electrochemical kinetics

To better understand the biofilms based on the two enrichment, we performed an analysis of polarization curves using the Butler-Volmer-Monod (BVM) model[9]. This enabled us to get a better understanding of the electrochemical kinetics and gives information about the metabolic process that enables the oxidation of substrate through Monod general enzyme kinetics and also about the transfer of electrons to the anode from bacteria, using the Butler-Volmer relationship. Equation (45) gives the current density obtained using the BVM model[168].

$$I = I_{MAX}\frac{1 - e^{-\left(\frac{F}{RT}\right)\eta}}{K_1 e^{-\left(\frac{(1-\alpha)F}{RT}\right)\eta} + K_2 e^{-\left(\frac{F}{RT}\right)\eta} + \left(\frac{K_M}{S} + 1\right)} \qquad (45)$$

Table lists all the elements present in equation (45):

Table 14: Definition of elements for equation (45).

Equation Element	Definition
F	Faraday constant
R	Gas Constant
α	Transfer co-efficient
η	Anodic Overpotential
K_M	Michaelis–Menten constant (substrate affinity constant)
S	Concentration of substrate
T	Absolute temperature
I_{MAX}	Maximum current density obtainable
K_1 & K_2	These are the parameters related to kinetics

The results obtained by using this BVM model to fit the experimental data are plotted in Figure 42. The value of the transfer co-efficient, α calculated for using this model was 0.5 (GE enrichment based MFCs) and 0.78 (FeC enrichment based MFCs). This is in line with the values that are generally obtained for bio-electrochemical reactions (in the range of 0.4 to 0.8)[169,170]. As for the parameter K_1, the obtained result for GE enrichment based MFCs was 0 which points to an

electron transfer process which is very fast (relative to the oxidation of substrate). In contrast, the K_1 value obtained for FeC enrichment based MFCs was 2.3 which points to a less efficient process of electron transfer. Therefore, these results are consistent with the results obtained from CV and EIS in which it was found that GE enrichment based MFCs exhibited a more efficient process of electron transfer. Lastly, the values obtained for K_2 are: 10.5 (GE) and 20.2 (FeC) which are consistent with the results found for bacteria that metabolize organic matter for survival[168].

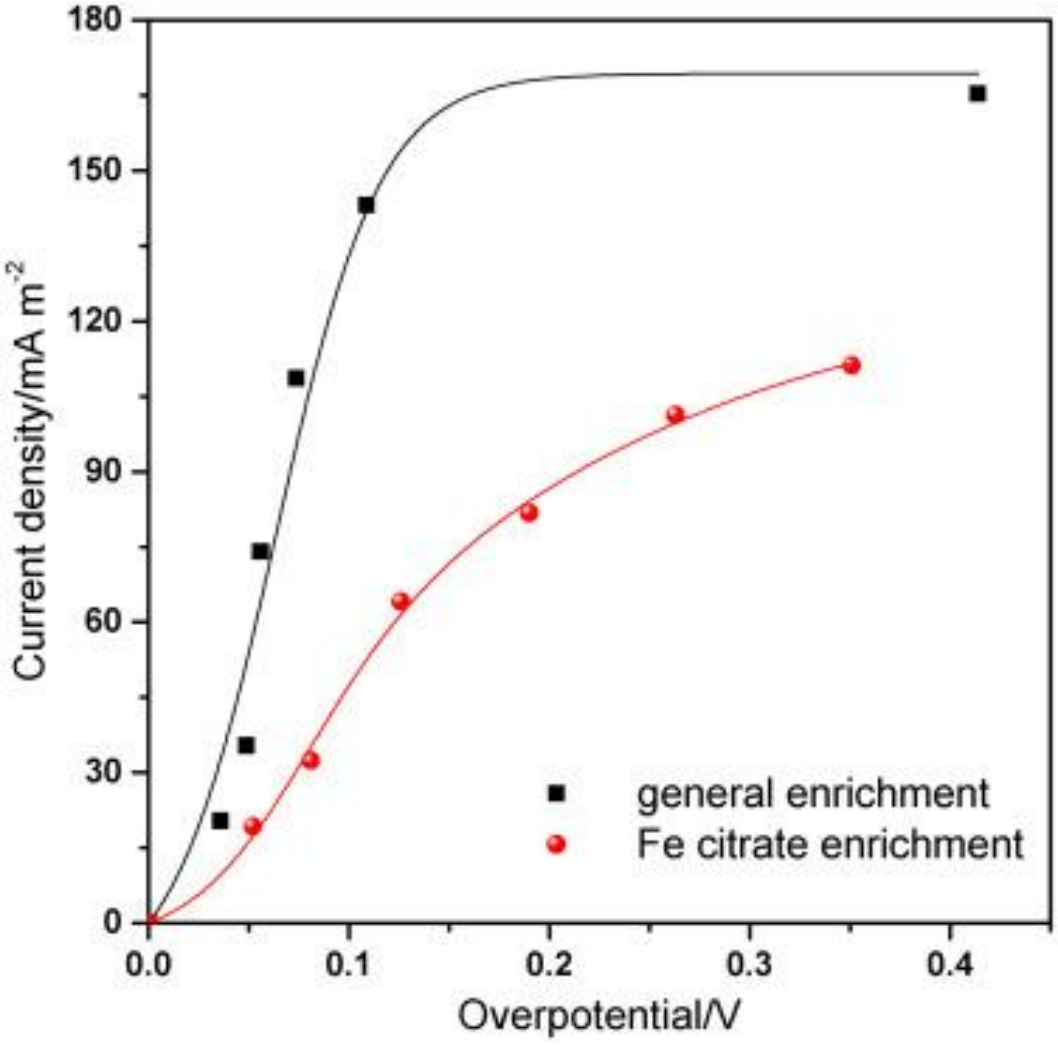

Figure 42: Polarization curves of the two bioanodes from the two different enrichments and their relative fitting using the Butler-Volmer-Monod model.

5.3.2.6 Bioanode Imaging

To have a visual representation of the biofilm that had formed in the two types of MFCs, imaging of the anodes was performed using the procedure described in section 5.2.2. This helped us in analyzing the distribution, density and heterogeneity of the formed biofilms.

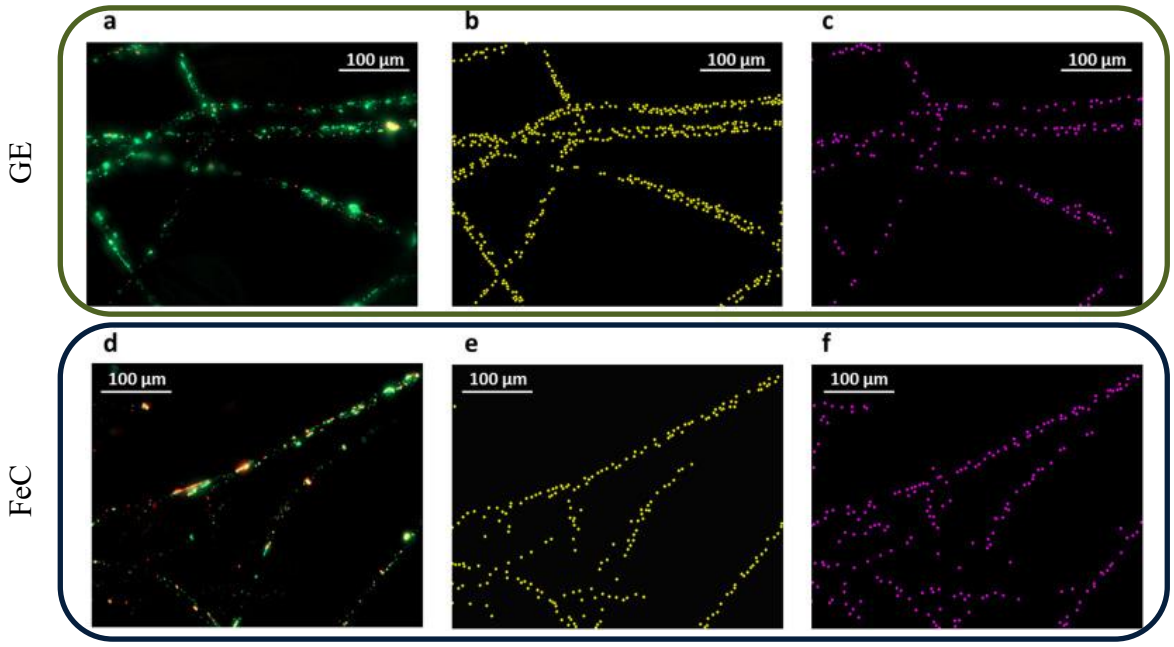

Figure 43: Biofilm fluorescence imaging of live/dead staining. (a) Gen-enriched biofilm, Max Intensity Projection (MaxIP) merge of green (live organisms) and red (dead organisms) channels. (b) Automated spot count relative to green channel. (c) Automated spot count relative to red channel. (d) FeC-enriched biofilm, MaxIP merge of green and red channels. (e) Automated spot count relative to green channel. (f) Automated spot count relative to red channel.

Figure 43 shows the results obtained from the imaging. It can be seen that the biofilms were not able to produce a dense mat on top of the carbon felt therefore, the calculation of the thickness of the biofilm was not possible. Nevertheless, the way the bacteria colonized the 3D structure of the anode was seen using multiple z-stacks for the entire thickness of the anode material (500 µm). Using the z-stacks, it was found that in the GE enrichment based MFCs, the biofilm almost completely penetrated the depth of the anode, 428 µm ± 31. In contrast, the biofilm of the FeC enrichment based MFCs was only able to occupy the anode to a depth of 325 µm ± 38. Moreover, using the imaging technique, a live (green dot)/dead (red dot) was also performed. The ratio between the living and dead bacteria (living:dead) was found out to be 2.9 ± 0.5 for the MFCs based on GE enrichment. On the contrary, for MFCs based on FeC enrichment, the ratio was found out to be 1.4 ± 0.4. Both

obtained results allowed to confirm that GE enrichment based MFCs showed a better formation of the biofilm. Furthermore, the higher charge transfer resistances seen in the FeC enrichment based MFCs' anode – electrolyte process in Table 12 can be explained by the fact that the FeC enrichment based MFC had a lower live/dead ratio thus having a larger resistance towards the anode – electrolyte process.

5.4 Conclusion

In this work, a complete electrochemical analysis was performed on the anodes of two different types of MFCs (different in terms of the enrichment method used) which had bacteria coming from a mixed community. Furthermore, the EIS data obtained was fitted through the EEC and to acquire the relevant electric parameters. The results indicated the presence of the different electrochemical processes within the anodic chamber: anode-electrolyte interface process, biofilm process and diffusion of substrate process. This impedance data was collected for all the polarization points thus revealing the relationship between the processes and the external polarization condition. For both types of enrichments, the MPP from the polarization test coincided with the minimum internal impedance calculated through EIS. Furthermore, in terms of performance, charge transfer process and the diffusion process, GE enrichment based MFCs dominated the FeC enrichment based MFCs. Delving into deeper details, FeC enrichment based MFCs had a slower diffusion rate, higher resistance and lower capacitance related to the biofilm process and a higher resistance for the anode – electrolyte interface process. Further evaluations such as a kinetics analysis, bioanode imaging and CV all confirmed the results obtained through EIS. To conclude, the GE enrichment-based bio anodes performed better and had a more efficient charge transfer process when compared to the FeC enrichment based bioanodes.

6 Moving Towards an in-situ Practical Application of MFCs as Power Sources

MFCs have a potential to be used as power sources for sensors used in remote places such as a marine environment. Such sensors commonly need to transmit data only a couple of times a day to monitor the quality of sea water or of the environment. Therefore, the low power output that the MFCs provide is not an issue. Power extracted throughout the day can be used to record and transmit data once or twice a day. In such a location the ideal type of MFC to be used is known as the sedimentary microbial fuel cell (sMFC). The setup of an sMFC has been discussed in detail in section 3.5. As expected, many works in the literature have proposed their use as remote power sources for a sustainable and clean source of energy. Nonetheless, the setups proposed are too big and immobile and therefore cannot be used when mobility and compact size are necessary. In this work we designed and studied a new, small, mobile and inexpensive architecture of an MFC, which was setup as a floating device. Furthermore, for the biofilm formation and development phase we conducted experiments to compare a biofilm formed in the lab and one that was formed in-situ i.e. in the real marine environment. The biofilm formed in-situ proved to be robust and showed a good level of stability in terms of electricity production even though the environment was not a controlled one like a scientific laboratory. Part of this chapter, relating to the experiments, results and discussions are also issued in an article published in Applied Energy:

Massaglia, G., Margaria, V., Sacco, A., Tommasi, T., Pentassuglia, S., Ahmed, D., Mo, R., Pirri, C.F. and Quaglio, M., 2018. In situ continuous current production from marine floating microbial fuel cells. Applied Energy, 230, pp.78-85.

6.1 Introduction

As discussed in the previous chapters, MFCs have the potential to be used as devices that provide electrical energy by metabolizing organic substrates[171,172]. Furthermore, they can also be used to treat waste water reducing the expenses incurred in waste water treatment while producing energy[17,22,37,62]. On the other hand, MFCs can be used in the sMFC configuration to provide a sustainable source of green energy to systems that require energy in the remote marine environment. The most exciting feature of the SMFC technology is their ability to use the organic substrates already present in the sediment and seawater to produce electrons. This produced electrical energy can then be harvested through a PMS, providing power to a system, such as a sensor, which monitors seawater health. In addition, these devices have minimal maintenance needs and costs and can keep on working for extended periods of time. Nonetheless, there are also some disadvantages that are associated with sMFCs. Firstly, sMFCs generally produce relatively lower voltages. Secondly, the ohmic losses experienced by the sMFCs are larger due to the increased dimensions. Lastly, the oxygen availability at the cathode is low due to the limited oxygen absorption into the water[173]. Furthermore, sMFCs also lack in terms of a stable voltage output[25].

Mostly, sMFCs that have been employed for practical applications in the oceans have a large size[174,175]. For example, an array of sMFCs which was 30 meters in length, was used by Arias-Thode and co-workers to provide electrical energy to a sensors that is used to sense passing ships known as a magnetometer[176].

Considering the size requirements and other limitations related to an sMFC, a variation of the sMFC has been anticipated recently which is known as floating MFC (fMFC). These new types of MFCs have been proposed for use in marine environments[177] and also in waste water[178]. fMFCs float near the surface of the water with the cathode directly exposed to the air while, the anode is present in the underlying water. This not only enables the availability of more oxygen on the cathode but also ensures that the overall losses in terms of ohmic resistance are reduced.

Figure 44: A floating MFC setup used by Martinucci et al. [177] This image is re-printed with permission from Elsevier 2015©.

All the works related to fMFCs up till now employ setups that are fixed and are not free to move on the surface of the water. For this reason, their applications are limited. In the present work, the main aim was to develop a floating MFC system that could enable the device to be portable while having compact dimensions. Portability is an important pre-requisite in many applications such as sensors etc. For this purpose, we used small scale MFCs in the single chamber configuration. These MFCs can produce electrical energy in a continuous manner using the organic matter present in sea water as their substrate for metabolism. Furthermore, the seawater acts as an electrolyte for the MFC. Another important aspect of the study is that we have compared the development and colonization of biofilm in-situ with the development and colonization of the biofilm using the standard enrichment approach conducted in a laboratory. By enabling the development of biofilm in-situ we also explored the use of aquatic biological environment as catalyst for biofilm

formation. Furthermore, we used a synthetic solid-state electrolyte (SSE), proposed recently by our group[179], which is based on agar to increase the metabolism of the bacteria in the biofilm during the startup phase. This SSE contained nitrogen and organic resources to boost the growth of biofilm. Apart from providing important nutrients the SSE, also acts as a physical layer between the O_2 from the cathode side and the anode one, maintaining thus the required anerobic condition on the anode. Air-cathode MFCs usually are equipped with a Pt/C catalyst layer on the cathode, which is expensive but improves the performance of an MFC. For this experiment, we did not use a catalyst layer on the cathode but allowed the unprompted formation of a biofilm (aerobic) on the cathode able to reduce oxygen. This has been explored previously by other groups as well[180]. The devices were setup and tested in a real marine environment (La Spezia bay, northern Italy) by using a data acquisition and transmission system and also in laboratory. Furthermore, the in-situ experiments were performed two times (in summers and winters) to study changes in performance due to the weather and temperature.

6.2 Experiment Structure

6.2.1 Scheme of experiment

The work performed for this experiment was divided into a series of experiments to have a complete analysis of the proposed approach with the one generally used in the laboratories. Furthermore, for this experiment two main kind of MFCs were setup for comparison:

i. *is-MFCs*. MFCs based on a novel enrichment method for the biofilm formation on the anodes. This enrichment method is explained in section 6.2.2.1.
ii. *st-MFCs*. MFCs based on anodic electrodes which used the general enrichment approach which was explained in section 5.2.2.

The two types of MFCs i.e. is-MFCs and st-MFCs were set up in the laboratory and monitored, in the laboratory, using a voltage monitoring system (with fixed load) and their performances were compared. Furthermore, EIS was also performed on the two types of MFCs. Both types of MFCs showed similar results in terms of

performance. Consequently, for further tests, is-MFCs were used. It is important to specify that is-MFCs did not consume any energy, effort and reagents for their enrichment process which is common for st-MFCs. For the purpose of subsequent experiments, six different MFCs were setup using in-situ colonized electrodes. Once these MFCs were setup, they were mounted on a floating system so that they could be deployed in a real marine environment for power production and monitoring. Two main campaigns were carried out for in-situ performance monitoring:

i. Summer Campaign
ii. Winter/Autumn Campaign

The summer campaign (which used all 6 MFCs) was carried out for a period of 58 days. On the other hand, the winter/autumn campaign (which used 4 out of the 6 initially prepared MFCs) went on for 45 days. During these campaigns, a fixed external resistance was used as the load and the voltage was monitored through a data acquisition and transmission system for acquiring data to be used in performance analysis. In between the two campaigns, the devices were moved to our laboratories from La Spezia bay.

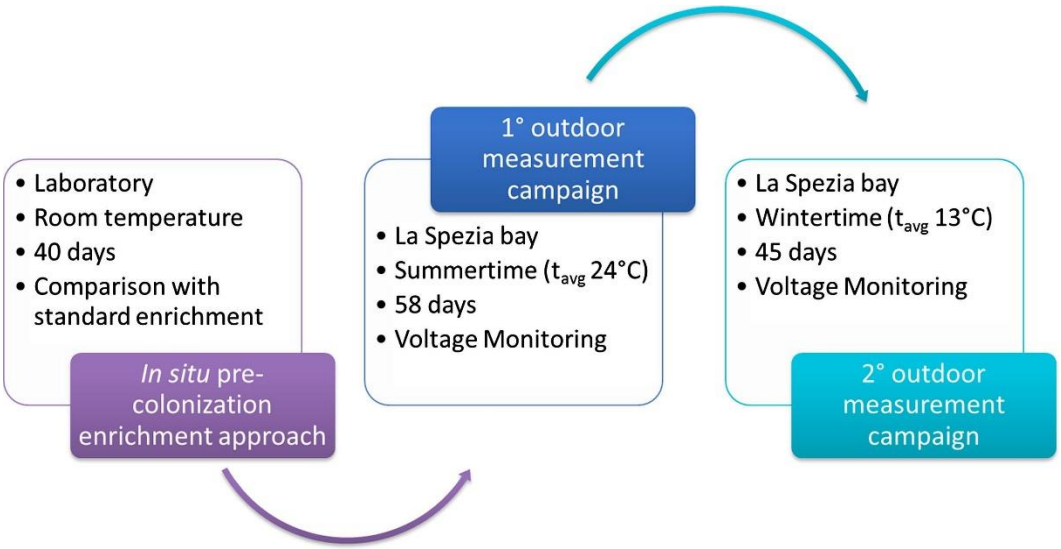

Figure 45: Highlights of the overall in-situ experiment. This image is re-printed with permission from Elsevier 2018©.

6.2.2 The two enrichment procedures explained

As discussed earlier, the work started with developing anodic biofilms using two different methods of enrichments. This section describes the two techniques

used. The resulting anodes from these enrichment methods were compared in terms of power production over an extended period. This was done by monitoring the voltage produced by the MFCs with an external resistance attached. It should be noted that all reagents used in this experiment were bought from Sigma-Aldrich unless specified otherwise and no purification steps were taken for the reagents.

6.2.2.1 In-situ pre-colonization enrichment

In this enrichment technique, the biofilm was allowed to form directly on the carbon felt (Soft felt SIGRATHERM GFA5, SGL Carbon) which was later used as the anodes of the MFCs. To maximize the formation of biofilm, the carbon felt was initially immersed in PBS which contained sodium acetate having a concentration of 2.5 g/L. Then, the carbon felt was placed in-situ i.e. in the sediment 3 meters under water, for the process of biofilm formation. This was done in the La Spezia bay (northern Italy).

6.2.2.2 Standard pre-colonization enrichment

In the case of the standard method, carbon felt (same as the one used for in-situ method) was placed inside bottles containing seawater sediment sample which was enriched in 250mL serum. The fluid inside the bottle comprised of seawater with the following compounds dissolved in it:

i. Ammonium Chloride (5.8 mM with concentration 0.75 g/L) as a source of nitrogen
ii. Sodium Acetate (30 mM with concentration 2.5 g/L) as a source of carbon

The above-mentioned compounds were added to enhance the formation of biofilm on the surface of the anode. A total of three enrichments were performed over a period of one month for the purpose of sub culturing. Throughout this period, the microbial cultures were placed under a gentle orbital shaking at 150 rpm at room temperature (21 ± 2°C). Lastly, at each step of enrichment, fresh media was used to inoculate 10% (v/v) of microbial cultures.

6.2.3 MFC setup

The structure of the MFC used in this experiment was made using a 3-D printer, OBJET 30 by Stratasys. Polymethyl-methacrylate (PMMA), a material which is polymeric and UV-curable, was used to print these MFCs. The material used for both the cathode and anode was the same – carbon felt. Both the anode and the cathode had a nominal geometric area of 5.76 cm^2. In the case of cathodes, additional layers of polytetrafluoroethylene were added to assist in oxygen diffusion. A total of four layers were applied on the external part of the cathode. The reactor had a volume of 12.5 ml. Furthermore, titanium wires were used as current collectors and were threaded into the electrodes to establish an electrical connection. For the addition of SSE to each anode's surface, 6 ml of the SSE at around 50 °C (in liquid form) was transferred onto a petri dish and left to solidify. Once in solid state, it was broken down into smaller pieces. Lastly, these pieces were placed on the surface of the anode.

6.2.4 Experiments conducted in Laboratory

For the experiments conducted in the laboratory, triplets (nominally identical) of MFCs pertaining to each type of enrichment method (standard and in-situ) for the biofilm were made. All the devices were immersed inside a container full of seawater. The placement was done in such a manner that the cathodes of each device were exposed to air, while the anodes remained submerged in seawater. The devices were kept at room temperature condition i.e. 21 ± 2 °C. To maintain the level of seawater in the container, seawater was replenished on weekly basis and apart from this no other nutrients or fluids were added during the whole experiments. Each MFC was connected to a 560 Ω resistor and the voltage across the MFC was measured using a multi-channel data acquisition system – Agilent 34972A. The voltages across the MFCs were recorded for a period of 40 days. Following the voltage monitoring campaign, impedance measurements were performed using a potentiostat – VSP Biologic. The parameters used for EIS are listed in Table 15.

Table 15: Parameters used for EIS.

EIS Parameters	
Frequency Range	20 Khz – 10 mHz
Signal Amplitude	10 mV
Configuration	2-electrode (Anode – Working Electrode, Cathode – Counter Electrode)

The EIS measurements were conducted with the external resistance of 560 Ω connected to the MFCs.

6.2.5 Experiments conducted in-situ

For the tests performed in-situ, a floating system that could support the MFCs was designed. This floating system was placed in the water 2 meters away from the wharf and anchored there. This location was in the Mediterranean Sea near the La Spezia bay. Figure 46 shows an overall sketch of the system and the actual pictures taken of the system being deployed.

In order to collect the voltage production data of the cells and to monitor their performance, a cable (Igus CF9.02.12, multipolar) was employed. On one end, this cable was connected to the respective anodes and cathodes. While on the other end, it was connected to the data acquisition system (a schematic of which is also shown in Figure 46 (a) which was present in the control room. The data acquisition system consisted of a Raspberry Pi which acts as a portable mini-computer, in conjunction with a relay board which is programable (Devantech ETH8020). There were 8 channels on this data acquisition board with the possibility of introducing different resistances to the MFCs as loads by programing the relay board. Once the voltage data was received through the relay board, the Raspberry Pi (acting as the control board) converted these signals to digital values through an on-board analog to digital converter. Lastly, a modem (connected to the Raspberry Pi) was used to transmit the data collected so that it could be accessed remotely. To perform the

data acquisition and transmission, control the overall operation and to program the relay board remotely using the internet, a custom software was developed and deployed on the Raspberry Pi. On the floating MFC side, the multiple wires inside the cable were connected to the titanium current collectors of the cathodes and anodes of respective MFCs. For the purpose of providing an insulation for the connections on the fMFCs side, a thermosetting resin was applied.

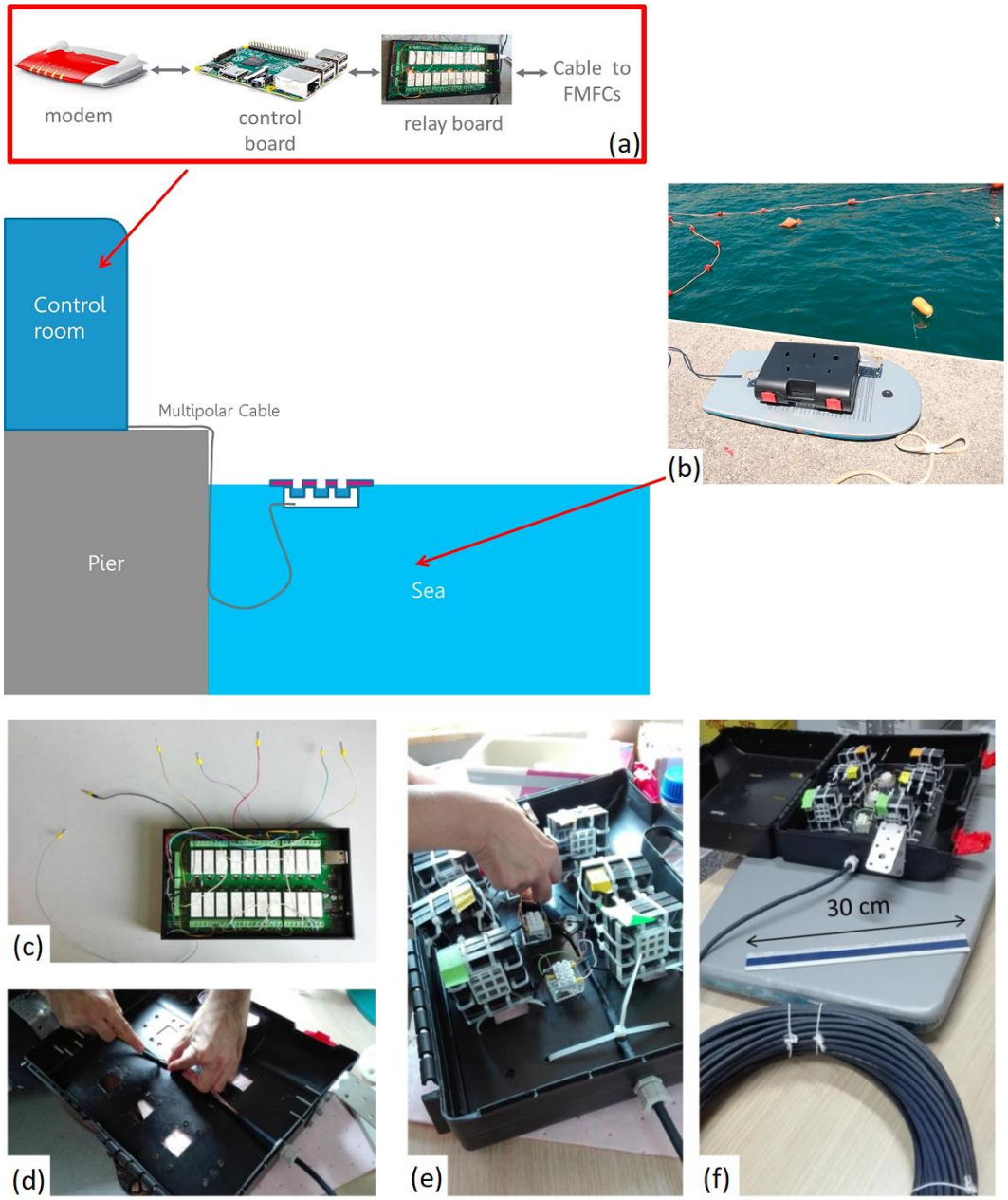

Figure 46: Scheme of the in-situ experiments: (a) data acquisition system; (b) floating housing system (bottom view); (c) Programable relay board; (d) fMFC housing; (e) Inside view of the fMFC housing with the MFCs being attached; (f) Complete setup with the multipolar cable (bottom of sub image) and the floating panel (grey). This image is adapted with permission from Elsevier 2018©.

A total of two voltage monitoring campaigns were conducted for the in-situ experiments. For the first campaign (summer), a total of six MFCs that were

nominally identical were used and this campaign lasted for 58 days (22nd July 2016 to 18th September 2016). All of these MFCs were kept under a load of 560 Ω. Throughout the period of the campaign, the voltage was monitored using the data acquisition system and recorded. After the completion of this period, the MFCs were transferred to our laboratory and were kept submerged in seawater. During this period, the voltages were monitored using a commercial data acquisition system by Agilent (34972A). The second campaign (winter/autumn) began on 1st December 2016 and went on for 45 days until 15th January 2017. In contrast to the first campaign, only four out of the six original MFCs were used. All the four MFCs were kept under a load of 560 Ω throughout the experiment and the voltages were monitored using the data acquisition system.

Furthermore, important parameters related to the seawater, such as pH, salinity, temperature etc., were monitored using Geoves SMx-485 meter.

6.3 Results and Discussion

6.3.1 Experiments Conducted in Laboratory

Initial part of the experiment was related to the comparison of different enrichment approaches for the pre-colonization and preparation of anode. One of the two techniques compared was based on the standard enrichment method. The second enrichment was performed based on an in-situ approach. For each approach, three nominally identical MFCs were set up and the performance of these MFCs was recorded using voltage monitoring with an external resistance attached. These results are displayed in Figure 47.

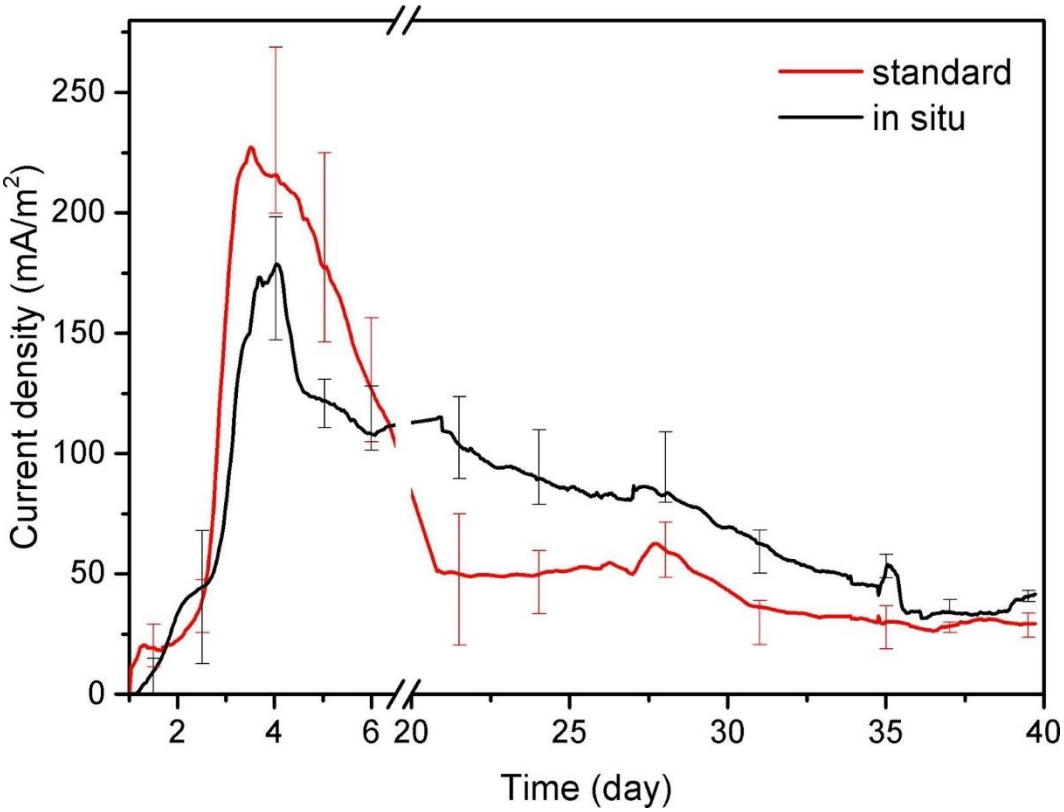

Figure 47: Average current densities vs. time obtained from three (for each enrichment type) nominally identical MFCs based on in-situ and standard enrichment techniques. Error bars are also reported. The discontinuity between days 7 to 20 was due to an electrical malfunction. This image is re-printed with permission from Elsevier 2018©.

It can be seen from Figure 47 that both is-MFCs and st-MFCs showed an initial increase in the production of power in the first four days. The maximum values of power density achieved by the two types of MFCs are presented in Table 16.

Table 16: Maximum Average Power Densities for the two types of enrichments.

MFC	Maximum Average Power Density (mW/m^2)
is-MFCs	10 ± 3
st-MFCs	18 ± 2

This increase in the current density in the start, followed by a decrease after day 4 in both the types of MFCs, can be ascribed to the SSE which was present on the anodes. The SSE is comprised of organic and nitrogenous sources which have proven to improve the metabolism of EABs[181]. Therefore, in the first few days with the presence of these sources, the MFCs' performance improved but as the sources were depleted, the MFCs' power production also started to decrease. The only remaining source of nutrition, after this point, to support bacterial metabolism were

the substrates present in seawater which had a concentration much lower than that in SSE. Furthermore, it can also be seen in Figure 47 that the is-MFCs showed a better average performance in terms of current density than that of st-MFCs after day six. Another important point to notice here is that the data in between day 6 and day 20 is missing. This was due to an electrical failure of the data acquisition system. This behavior of the is-MFCs can be attributed to the fact that the bio anodes of these MFCs were developed in the environment that these voltage monitoring experiments were conducted. Therefore, even in the earlier stages, these MFCs were more adapt to a seawater medium than the st-MFCs. On the other hand, st-MFCs needed some time to get acclimated to the seawater medium as their primary source of organic compounds and nutrition. As it can be seen from Figure 47, after a period of about 35 days, both types of MFCs exhibited similar and stable current density. The values of current densities were 40 mA/m^2 and 33 mA/m^2 for is-MFCs and st-MFCs respectively. These values of current densities correspond to a power density in the range of 1 mW/m^2.

The results obtained from EIS are also in line with the voltage monitoring results. The Nyquist plots obtained using EIS data on the two types of MFCs are shown in Figure 48.

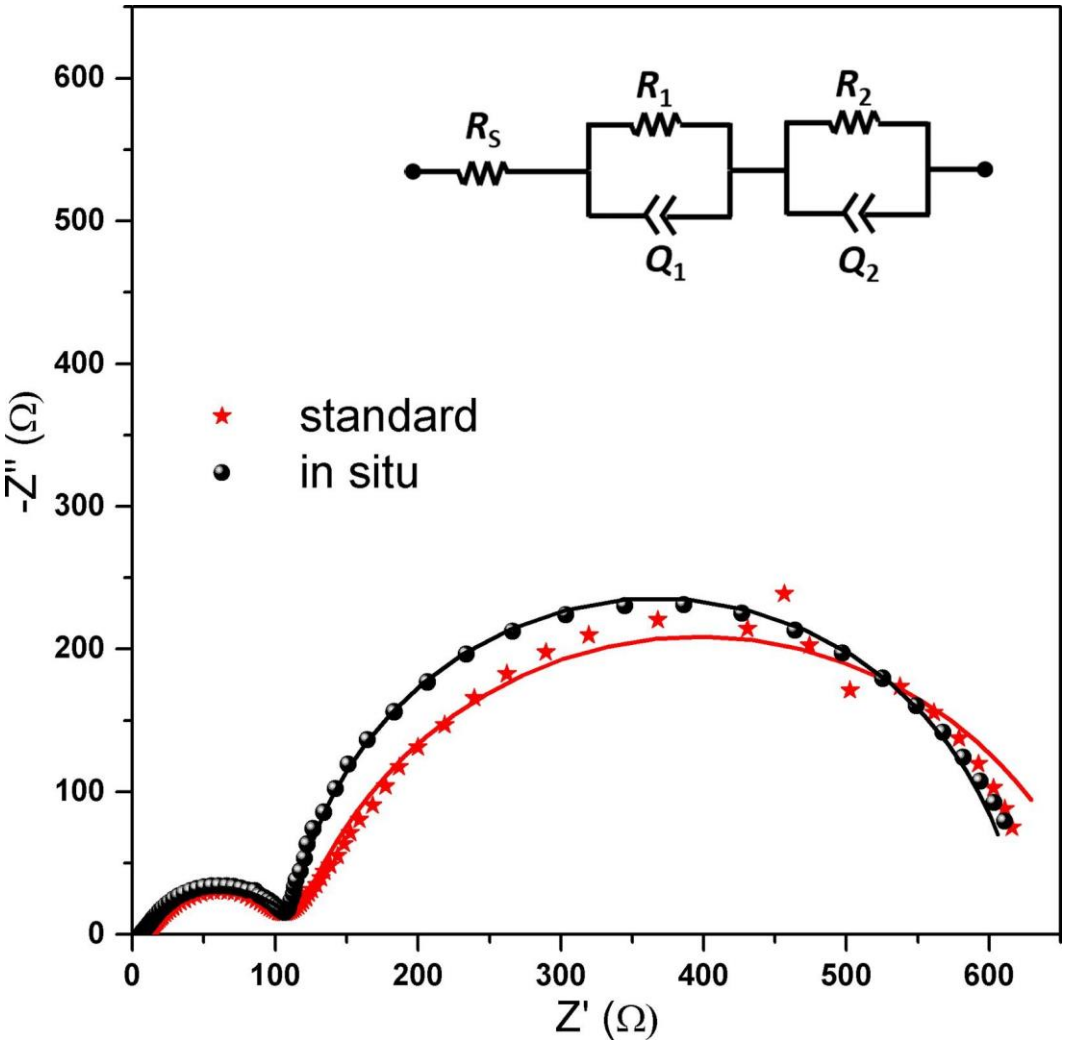

Figure 48: Nyquist plots obtained using EIS data of MFCs fabricated using two different enrichment methods. The points are based on experimental data, while the lines correspond to the fitting procedure performed using the circuit shown in the inset. This image is re-printed with permission from Elsevier 2018©.

The two semicircles that can be seen in Figure 48 correspond to two different processes. The one on the left is a high frequency process which is related to the cathode. As expected, this process exhibits very similar values for both the types of enrichments. This is because the electrodes used in all the MFCs were made from the same material and with the same dimensions.

On the other hand, the second semicircle (on the left side of the image) corresponds to a slower process (occurring at a lower frequency). This process is related to the anode. Moreover, as it can be seen from the EEC (inset of Figure 48) that the EIS data did not show a process related to the diffusion of substrate. This is most likely because the diffusion process was masked by the large capacitance exhibited by the electrodes composed of carbon felt[9]. The second process exhibits different characteristics in the two types of MFCs. This is again an expected

outcome since this process, related to the anode, must be different since two different types of bioanodes have evolved due to the different enrichment methods used. A lower resistance related to the anodic process is seen in the is-MFCs compared to the st-MFCs.

To acquire the values of the parameters related to the different processes, the EIS data were fitted through EECs. The same EEC was employed for both the types of MFCs which comprised of a series resistance R_s which is caused by the ohmic contributions of the medium, wires used etc. Furthermore, the two processes related to the cathodic and anodic interfaces were fitted using a parallel combination of a charge transfer resistance and a double layer capacitance. Both these parallel combinations R_1 and Q_1 for the cathodic process and R_2 and Q_2 for the anodic process were in series to each other in the overall EEC. Both the capacitances obtained through fitting were actually CPEs which were discussed in detail in section 4.4. The resistances obtained using fitting results are given in Table 17.

Table 17: Resistance values obtained through fitting of EIS data.

Type of MFC	R_s (Ω)	R_1 (Ω)	R_2 (Ω)
st-MFC	11.5 ± 2.6	131.7 ± 26.1	500.4 ± 22.3
is-MFC	12.3 ± 1.5	128.9 ± 20.7	448.3 ± 18.6

It can be seen from Table 17 that both R_s and R_1 have very similar values for both types of MFCs and the only substantial difference lies in the value of R_2 – related to the anodic process. A smaller anodic resistance of the is-MFCs is in line with the earlier results related to the current density of the two MFCs in which the is-MFCs show a better performance.

Both the results obtained through EIS and voltage monitoring point to the fact that the novel in-situ enrichment method that we have adopted successfully colonizes a bioanode and eradicates the need of using the procedures used in the standard enrichment technique. This reduces the amount of time, effort and reagents required to start an MFC. An in-situ pre-colonization also ensures that the EAB are kept in a natural habitat throughout the growth cycle thus reducing any effects that a synthesized environment might have on the diversity of the consortia which

develops. To summarize, the in-situ enrichment approach that we have proposed has the following advantages:

i. Reduction in manual tasks since the only requirement is to put the anodes inside the sediment and later, their immersion into seawater.
ii. Reduced need of reagents.
iii. Natural habitat for the microbial consortia development.

Due to all the benefits listed above and competitive performance, in-situ enrichment method was used for bioanode formation to be used in the rest of the experiments.

6.3.2 Experiments conducted in-situ

Once the laboratory experiments were over and the in-situ enrichment approach was chosen as the primary enrichment method, six fMFCs which were nominally identical were constructed. These fMFCs comprised of bioanodes which were enriched using the in-situ enrichment method. During the in-situ experiments, some important parameters relating to the experimental conditions were also recorded and are reported in Table 18.

Table 18: Average of the measurements of different parameters during the in-situ experiments.

Period	Temperature (°C)	Conductivity (mS/cm)	Salinity (‰)	pH	Dissolved O_2 (mg/L)
Summertime	26.6 ± 2.5	59.0 ± 2.9	38.1 ± 0.3	7.9 ± 0.3	8.7 ± 0.5
Winter / Autumn	15.1 ± 2.0	38.3 ± 2.7	32.5 ± 0.6	8.3 ± 0.2	9.0 ± 0.5

6.3.2.1 Summertime campaign

Once the fMFCs were assembled, they were deployed in the La Spezia bay, through summers, and their performance in terms of production of power was monitored. Figure 49 shows the average current density from these fMFCs. For the calculation of this average current density, data from MFC4 and MFC5 were not used, as explained later. Instead, the current density measurements for these fMFCs are shown separately on Figure 49.

It can be seen in Figure 49 that the fMFCs initially produced a high current density which gradually reduced till day 15. This is similar to what was seen in the tests conducted in the laboratory. After this initial phase, the fMFCs stabilized and produced a current density of 135 mA/m^2 towards the end of the experiment. This value of current density corresponds to a power density of 6 mW/m^2. This performance in terms of power density is better when compared to the experiments conducted in the laboratory. Improved performance of the fMFCs operating in-situ is attributed to the fact that the fMFCs have an abundant supply of fresh seawater at their disposal. Furthermore, in this setup, the seawater is continuously moving due to ripples and waves which results in an efficient flow of the seawater through the fMFCs. Both these factors contribute to the fMFCs' improved performance relative to the MFCs in laboratory.

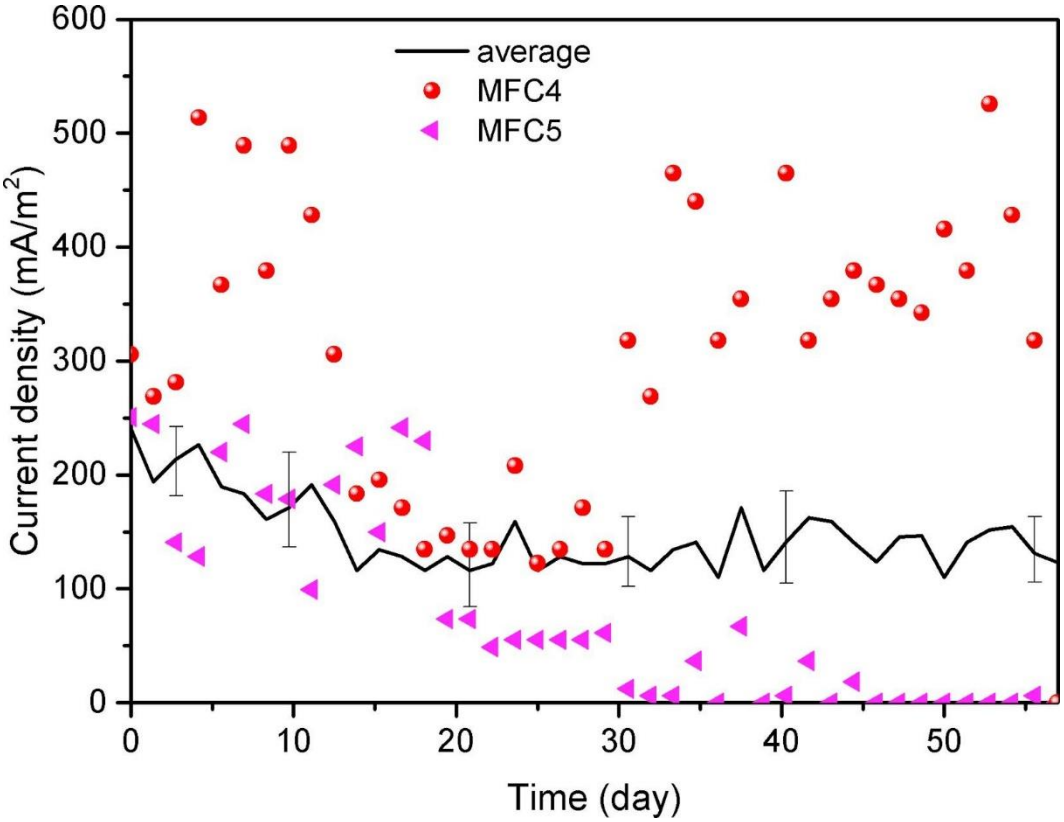

Figure 49: Current density measurements during the summertime campaign are reported in this figure. The black line is an average of the current densities of MFCs 1, 2, 3, and 6 while the points related to MFC 4 and 5 are shown separately. Error bars related to the average current density line are also reported. This image is re-printed with permission from Elsevier 2018©.

An interesting feature that we can extract from the data we collected is the effect of change in temperature on the voltage produced by the fMFCs. These cyclic temperature changes occurred due to the temperature difference in between the day and the night. Figure 50 shows the current density data recorded during days 34 and

40. It is clearly evident that variation in temperature has a significant effect on the current density produced. The minima occurred around 5am while the maxima occurred around 1pm. Furthermore, the change in current density recorded was of approximately ± 50 %. A variation in the performance of an MFC, due to external factors, has been widely studied and experienced both in the laboratory and in field experiments. The main factors that affect the performance of an MFC are:

i. Temperature
ii. pH
iii. Salinity
iv. External load applied

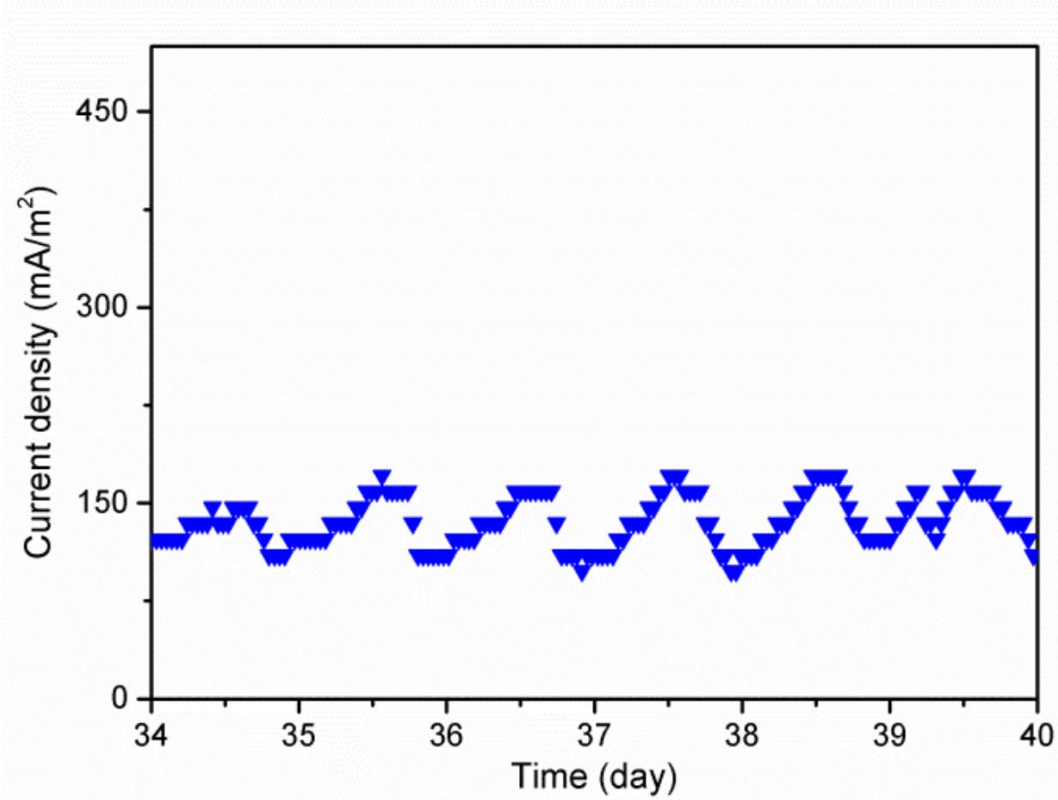

Figure 50: The effect of temperature variation evident in the current density data from day 34 to day 40. This image is re-printed with permission from Elsevier 2018©.

A study by Velasquez-Orta et al. discovered that the most relevant external factor which had a noteworthy impact on the performance of an MFC was the ambient temperature[182]. On the other hand, Ren and co-workers studied the effect of operational temperature range, in order to find an optimal, to improve performance in terms of power in a miniaturized MFC[70]. On the basis of our results and the results from literature, it is evident that the metabolic activity of EABs are

affected by the ambient temperature. Nevertheless, as it can be seen in Figure 50 the effect of temperature is cyclic in nature and thus results in an average current density value that is consistent over longer periods of time.

The data shown in Figure 49 has the average of fMFCs 1,2,3 and 6 as a single line while, the data related to fMFCs 4 and 5 are shown separately as data points. This is because the two devices behaved differently from others either due to a malfunction in the data acquisition system (fMFC 4) or because the device itself did not perform as expected (fMFC 5). In the case of fMFC 4, the main issue was the connection of this device with the data acquisition system and the load resistance. Due to this problem, it kept on connecting and disconnecting causing erratic data points and not the actual ones. On the other hand, fMFC 5 suddenly experienced a decrease in performance from day 19. This followed another rapid decrease in performance on the 30th day. Following this point, fMFC 5 produced a very low current density (9 mA/m^2) until the end of summertime campaign.

On the 58th day, at the end of summertime campaign, all the MFCs were unmounted from the floating system and moved to our laboratory. This was done in order to understand the connection failure of MFC 4 and the decrease in performance of MFC 5. All the devices were placed in the same way they were placed for the first phase in in-lab experiments. Furthermore, the voltage was also monitored. The results of the voltage monitoring showed a consistent power density production of around 2 mW/m^2 for all of the six MFCs. This value of power density is in line with the results discussed in section 6.3.1. During this intermediate in-lab voltage monitoring, MFC 4 did not exhibit any issues related to the electrical connections. Considering these outcomes, 4 out of the six original devices were shortlisted to be used for the winter/autumn campaign. More precisely, MFCs 3,4,5 and 6 were selected for use in the second in-situ measurements campaign. On the other hand, MFCs 1 and 2 were kept in laboratory for other experiments which were not a part of this study.

6.3.2.2 Winter/Autumn campaign

The second part of the in-situ experiments were related to assessing the performance of the devices in a different season. Figure 51 shows the current density results obtained from this campaign. It is important to notice that Figure 51 does not contain data related to fMFC 4. This is because fMFC 4 once again

experienced problems related to the electrical connection resulting in erratic current density data points. Therefore, results related to fMFC 4 were not included in Figure 51. Moreover, it can be seen in Figure 51 that fMFC 5 also showed a similar behavior to the summertime campaign. Initially, it performed well. The values of current densities were even better than fMFCs 3 and 6 until day 15. Nonetheless, fMFC 5 experienced an abrupt decline in current density values following day 15 and continued this declined behavior till the end of the winter/autumn campaign.

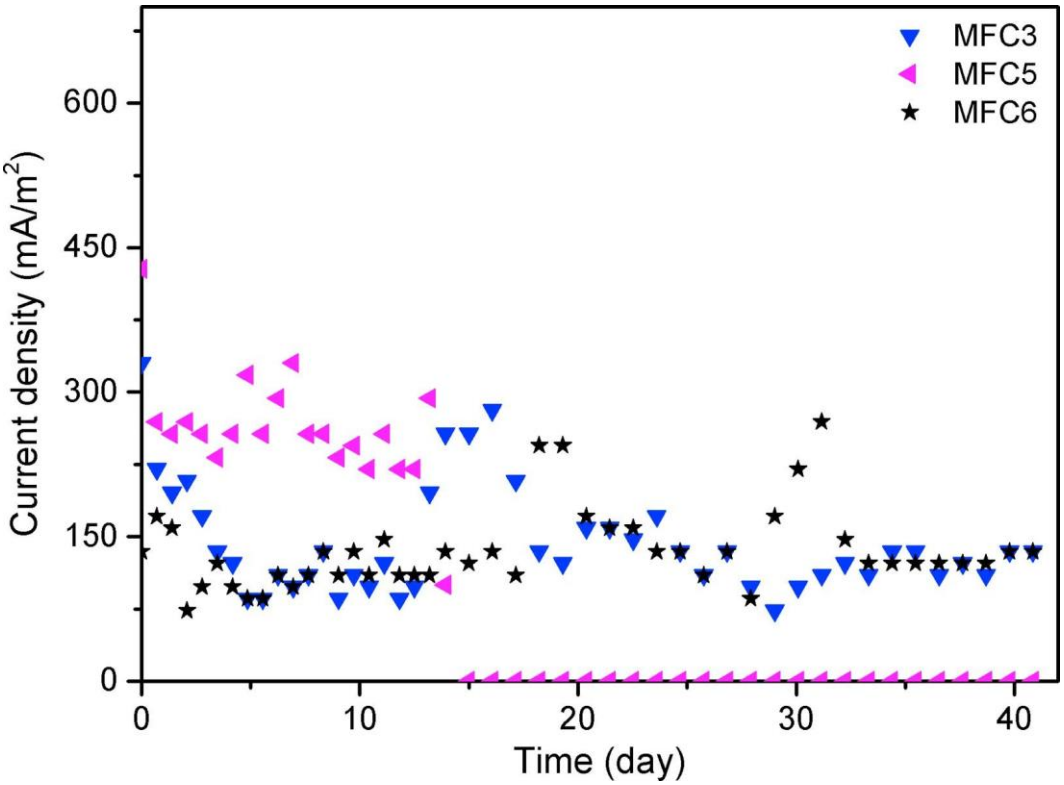

Figure 51: Current density results related to the winter/autumn campaign. This image is re-printed with permission from Elsevier 2018©.

As for fMFCs 3 and 6, they performed consistently producing a stable current density throughout the second experimental campaign. Therefore, the results pertaining to these two fMFCs can be used for a comparison between the two seasonal campaigns. Even though the two campaigns had a difference in temperature of about 10 °C (Table 18), the performance in terms of current density did not show a significant change. This slow and steady change in temperature (due to a seasonal change) allowed the EABs to adapt their metabolic activity according to the ambient changes thus resulting in comparable performances to the summertime campaign. On the other hand, the changes seen in the performance of the fMFCs due to the change in temperature from daytime to nighttime is due to the

fact that these changes occur too quickly for the microbes to adapt to them thus resulting in a change in the performance. This effect of rapid temperature change has been observed in previous works as well[183,184].

The results that have been obtained from the two in-situ campaigns clearly indicated the utility of small-scale fMFCs. Both Figure 49 and Figure 51 show that small-scale fMFCs can produce stable electrical power which can be used in a variety of applications. Not only this, the source of organic compounds (which the EAB use as fuel) was the abundant sea water. Furthermore, these devices are constructed using materials and components that have a very low cost. For such a device to be functional, only the following components are required:

i. Carbon felt – to be used as electrodes.
ii. Housing for the floating setup composed of a polymeric material.

Moreover, the convenience and minimal effort with which the anodes of these devices can be pre-colonized is unprecedented. All these factors point towards a source of sustainable energy which requires negligible maintenance, is inexpensive, does not require a fuel source (since it uses seawater as the source of organic compounds for the EAB to feed on) and is very easy to setup.

Table 19 lists works related to fMFCs and the results associated with them. Table 19 has been introduced in order to analyze the different results and performances achieved thus far and the different materials, architectures and experimental schemes used in the different works. Until recently, there were only two works that have reported the production of electrical power using fMFCs in-situ marine environments[178,185]. Both these research articles are based on experiments which used large scale MFCs. Moreover, these MFCs also contained PEMs. In the work by Huang and co-workers[178], an anode composed of granular graphite is used. For biofilm formation, standard method was employed in the laboratory. The anodic compartment is separated from the cathodic compartment using a PEM and the cathode also has a catalyst layer based on Pt. The cathode is composed of carbon fibers. The total volume of the cell is 4.5 L and has a tubular structure. The reported power produced by this system is 4 mW/m^2. This value of power density is similar to what we obtained using a small scale, easy to setup and inexpensive system.

Table 19: A summary of the data related to fMFCs found in literature. This table is re-printed with permission from Elsevier 2018©.

Architecture	Total volume (L)	Anode	Cathode	Carbon energy source	Electrolyte	Inoculum source	L/F	Maximum power density (mW/m^2)	Reference
Circular tube made of PEM	4.5	GG	Ni-coated GF + Pt/C layers	None	Seawater	50/50 mixture of anaerobic and aerobic sludge collected from a WW treatment plant	F	4[a]	185
Sediment-like MFC installed in a container	121	FB	FB	None	Lake water	Lake sediment layer	L	2.2	54
2 anodes, 1 PEM, 2 cathodes	0.6	Ti covered with iridium and tantalum oxides	Biofilm-covered SS	10 mM sodium acetate	Seawater	Marine biofilm samples	F	20	178
Rectangular box-type acrylic reactor	1.9	GG + GF	GC + Pt	Glucose, macro- and micro-nutrients, and sodium bicarbonate	Synthetic WW	Unknown	L	311.2	186
Cylindrical polyacryl-pipe, 1 PEM	0.1	CF	CF	0–50 mM sodium acetate	Synthetic WW	ADF and WI, collected from a domestic brewery WW treatment plant	L	6	187
Hybrid sediment/plant MFC	3.1	GC	GC	Initially, 3 g/kg sodium acetate	Lake water	Unknown	F	12.2	188

[a] Calculated value. L/F: laboratory/field; PEM: proton exchange membrane; GG: granular graphite; GF: graphite fibers; Pt/C: platinum-covered porous carbon; WW: wastewater; FB: fiber brushes; SS: stainless steel; GC: graphite cloth; CF: carbon felt; ADF: anaerobic digestion fluid, WI: wastewater influent.

On the other hand, Erable and co-workers[185] used anodes in their setup which were composed of titanium with a coating of tantalum oxide and iridium oxide. Cathode was composed of stainless steel. Moreover, they also employed acetate in addition to seawater as the source of organic compounds for microbial metabolism. This work reported a power density of 20 mW/m^2. Although this value is larger than the power density we obtained for our system, it is important to point out that the materials we used for constructing our MFCs were much cheaper. Furthermore, the biofilm pre-colonization phase was conducted in laboratory for this work using the standard approach which increases operational complexity and overall cost. In addition, catalyst layer was also used which add to the cost of the system.

On the other hand, Table 19 also reports works that conducted experiments in the laboratory. In all of these cases, with only one exception, the produced power densities were quite low. The exception was a work by Song and co-workers[186]. Their device achieved a power density of 311.2 mW/m^2 and used a cathode based on carbon with a catalyst (Pt) layer, a composite anode and glucose in addition to other nutrients for microbial metabolism.

The power densities we were able to obtain from our fMFC devices were in the range of some milli watts. Although this range of power density is low, it is still quite useful in applications that require energy in remote environments such as the ocean. An example of such an application is a sensor to detect the quality of the marine environment. Different works in the literature have managed to successfully power different sensors using MFCs which produce power in a similar range. Zhang and co-workers were able to use energy extracted from an SMFC to operate a wireless temperature sensor[54]. For this work, Zhang et al. designed a PMS which used a supercapacitor as the energy storage element and the power density their device produced was 2.2 mW/m^2. In addition, Gong and co-workers powered a sensor, using MFCs, which sensed oxygen levels in the seawater and the temperature and communicated them through an acoustic modem[60]. It is evident from the above worked that if we use our system with a custom designed PMS, we can use our fMFCs to power devices that require low energy such as sensors. Furthermore, our devices offer the added benefits of compact size and mobility.

Having all the benefits discussed, our system still has room for improvement. Clear indication of this comes from the experience we had with the electrical

connection of MFC 4 in the floating system. This problem was related to the relay board which was used to program appropriate connections in between the fMFCs, data acquisition system and the external loads. This indicates the need to develop a more robust electronic control system to avoid such failures when the devices are meant to function in inaccessible remote areas without maintenance and supervision. Furthermore, another fault that was experienced in this setup was the one related to MFC 5. Through both summertime and winter/autumn campaigns, MFC 5 exhibited a strange behavior in which initially the device performed as expected but as later at some point the performance of MFC 5 reduced drastically. One explanation for this could be the fact that the floating MFC system was operating in real environment which is characterized by constant waves and ripples which cause the devices to physically move at all times. We believe that at some point, due to these movements, the connection between either of the electrodes and their current collectors (titanium wires) loosened causing this irregularity. Such a problem can be tackled by optimizing the design of the MFC devices allowing all the connections to more steadfast and robust. The abovementioned improvements in the MFCs' design and electronic units' development can be easily implemented to reduce the possibility of failure in these devices.

In future works we also plan to consider the implementation of an fMFC livestock. An fMFC livestock is basically a collection of several fMFCs which are pre-colonized using the in-situ method. All of their performances will be monitored and an intelligent electronic control unit will decide to use only the best performing fMFCs to extract power in an optimal way. Moreover, the devices that cease to function in a proper manner can be discarded and new ones can be used in their place. This concept will allow to have back up fMFCs readily available to power a variety of low power electronic systems.

6.4 Conclusion

The main aim of this work is to propose a real application of fMFCs that are able to provide sufficient power for different applications. Furthermore, another important motive of this study was to propose a device which requires minimal time, effort and finances to start functioning as a source of sustainable and clean

energy. Moreover, the physical size of the device was kept small in order to make compact and mobile fMFCs able to work in remote locations.

An innovative enrichment method i.e. the in-situ pre-colonization together with an SSE was proposed to ensure that the formed biofilms require very low effort to start up and are acclimated to the natural marine environments from the very start. fMFCs based on bioanodes enriched with this method were developed and tested in the La Spezia bay during two lengthy campaigns (one in the summertime and the second in winter/autumn). These fMFCs were able to produce 6 mW/m^2 of average power density during the two campaigns and showed almost no dependence on the temperature. There were some setbacks that were experienced through the experiments which were related to improper connections, but such issues can be easily dealt with in the future. To improve the robustness of these devices, we will use the fMFCs livestock concept to ensure that if one or more of the fMFCs are not working properly, there are fully functional backup fMFCs which can replace the malfunctioning fMFCs. This will ensure a smooth operation of the overall system.

In the future, we will test our devices in different marine and aquatic environments to investigate if the results we have obtained are reproducible or not. In case the results differ, we will examine the conditions and parameters that cause any variation in the performances of fMFCs.

7 Conclusion

The present dissertation is an in-depth study of Microbial Fuel Cells (MFCs) as sustainable source for renewable energy. MFCs are fuel cells that are based on electroactive bacteria (EAB) forming a biofilm on the anode. These EAB feed on substrates present inside the electrolyte of an MFC. The medium acting as an electrolyte to the MFC can be an artificial one prepared in the laboratory for experimental purposes and, as many works have proposed, it can also be wastewater. EABs process the organic compounds present inside the wastewater (treating it in the process) and produce energy. Thus, proving to be an effective way to treat wastewater. Moreover, MFCs also have applications in bio-sensing. Changes in an MFC's environment such as the temperature, pH etc. affect the performance since these are devices based on living organisms which are sensitive to such changes. Moreover, MFCs can be used in the marine environment in the form of sedimentary MFCs (SMFCs) and floating MFCs (fMFCs). These variations of MFCs allow their application in the marine environment as devices that can produce energy in the remote locations and with the use of proper power management systems (PMSs), can power low energy systems such as environmental sensors.

Another important aspect of this thesis is the detailed discussion of Electrochemical Impedance Spectroscopy (EIS). EIS is a non-invasive electrochemical technique which enables us to study the impedance response of an electrochemical device. The impedance response of a device can provide valuable information about a device related to the different interfaces present in the device and also the different electrochemical processes that are taking place in the device. Moreover, EIS can also help us understand the effects of different parameters and external conditions on a device.

EIS has been used on a wide variety of devices and the interest in use of EIS to investigate MFCs has risen in the past years. A comprehensive work related to the use of EIS to investigate MFCs, based on different enrichments methods has been discussed in detail in this thesis. At the time this work was published, most of the

works in the literature dealing with the use of EIS to investigate MFCs were using a pure culture mostly related to the following strains of bacteria:

- Geobacter sulfurreducens
- Shewanella oneidensis

In the work that we performed, we focused on the use of mixed community bacteria for practical applications of MFCs. To start the culture, we used two different types of enrichment methods 1) General Enrichment (GE) and 2) Ferric Citrate based enrichment (FeC). This was done to study the effect of an iron-based enrichment method and its effects on the growth and health of the biofilm resulting from it. The MFCs based on GE were used to compare the effects of the FeC based method.

To compare the two methods, a comprehensive electrochemical analysis was performed which involved the use of polarization tests, cyclic voltammeter and EIS. In addition, a biological analysis was also performed on the MFCs' biofilms. A major focus was put on the analysis of EIS results based on experiments conducted in different polarization conditions and their proper interpretation. EIS was performed in a half cell (with three electrodes configuration) to gather in-depth information related to the evolution of the biofilm on the anode. Furthermore, the results obtained through EIS were fitted using different models to propose suitable equivalent electrical circuits. Parameters derived from these circuits prove to be very important when it comes to the quantitative analysis (in terms of time constants) of the processes occurring inside an electrochemical device. Furthermore, EIS also sheds light on the changes occurring in the electrochemical processes due to the variation in conditions and performance of the MFCs.

The results obtained from EIS showed the presence of various electrochemical processes and interfaces present within the anodic chamber. Three main processes were identified:

i. anode-electrolyte interface process,
ii. biofilm process,
iii. diffusion of substrate process.

Moreover, these EIS tests were performed on different points of the polarization curves and thus an understanding of the relationship between polarization condition and the performance (in terms of the efficiency of internal processes) of an MFC was also developed. The maximum power point (inferred from the polarization test) occurred at the same polarization point at which both types of MFCs exhibited lowest internal impedance. When the performances of the two types of enrichments were compared, it was deduced that the MFCs based on a GE based enrichment method performed better than the MFCs based on FeC based enrichment method. These results were confirmed by all the analysis techniques used during the experiments. If we consider the results from EIS, GE enrichment based MFCs performed better when considering the parameters relating to the charge transfer process and the diffusion process. EIS results showed that the FeC enrichment based MFCs had a diffusion process rate that was slower and generally exhibited larger resistances than the GE enrichment based MFCs. To summarize, the GE enrichment-based bio anodes performed better and had a more efficient charge transfer process when compared to the FeC enrichment based bioanodes.

MFCs are devices intended to be used primarily for energy harvesting in real and practical situations. They provide a sustainable source of green energy that can sustain devices which require low power. Moving towards their widescale implementation as energy harvesting devices it is important to develop techniques and methods which allow an easy, in-situ and reliable implementation of MFCs as sources of clean energy. In order to develop such methods and devices, we explored the use of an innovative class of MFCs known as floating MFCs (fMFCs). fMFCs, are single chamber, air-cathode devices which operated mainly in marine and aquatic locations. In such applications, MFCs are mostly used to power sensors at remote locations, for example in the sea. To be able to do that efficiently, it is also important that these devices offer mobility and compact dimensions. At the time of publication of this work, the fMFCs designed were of large dimensions and immobile. The main aim of our work was to cater for the challenges related to mobility and size, meanwhile developing an MFC acclimation technique that requires minimal input for setting up the devices and making them functional. In addition, the technique we investigated also reduces the cost of setting up the fMFC

since no reagents and catalyst layers were used for acclimation and operation of the fMFCs.

Initially, we compared a standard enrichment technique to an in-situ enrichment approach that we have proposed. In this novel technique, anode material (carbon felt) was directly buried inside seawater sediment (La Spezia bay, north Italy) for the formation of the biofilm on the anode. The two types enrichment methods of fMFCs were compared using voltage monitoring and EIS to assess differences in their performances. All the results we obtained in the comparisons of the two enrichment methods pointed out that the in-situ enrichment method was able to successfully acclimate the biofilm on to the anodes. Moreover, the performance in terms of power also indicated a more robust biofilm formed on the in-situ acclimated anode. Such an enrichment approach has several benefits such as a reduction in the work required to get the devices functional, a decrease in the number of reagents needed for start-up and it allows the bacteria to form a biofilm which proliferates in its natural habitat and the one in which it is intended to work for its functional life time. After this stage of the experiment, we moved on with MFCs acclimated in-situ and constructed fMFCs from them to test their performance in a real marine environment through voltage monitoring in an external load. This was done in two separate comprehensive seasonal campaigns (summertime and winter/autumn). The results showed a stable power density output from these devices with an average of 6 mW/m^2. The devices did not show a variation in performance between the two seasonal campaigns thus proving themselves to be reliable. Power density output in this range has been used in the literature to provide energy to low power remote sensing systems in literature thus, affirming the utility of these devices. Such an approach of using fMFCs whose biofilms were acclimated in-situ not only prove to be stable sources of sustainable energy but also reduces the time and effort required to get these devices functional. Moreover, our design further improves the fMFCs' mobility and reduces their dimensions which ensures their application in real marine environments where mobility and compact design are a pre-requisite.

This dissertation starts with a comprehensive description of MFCs, their types and the main factors that affect their performance. Applications of MFCs as sustainable power sources has also been explored. Additionally, to improve their

performance, an in-depth analysis of the electrochemical technique – EIS is also performed. Then, an experimental work which we published in Electrochemical Acta has been thoroughly reported in which EIS was used as a tool to investigate the performances of biofilms in MFCs started from two different enrichment methods. Henceforth, another work we published in Applied Energy has been described which focuses on the real applications of MFCs as devices that provide renewable energy in remote locations.

All the experiments performed, and the results inferred from them, point towards the utility of MFCs as a source of renewable energy in low power applications. Even though at present, MFCs are not implemented on a wide scale we believe that they have immense potential to be used as reliable and sustainable energy sources with the help of upcoming efforts and future developments in the devices.

7.1 Future Scope

In the present day and age, it is very important to explore alternate options for energy generation that are clean and reliable. Some of the main reasons why this is necessary are the depletion of fossil fuels, the escalating issue of pollution and the growing population of the world. MFCs provide one such source of clean and renewable energy. Furthermore, in the process of making energy, MFCs can also be used to clean wastewater. Though the energy produced from MFCs is low, they have a huge potential in applications that require low energy but in remote locations. One important example of such applications is the monitoring of marine life using sensors powered by MFCs. Not only do MFCs provide energy for the sensors in remote marine locations but do so without perturbating the natural habitat of marine life. Especially, advances in MFC technology such as the use of sMFC stacks make the use of MFCs as power sources more reliable. An MFC stack connected in parallel would provide a higher current while one connected in series provides higher operational voltage. Moreover, in a stack configuration, if an MFC fails or malfunctions, an intelligent electrical circuit can be used to switch the system over to other MFC(s) available for power production thus ensuring a continuous supply of energy.

To improve the production of power and performance of MFCs, it is important to understand the electron transfer mechanisms and the diffusion of substrate that occurs within the different types of MFCs. For this reason, EIS has been widely used to perform electrochemical analysis on MFCs. The use of EIS for analyzing MFCs is promising since it provides a non-invasive method to investigate the different processes occurring inside MFCs. It also provides a quantitative analysis of the resistive elements present inside an MFCs and thus helps in exploring materials and methods that help reduce the internal resistance of an MFC. Therefore, EIS will remain an important technique, even in the future, to understand the internal processes of MFCs.

With more research in improving their power generation and reducing their internal resistance, MFCs will eventually reach a level of power generation and robustness enough to warrant their use as commercially available devices.

8 Bibliography

1. Chu S, Majumdar A. Opportunities and challenges for a sustainable energy future. *Nature*. 2012;488(7411):294-303. doi:10.1038/nature11475
2. Dincer I. Renewable energy and sustainable development: a crucial review. *Renew Sustain Energy Rev*. 2000;4(2):157-175. doi:10.1016/S1364-0321(99)00011-8
3. Eleven EU countries hit 2020 renewable energy targets | EMIS. https://emis.vito.be/nl/artikel/eleven-eu-countries-hit-2020-renewable-energy-targets. Accessed January 9, 2019.
4. Logan BE. Exoelectrogenic bacteria that power microbial fuel cells. *Nat Rev Microbiol*. 2009;7(5):375-381. doi:10.1038/nrmicro2113
5. Velasquez-Orta SB, Head IM, Curtis TP, Scott K. Factors affecting current production in microbial fuel cells using different industrial wastewaters. *Bioresour Technol*. 2011;102(8):5105-5112. doi:10.1016/J.BIORTECH.2011.01.059
6. Logan BE, Hamelers B, Rozendal R, et al. Microbial Fuel Cells: Methodology and Technology †. *Environ Sci Technol*. 2006;40(17):5181-5192. doi:10.1021/es0605016
7. Rabaey K, Boon N, Höfte M, Verstraete W. Microbial phenazine production enhances electron transfer in biofuel cells. *Environ Sci Technol*. 2005;39(9):3401-3408. http://www.ncbi.nlm.nih.gov/pubmed/15926596. Accessed September 16, 2018.
8. Watanabe K. Recent Developments in Microbial Fuel Cell Technologies for Sustainable Bioenergy. *J Biosci Bioeng*. 2008;106(6):528-536. doi:10.1263/JBB.106.528
9. Agostino V, Ahmed D, Sacco A, Margaria V, Armato C, Quaglio M. Electrochemical analysis of microbial fuel cells based on enriched biofilm communities from freshwater sediment. *Electrochim Acta*. 2017;237:133-143. doi:10.1016/J.ELECTACTA.2017.03.186
10. Huang L, Regan JM, Quan X. Electron transfer mechanisms, new applications, and performance of biocathode microbial fuel cells. *Bioresour Technol*. 2011;102(1):316-323. doi:10.1016/J.BIORTECH.2010.06.096
11. Schröder U. Anodic electron transfer mechanisms in microbial fuel cells and their energy efficiency. *Phys Chem Chem Phys*. 2007;9(21):2619-2629. doi:10.1039/B703627M
12. Logan BE. *Microbial Fuel Cells*. Hoboken, NJ, USA; 2007. doi:10.1002/9780470258590
13. Sydow A, Krieg T, Mayer F, Schrader J, Holtmann D. Electroactive bacteria—molecular mechanisms and genetic tools. *Appl Microbiol Biotechnol*. 2014;98(20):8481-8495. doi:10.1007/s00253-014-6005-z
14. Gorby YA, Yanina S, McLean JS, et al. Electrically conductive bacterial nanowires produced by Shewanella oneidensis strain MR-1 and other microorganisms. *Proc Natl Acad Sci U S A*. 2006;103(30):11358-11363. doi:10.1073/pnas.0604517103
15. Shizas I, Bagley DM. Experimental Determination of Energy Content of

Unknown Organics in Municipal Wastewater Streams. *J Energy Eng*. 2004;130(2):45-53. doi:10.1061/(ASCE)0733-9402(2004)130:2(45)

16. Pandey P, Shinde VN, Deopurkar RL, Kale SP, Patil SA, Pant D. Recent advances in the use of different substrates in microbial fuel cells toward wastewater treatment and simultaneous energy recovery. *Appl Energy*. 2016;168:706-723. doi:10.1016/J.APENERGY.2016.01.056
17. and BM, Bruce E. Logan* †,‡. Continuous Electricity Generation from Domestic Wastewater and Organic Substrates in a Flat Plate Microbial Fuel Cell. 2004. doi:10.1021/ES0491026
18. Min B, Kim J, Oh S, Regan JM, Logan BE. Electricity generation from swine wastewater using microbial fuel cells. *Water Res*. 2005;39(20):4961-4968. doi:10.1016/J.WATRES.2005.09.039
19. Cheng S, Liu H, Logan BE. Increased performance of single-chamber microbial fuel cells using an improved cathode structure. *Electrochem commun*. 2006;8(3):489-494. doi:10.1016/J.ELECOM.2006.01.010
20. Sell D, Kr[?]mer P, Kreysa G. Use of an oxygen gas diffusion cathode and a three-dimensional packed bed anode in a bioelectrochemical fuel cell. *Appl Microbiol Biotechnol*. 1989;31(2):211-213. doi:10.1007/BF00262465
21. Reimers* CE, Tender* LM, Fertig S, Wang W. Harvesting Energy from the Marine Sediment−Water Interface. 2000. doi:10.1021/ES001223S
22. Liu H, Ramnarayanan R, Logan BE, Hong Liu †, Ramanathan Ramnarayanan ‡ and, Bruce E. Logan* †. Production of Electricity during Wastewater Treatment Using a Single Chamber Microbial Fuel Cell. *Environ Sci Technol*. 2004;38(7):2281-2285. doi:10.1021/es034923g
23. Dewan A, Ay SU, Karim MN, Beyenal H. Alternative power sources for remote sensors: A review. *J Power Sources*. 2014;245:129-143. doi:10.1016/J.JPOWSOUR.2013.06.081
24. Yang H, Zhou M, Liu M, Yang W, Gu T. Microbial fuel cells for biosensor applications. *Biotechnol Lett*. 2015;37(12):2357-2364. doi:10.1007/s10529-015-1929-7
25. Donovan C, Dewan A, Heo D, Beyenal H. Batteryless, Wireless Sensor Powered by a Sediment Microbial Fuel Cell. *Environ Sci Technol*. 2008;42(22):8591-8596. doi:10.1021/es801763g
26. Abazarian E, Gheshlaghi R, Mahdavi MA. The effect of number and configuration of sediment microbial fuel cells on their performance in an open channel architecture. *J Power Sources*. 2016;325:739-744. doi:10.1016/J.JPOWSOUR.2016.06.080
27. Sherafatmand M, Ng HY. Using sediment microbial fuel cells (SMFCs) for bioremediation of polycyclic aromatic hydrocarbons (PAHs). *Bioresour Technol*. 2015;195:122-130. doi:10.1016/J.BIORTECH.2015.06.002
28. Ewing T, Ha PT, Babauta JT, Tang NT, Heo D, Beyenal H. Scale-up of sediment microbial fuel cells. *J Power Sources*. 2014;272:311-319. doi:10.1016/J.JPOWSOUR.2014.08.070
29. Bhande R, Noori MT, Ghangrekar MM. Performance assessment of sediment microbial fuel cell by enriching the sediment with cellulose: Kinetics of cellulose degradation. *Environ Technol Innov*. November 2018. doi:10.1016/J.ETI.2018.11.003
30. Zhao Q, Ji M, Li R, Ren ZJ. Long-term performance of sediment microbial fuel cells with multiple anodes. *Bioresour Technol*. 2017;237:178-185. doi:10.1016/J.BIORTECH.2017.03.002

31. Bruce E. Logan *,‡, Bert Hamelers §, René Rozendal §,‖, et al. Microbial Fuel Cells: Methodology and Technology†. 2006. doi:10.1021/ES0605016
32. Chaudhuri SK, Lovley DR. Electricity generation by direct oxidation of glucose in mediatorless microbial fuel cells. *Nat Biotechnol*. 2003;21(10):1229-1232. doi:10.1038/nbt867
33. Kim JR, Jung SH, Regan JM, Logan BE. Electricity generation and microbial community analysis of alcohol powered microbial fuel cells. *Bioresour Technol*. 2007;98(13):2568-2577. doi:10.1016/J.BIORTECH.2006.09.036
34. Zhiyong Ren †, Thomas E. Ward † and, John M. Regan* †,‡. Electricity Production from Cellulose in a Microbial Fuel Cell Using a Defined Binary Culture. 2007. doi:10.1021/ES070577H
35. Hong Liu †, Shaoan Cheng † and, Bruce E. Logan* †,‡. Production of Electricity from Acetate or Butyrate Using a Single-Chamber Microbial Fuel Cell. 2004. doi:10.1021/ES048927C
36. Ieropoulos IA, Ledezma P, Stinchcombe A, Papaharalabos G, Melhuish C, Greenman J. Waste to real energy: the first MFC powered mobile phone. *Phys Chem Chem Phys*. 2013;15(37):15312. doi:10.1039/c3cp52889h
37. Ge Z, Wu L, Zhang F, He Z. Energy extraction from a large-scale microbial fuel cell system treating municipal wastewater. *J Power Sources*. 2015;297:260-264. doi:10.1016/J.JPOWSOUR.2015.07.105
38. Shaoan Cheng †, Hong Liu † and, Bruce E. Logan* †,‡. Power Densities Using Different Cathode Catalysts (Pt and CoTMPP) and Polymer Binders (Nafion and PTFE) in Single Chamber Microbial Fuel Cells. 2005. doi:10.1021/ES0512071
39. Zhao F, Harnisch F, Schröder U, Scholz F, Bogdanoff P, Herrmann I. Application of pyrolysed iron(II) phthalocyanine and CoTMPP based oxygen reduction catalysts as cathode materials in microbial fuel cells. *Electrochem commun*. 2005;7(12):1405-1410. doi:10.1016/J.ELECOM.2005.09.032
40. Zhang L, Liu C, Zhuang L, Li W, Zhou S, Zhang J. Manganese dioxide as an alternative cathodic catalyst to platinum in microbial fuel cells. *Biosens Bioelectron*. 2009;24(9):2825-2829. doi:10.1016/J.BIOS.2009.02.010
41. Wen Q, Wang S, Yan J, et al. MnO2–graphene hybrid as an alternative cathodic catalyst to platinum in microbial fuel cells. *J Power Sources*. 2012;216:187-191. doi:10.1016/J.JPOWSOUR.2012.05.023
42. Morris JM, Jin S, Wang J, Zhu C, Urynowicz MA. Lead dioxide as an alternative catalyst to platinum in microbial fuel cells. *Electrochem commun*. 2007;9(7):1730-1734. doi:10.1016/J.ELECOM.2007.03.028
43. Bergel A, Féron D, Mollica A. Catalysis of oxygen reduction in PEM fuel cell by seawater biofilm. *Electrochem commun*. 2005;7(9):900-904. doi:10.1016/J.ELECOM.2005.06.006
44. Wang H, Park J-D, Ren ZJ. Practical Energy Harvesting for Microbial Fuel Cells: A Review. *Environ Sci Technol*. 2015;49(6):3267-3277. doi:10.1021/es5047765
45. Walter XA, Stinchcombe A, Greenman J, Ieropoulos I. Urine transduction to usable energy: A modular MFC approach for smartphone and remote system charging. *Appl Energy*. 2017;192:575-581. doi:10.1016/J.APENERGY.2016.06.006
46. Oh S-E, Logan BE. Proton exchange membrane and electrode surface areas as factors that affect power generation in microbial fuel cells. *Appl Microbiol*

Biotechnol. 2006;70(2):162-169. doi:10.1007/s00253-005-0066-y
47. Fan Y, Sharbrough E, Liu H. Quantification of the internal resistance distribution of microbial fuel cells. *Environ Sci Technol*. 2008;42(21):8101-8107. doi:10.1021/es801229j
48. Ieropoulos IA, Ledezma P, Stinchcombe A, Papaharalabos G, Melhuish C, Greenman J. Waste to real energy: the first MFC powered mobile phone. *Phys Chem Chem Phys*. 2013;15(37):15312. doi:10.1039/c3cp52889h
49. Yang F, Zhang D, Shimotori T, Wang K-C, Huang Y. Study of transformer-based power management system and its performance optimization for microbial fuel cells. *J Power Sources*. 2012;205:86-92. doi:10.1016/J.JPOWSOUR.2012.01.025
50. Yang F, Zhang D, Shimotori T, Wang K-C, Huang Y. Study of transformer-based power management system and its performance optimization for microbial fuel cells. *J Power Sources*. 2012;205:86-92. doi:10.1016/J.JPOWSOUR.2012.01.025
51. Donovan C, Dewan A, Peng H, Heo D, Beyenal H. Power management system for a 2.5 W remote sensor powered by a sediment microbial fuel cell. *J Power Sources*. 2011;196(3):1171-1177. doi:10.1016/J.JPOWSOUR.2010.08.099
52. Zhang D, Yang F, Shimotori T, Wang K-C, Huang Y. Performance evaluation of power management systems in microbial fuel cell-based energy harvesting applications for driving small electronic devices. *J Power Sources*. 2012;217:65-71. doi:10.1016/J.JPOWSOUR.2012.06.013
53. Wang H, Park J-D, Ren Z. Active Energy Harvesting from Microbial Fuel Cells at the Maximum Power Point without Using Resistors. *Environ Sci Technol*. 2012;46(9):5247-5252. doi:10.1021/es300313d
54. Zhang F, Tian L, He Z. Powering a wireless temperature sensor using sediment microbial fuel cells with vertical arrangement of electrodes. *J Power Sources*. 2011;196(22):9568-9573. doi:10.1016/J.JPOWSOUR.2011.07.037
55. Meehan A, Gao H, Lewandowski Z. Energy harvesting with microbial fuel cell and power management system. *IEEE Trans Power Electron*. 2011;26(1):176-181. doi:10.1109/TPEL.2010.2054114
56. Alaraj M, Ren ZJ, Park J-D. Microbial fuel cell energy harvesting using synchronous flyback converter. *J Power Sources*. 2014;247:636-642. doi:10.1016/J.JPOWSOUR.2013.09.017
57. Zhang X, Ren H, Pyo S, Lee J-I, Kim J, Chae J. A High-Efficiency DC–DC Boost Converter for a Miniaturized Microbial Fuel Cell. *IEEE Trans Power Electron*. 2015;30(4):2041-2049. doi:10.1109/TPEL.2014.2323075
58. Park J-D, Ren Z. High efficiency energy harvesting from microbial fuel cells using a synchronous boost converter. *J Power Sources*. 2012;208:322-327. doi:10.1016/J.JPOWSOUR.2012.02.035
59. Li X, Liu G, Sun S, et al. Power generation in dual chamber microbial fuel cells using dynamic membranes as separators. *Energy Convers Manag*. 2018;165:488-494. doi:10.1016/J.ENCONMAN.2018.03.074
60. Gong Y, Radachowsky SE, Wolf M, Nielsen ME, Girguis PR, Reimers CE. Benthic Microbial Fuel Cell as Direct Power Source for an Acoustic Modem and Seawater Oxygen/Temperature Sensor System. *Environ Sci Technol*. 2011;45(11):5047-5053. doi:10.1021/es104383q
61. Ma F, Fu C, Rong X. Performance evaluation of sediment microbial fuel

cells Powering electronic devices with maximum power point tracking. In: *2017 Chinese Automation Congress (CAC)*. IEEE; 2017:7362-7367. doi:10.1109/CAC.2017.8244108

62. Hong Liu †, Ramanathan Ramnarayanan ‡ and, Bruce E. Logan* †,§. Production of Electricity during Wastewater Treatment Using a Single Chamber Microbial Fuel Cell. 2004. doi:10.1021/ES034923G
63. Zhen He †, Shelley D. Minteer ‡ and, Largus T. Angenent* †. Electricity Generation from Artificial Wastewater Using an Upflow Microbial Fuel Cell. 2005. doi:10.1021/ES0502876
64. Moon H, Chang IS, Jang JK, Kim BH. Residence time distribution in microbial fuel cell and its influence on COD removal with electricity generation. *Biochem Eng J*. 2005;27(1):59-65. doi:10.1016/J.BEJ.2005.02.010
65. Jang JK, Pham TH, Chang IS, et al. Construction and operation of a novel mediator- and membrane-less microbial fuel cell. *Process Biochem*. 2004;39(8):1007-1012. doi:10.1016/S0032-9592(03)00203-6
66. • Projected spending on water and wastewater infrastructure U.S. 2018 | Statistic. https://www.statista.com/statistics/618215/us-spending-on-water-and-wastewater-infrastructure-projection/. Accessed September 17, 2018.
67. Korneel Rabaey *,‡, Kirsten Van de Sompel ‡, Lois Maignien ‡, et al. Microbial Fuel Cells for Sulfide Removal†. 2006. doi:10.1021/ES060382U
68. Hong Liu †, Stephen Grot ‡ and, Bruce E. Logan* †. Electrochemically Assisted Microbial Production of Hydrogen from Acetate. 2005. doi:10.1021/ES050244P
69. Liu Y, Climent V, Berná A, Feliu JM. Effect of Temperature on the Catalytic Ability of Electrochemically Active Biofilm as Anode Catalyst in Microbial Fuel Cells. *Electroanalysis*. 2011;23(2):387-394. doi:10.1002/elan.201000499
70. Ren H, Jiang C, Chae J. Effect of temperature on a miniaturized microbial fuel cell (MFC). *Micro Nano Syst Lett*. 2017;5(1):13. doi:10.1186/s40486-017-0048-8
71. Li LH, Sun YM, Yuan ZH, Kong XY, Li Y. Effect of temperature change on power generation of microbial fuel cell. *Environ Technol*. 2013;34(13-14):1929-1934. doi:10.1080/09593330.2013.828101
72. Wang X, Cheng S, Zhang X, Li X, Logan BE. Impact of salinity on cathode catalyst performance in microbial fuel cells (MFCs). *Int J Hydrogen Energy*. 2011;36(21):13900-13906. doi:10.1016/J.IJHYDENE.2011.03.052
73. Adelaja O, Keshavarz T, Kyazze G. The effect of salinity, redox mediators and temperature on anaerobic biodegradation of petroleum hydrocarbons in microbial fuel cells. *J Hazard Mater*. 2015;283:211-217. doi:10.1016/J.JHAZMAT.2014.08.066
74. He Z, Huang Y, Manohar AK, Mansfeld F. Effect of electrolyte pH on the rate of the anodic and cathodic reactions in an air-cathode microbial fuel cell. *Bioelectrochemistry*. 2008;74(1):78-82. doi:10.1016/J.BIOELECHEM.2008.07.007
75. Puig S, Serra M, Coma M, Cabré M, Balaguer MD, Colprim J. Effect of pH on nutrient dynamics and electricity production using microbial fuel cells. *Bioresour Technol*. 2010;101(24):9594-9599. doi:10.1016/J.BIORTECH.2010.07.082
76. Margaria V, Tommasi T, Pentassuglia S, et al. Effects of pH variations on

anodic marine consortia in a dual chamber microbial fuel cell. *Int J Hydrogen Energy*. 2017;42(3):1820-1829. doi:10.1016/J.IJHYDENE.2016.07.250

77. Shen YJ, Lefebvre O, Tan Z, Ng HY. Microbial fuel-cell-based toxicity sensor for fast monitoring of acidic toxicity. *Water Sci Technol*. 2012;65(7):1223-1228. doi:10.2166/wst.2012.957
78. Dávila D, Esquivel JP, Sabaté N, Mas J. Silicon-based microfabricated microbial fuel cell toxicity sensor. *Biosens Bioelectron*. 2011;26(5):2426-2430. doi:10.1016/J.BIOS.2010.10.025
79. Jiang Y, Liang P, Zhang C, et al. Enhancing the response of microbial fuel cell based toxicity sensors to Cu(II) with the applying of flow-through electrodes and controlled anode potentials. *Bioresour Technol*. 2015;190:367-372. doi:10.1016/J.BIORTECH.2015.04.127
80. Lasia A. Electrochemical Impedance Spectroscopy and its Applications. In: *Modern Aspects of Electrochemistry*. Boston: Kluwer Academic Publishers; 2002:143-248. doi:10.1007/0-306-46916-2_2
81. Manickam A, Chevalier A, McDermott M, Ellington AD, Hassibi A. A CMOS Electrochemical Impedance Spectroscopy (EIS) Biosensor Array. *IEEE Trans Biomed Circuits Syst*. 2010;4(6):379-390. doi:10.1109/TBCAS.2010.2081669
82. Tan YJ, Bailey S, Kinsella B. An investigation of the formation and destruction of corrosion inhibitor films using electrochemical impedance spectroscopy (EIS). *Corros Sci*. 1996;38(9):1545-1561. doi:10.1016/0010-938X(96)00047-9
83. Mansfeld F. Electrochemical impedance spectroscopy (EIS) as a new tool for investigating methods of corrosion protection. *Electrochim Acta*. 1990;35(10):1533-1544. doi:10.1016/0013-4686(90)80007-B
84. Jüttner K. Electrochemical impedance spectroscopy (EIS) of corrosion processes on inhomogeneous surfaces. *Electrochim Acta*. 1990;35(10):1501-1508. doi:10.1016/0013-4686(90)80004-8
85. Liu C, Bi Q, Leyland A, Matthews A. An electrochemical impedance spectroscopy study of the corrosion behaviour of PVD coated steels in 0.5 N NaCl aqueous solution: Part II.: EIS interpretation of corrosion behaviour. *Corros Sci*. 2003;45(6):1257-1273. doi:10.1016/S0010-938X(02)00214-7
86. Hjelm A-K, Lindbergh G. Experimental and theoretical analysis of LiMn2O4 cathodes for use in rechargeable lithium batteries by electrochemical impedance spectroscopy (EIS). *Electrochim Acta*. 2002;47(11):1747-1759. doi:10.1016/S0013-4686(02)00008-7
87. Itagaki M, Kobari N, Yotsuda S, Watanabe K, Kinoshita S, Ue M. In situ electrochemical impedance spectroscopy to investigate negative electrode of lithium-ion rechargeable batteries. *J Power Sources*. 2004;135(1-2):255-261. doi:10.1016/J.JPOWSOUR.2004.04.004
88. Li H, Huang X, Chen L. Electrochemical impedance spectroscopy study of SnO and nano-SnO anodes in lithium rechargeable batteries. *J Power Sources*. 1999;81-82:340-345. doi:10.1016/S0378-7753(99)00214-1
89. Zhang SS, Xu K, Jow TR. Electrochemical impedance study on the low temperature of Li-ion batteries. *Electrochim Acta*. 2004;49(7):1057-1061. doi:10.1016/J.ELECTACTA.2003.10.016
90. Cañas NA, Hirose K, Pascucci B, Wagner N, Friedrich KA, Hiesgen R. Investigations of lithium–sulfur batteries using electrochemical impedance spectroscopy. *Electrochim Acta*. 2013;97:42-51.

doi:10.1016/J.ELECTACTA.2013.02.101

91. Andre D, Meiler M, Steiner K, Wimmer C, Soczka-Guth T, Sauer DU. Characterization of high-power lithium-ion batteries by electrochemical impedance spectroscopy. I. Experimental investigation. *J Power Sources*. 2011;196(12). https://www.sciencedirect.com/science/article/abs/pii/S0378775311000681. Accessed December 4, 2018.
92. Guo J, Sun A, Chen X, Wang C, Manivannan A. Cyclability study of silicon–carbon composite anodes for lithium-ion batteries using electrochemical impedance spectroscopy. *Electrochim Acta*. 2011;56(11):3981-3987. doi:10.1016/J.ELECTACTA.2011.02.014
93. Deng Z, Zhang Z, Lai Y, Liu J, Li J, Liu Y. Electrochemical Impedance Spectroscopy Study of a Lithium/Sulfur Battery: Modeling and Analysis of Capacity Fading. *J Electrochem Soc*. 2013;160(4):A553-A558. doi:10.1149/2.026304jes
94. He C, Zheng Z, Tang H, Zhao L, Lu F. Electrochemical Impedance Spectroscopy Characterization of Electron Transport and Recombination in ZnO Nanorod Dye-Sensitized Solar Cells. *J Phys Chem C*. 2009;113(24):10322-10325. doi:10.1021/jp902523c
95. Shin I, Seo H, Son M-K, Kim J-K, Prabakar K, Kim H-J. Analysis of TiO2 thickness effect on characteristic of a dye-sensitized solar cell by using electrochemical impedance spectroscopy. *Curr Appl Phys*. 2010;10(3):S422-S424. doi:10.1016/J.CAP.2009.12.039
96. Chang B-Y, Park S-M. Electrochemical Impedance Spectroscopy. *Annu Rev Anal Chem*. 2010;3(1):207-229. doi:10.1146/annurev.anchem.012809.102211
97. Fabregat-Santiago F, Bisquert J, Garcia-Belmonte G, Boschloo G, Hagfeldt A. Influence of electrolyte in transport and recombination in dye-sensitized solar cells studied by impedance spectroscopy. *Sol Energy Mater Sol Cells*. 2005;87(1-4):117-131. doi:10.1016/J.SOLMAT.2004.07.017
98. Claudia Longo, A. F. Nogueira and, Paoli* M-A De, Cachet H. Solid-State and Flexible Dye-Sensitized TiO2 Solar Cells: a Study by Electrochemical Impedance Spectroscopy. 2002. doi:10.1021/JP014456U
99. Qing Wang, Jacques-E. Moser and, Grätzel* M. Electrochemical Impedance Spectroscopic Analysis of Dye-Sensitized Solar Cells. 2005. doi:10.1021/JP052768H
100. Motonari Adachi *,†, Masaru Sakamoto ‡, Jinting Jiu §, Yukio Ogata ‡ and, Isoda§ S. Determination of Parameters of Electron Transport in Dye-Sensitized Solar Cells Using Electrochemical Impedance Spectroscopy. 2006. doi:10.1021/JP061693U
101. Schichlein H, Müller AC, Voigts M, Krügel A, Ivers-Tiffée E. Deconvolution of electrochemical impedance spectra for the identification of electrode reaction mechanisms in solid oxide fuel cells. *J Appl Electrochem*. 2002;32(8):875-882. doi:10.1023/A:1020599525160
102. Asghari S, Mokmeli A, Samavati M. Study of PEM fuel cell performance by electrochemical impedance spectroscopy. *Int J Hydrogen Energy*. 2010;35(17):9283-9290. doi:10.1016/J.IJHYDENE.2010.03.069
103. Tamilselvi S, Raman V, Rajendran N. Corrosion behaviour of Ti–6Al–7Nb and Ti–6Al–4V ELI alloys in the simulated body fluid solution by electrochemical impedance spectroscopy. *Electrochim Acta*.

2006;52(3):839-846. doi:10.1016/J.ELECTACTA.2006.06.018
104. Nishikata A, Ichihara Y, Tsuru T. An application of electrochemical impedance spectroscopy to atmospheric corrosion study. *Corros Sci*. 1995;37(6):897-911. doi:10.1016/0010-938X(95)00002-2
105. Pebere N, Riera C, Dabosi F. Investigation of magnesium corrosion in aerated sodium sulfate solution by electrochemical impedance spectroscopy. *Electrochim Acta*. 1990;35(2):555-561. doi:10.1016/0013-4686(90)87043-2
106. Bonora PL, Deflorian F, Fedrizzi L. Electrochemical impedance spectroscopy as a tool for investigating underpaint corrosion. *Electrochim Acta*. 1996;41(7-8):1073-1082. doi:10.1016/0013-4686(95)00440-8
107. Mansfeld F. Use of electrochemical impedance spectroscopy for the study of corrosion protection by polymer coatings. *J Appl Electrochem*. 1995;25(3):187-202. doi:10.1007/BF00262955
108. Tang D, Yuan R, Chai Y, Dai J, Zhong X, Liu Y. A novel immunosensor based on immobilization of hepatitis B surface antibody on platinum electrode modified colloidal gold and polyvinyl butyral as matrices via electrochemical impedance spectroscopy. *Bioelectrochemistry*. 2004;65(1):15-22. doi:10.1016/J.BIOELECHEM.2004.05.004
109. Chuanmin Ruan †, Liju Yang ‡ and, Yanbin Li* †,‡. Immunobiosensor Chips for Detection of Escherichia coli O157:H7 Using Electrochemical Impedance Spectroscopy. 2002. doi:10.1021/AC025647B
110. Pei R, Cheng Z, Wang E, Yang X. Amplification of antigen–antibody interactions based on biotin labeled protein–streptavidin network complex using impedance spectroscopy. *Biosens Bioelectron*. 2001;16(6):355-361. doi:10.1016/S0956-5663(01)00150-6
111. Katz E, Willner I. Probing Biomolecular Interactions at Conductive and Semiconductive Surfaces by Impedance Spectroscopy: Routes to Impedimetric Immunosensors, DNA-Sensors, and Enzyme Biosensors. *Electroanalysis*. 2003;15(11):913-947. doi:10.1002/elan.200390114
112. and SP, Rothberg* L. Chemical Control of Electrode Functionalization for Detection of DNA Hybridization by Electrochemical Impedance Spectroscopy. 2005. doi:10.1021/LA048083A
113. Keighley SD, Li P, Estrela P, Migliorato P. Optimization of DNA immobilization on gold electrodes for label-free detection by electrochemical impedance spectroscopy. *Biosens Bioelectron*. 2008;23(8):1291-1297. doi:10.1016/J.BIOS.2007.11.012
114. Lisdat F, Schäfer D. The use of electrochemical impedance spectroscopy for biosensing. *Anal Bioanal Chem*. 2008;391(5):1555-1567. doi:10.1007/s00216-008-1970-7
115. Wang R, Di J, Ma J, Ma Z. Highly sensitive detection of cancer cells by electrochemical impedance spectroscopy. *Electrochim Acta*. 2012;61:179-184. doi:10.1016/J.ELECTACTA.2011.11.112
116. Hu Y, Zuo P, Ye B-C. Label-free electrochemical impedance spectroscopy biosensor for direct detection of cancer cells based on the interaction between carbohydrate and lectin. *Biosens Bioelectron*. 2013;43:79-83. doi:10.1016/J.BIOS.2012.11.028
117. Wei B, Tokash JC, Zhang F, Kim Y, Logan BE. Electrochemical analysis of separators used in single-chamber, air-cathode microbial fuel cells. *Electrochim Acta*. 2013;89:45-51. doi:10.1016/J.ELECTACTA.2012.11.004

118. Yoho RA, Popat SC, Fabregat-Santiago F, Giménez S, Heijne A ter, Torres CI. Electrochemical Impedance Spectroscopy as a Powerful Analytical Tool for the Study of Microbial Electrochemical Cells. In: *Biofilms in Bioelectrochemical Systems*. Hoboken, NJ, USA: John Wiley & Sons, Inc; 2015:249-280. doi:10.1002/9781119097426.ch8
119. Dominguez-Benetton X, Sevda S, Vanbroekhoven K, Pant D. The accurate use of impedance analysis for the study of microbial electrochemical systems. *Chem Soc Rev*. 2012;41(21):7228. doi:10.1039/c2cs35026b
120. Manohar AK, Bretschger O, Nealson KH, Mansfeld F. The use of electrochemical impedance spectroscopy (EIS) in the evaluation of the electrochemical properties of a microbial fuel cell. *Bioelectrochemistry*. 2008;72(2):149-154. doi:10.1016/J.BIOELECHEM.2008.01.004
121. He Z, Mansfeld F. Exploring the use of electrochemical impedance spectroscopy (EIS) in microbial fuel cell studies. *Energy Environ Sci*. 2009;2(2):215-219. doi:10.1039/B814914C
122. Sacco A. Electrochemical impedance spectroscopy: Fundamentals and application in dye-sensitized solar cells. *Renew Sustain Energy Rev*. 2017;79:814-829. doi:10.1016/J.RSER.2017.05.159
123. Min B, Cheng S, Logan BE. Electricity generation using membrane and salt bridge microbial fuel cells. *Water Res*. 2005;39(9):1675-1686. doi:10.1016/j.watres.2005.02.002
124. Kim JR, Premier GC, Hawkes FR, Rodríguez J, Dinsdale RM, Guwy AJ. Modular tubular microbial fuel cells for energy recovery during sucrose wastewater treatment at low organic loading rate. *Bioresour Technol*. 2010;101(4):1190-1198. doi:10.1016/J.BIORTECH.2009.09.023
125. Yi Zuo, Shaoan Cheng, Doug Call and, Logan* BE. Tubular Membrane Cathodes for Scalable Power Generation in Microbial Fuel Cells. 2007. doi:10.1021/ES0627601
126. Min B, Angelidaki I. Innovative microbial fuel cell for electricity production from anaerobic reactors. *J Power Sources*. 2008;180(1):641-647. doi:10.1016/J.JPOWSOUR.2008.01.076
127. Dewan A, Beyenal H, Lewandowski Z. Scaling up Microbial Fuel Cells. *Environ Sci Technol*. 2008;42(20):7643-7648. doi:10.1021/es800775d
128. Di Lorenzo M, Curtis TP, Head IM, Scott K. A single-chamber microbial fuel cell as a biosensor for wastewaters. *Water Res*. 2009;43(13):3145-3154. doi:10.1016/J.WATRES.2009.01.005
129. Nam J-Y, Kim H-W, Lim K-H, Shin H-S, Logan BE. Variation of power generation at different buffer types and conductivities in single chamber microbial fuel cells. *Biosens Bioelectron*. 2010;25(5):1155-1159. doi:10.1016/J.BIOS.2009.10.005
130. Huang L, Angelidaki I. Effect of humic acids on electricity generation integrated with xylose degradation in microbial fuel cells. *Biotechnol Bioeng*. 2008;100(3):413-422. doi:10.1002/bit.21786
131. Freguia S, Rabaey K, Yuan Z, Keller J. Sequential anode–cathode configuration improves cathodic oxygen reduction and effluent quality of microbial fuel cells. *Water Res*. 2008;42(6-7):1387-1396. doi:10.1016/J.WATRES.2007.10.007
132. Xing D, Zuo Y, Cheng S, Regan JM, Logan BE. Electricity Generation by *Rhodopseudomonas palustris* DX-1. *Environ Sci Technol*. 2008;42(11):4146-4151. doi:10.1021/es800312v

133. You S, Zhao Q, Zhang J, Liu H, Jiang J, Zhao S. Increased sustainable electricity generation in up-flow air-cathode microbial fuel cells. *Biosens Bioelectron*. 2008;23(7):1157-1160. doi:10.1016/J.BIOS.2007.10.010
134. Thygesen A, Poulsen FW, Min B, Angelidaki I, Thomsen AB. The effect of different substrates and humic acid on power generation in microbial fuel cell operation. *Bioresour Technol*. 2009;100(3):1186-1191. doi:10.1016/J.BIORTECH.2008.07.067
135. Zuo Y, Cheng S, Logan BE. Ion Exchange Membrane Cathodes for Scalable Microbial Fuel Cells. *Environ Sci Technol*. 2008;42(18):6967-6972. doi:10.1021/es801055r
136. Jung Rae Kim †, Shaoan Cheng †, Sang-Eun Oh †,§ and, Bruce E. Logan* †,‡. Power Generation Using Different Cation, Anion, and Ultrafiltration Membranes in Microbial Fuel Cells. 2007. doi:10.1021/ES062202M
137. Fan Y, Hu H, Liu H. Sustainable Power Generation in Microbial Fuel Cells Using Bicarbonate Buffer and Proton Transfer Mechanisms. *Environ Sci Technol*. 2007;41(23):8154-8158. doi:10.1021/es071739c
138. Shaoan Cheng †, Hong Liu † and, Bruce E. Logan* †,‡. Increased Power Generation in a Continuous Flow MFC with Advective Flow through the Porous Anode and Reduced Electrode Spacing. 2006. doi:10.1021/ES051652W
139. Bruce Logan *,†,‡, Shaoan Cheng †,‡, Valerie Watson † and, Estadt§ G. Graphite Fiber Brush Anodes for Increased Power Production in Air-Cathode Microbial Fuel Cells. 2007. doi:10.1021/ES062644Y
140. Cheng P, Shan R, Yuan H-R, Dong G, Deng L, Chen Y. Enhanced Rhodococcus pyridinivorans sp. strain HR-1 anode performance in microbial fuel cells by adding polymyxin B sulfate. *Electrochem commun*. 2018;93:171-174. doi:10.1016/J.ELECOM.2018.07.011
141. Chen Z, Niu Y, Zhao S, et al. A novel biosensor for p-nitrophenol based on an aerobic anode microbial fuel cell. *Biosens Bioelectron*. 2016;85:860-868. doi:10.1016/J.BIOS.2016.06.007
142. Yang W, Wei X, Fraiwan A, Coogan CG, Lee H, Choi S. Fast and sensitive water quality assessment: A μL-scale microbial fuel cell-based biosensor integrated with an air-bubble trap and electrochemical sensing functionality. *Sensors Actuators B Chem*. 2016;226:191-195. doi:10.1016/J.SNB.2015.12.002
143. Stein NE, Hamelers HVM, Buisman CNJ. The effect of different control mechanisms on the sensitivity and recovery time of a microbial fuel cell based biosensor. *Sensors Actuators B Chem*. 2012;171-172:816-821. doi:10.1016/J.SNB.2012.05.076
144. Stein NE, Hamelers HVM, Buisman CNJ. Influence of membrane type, current and potential on the response to chemical toxicants of a microbial fuel cell based biosensor. *Sensors Actuators B Chem*. 2012;163(1):1-7. doi:10.1016/J.SNB.2011.10.060
145. Stein NE, Hamelers HVM, Buisman CNJ. Stabilizing the baseline current of a microbial fuel cell-based biosensor through overpotential control under non-toxic conditions. *Bioelectrochemistry*. 2010;78(1):87-91. doi:10.1016/J.BIOELECHEM.2009.09.009
146. Di Lorenzo M, Thomson AR, Schneider K, Cameron PJ, Ieropoulos I. A small-scale air-cathode microbial fuel cell for on-line monitoring of water quality. *Biosens Bioelectron*. 2014;62:182-188.

doi:10.1016/J.BIOS.2014.06.050
147. Jiang Y, Liang P, Liu P, Wang D, Miao B, Huang X. A novel microbial fuel cell sensor with biocathode sensing element. *Biosens Bioelectron*. 2017;94:344-350. doi:10.1016/J.BIOS.2017.02.052
148. Kim BH, Chang IS, Gadd GM. Challenges in microbial fuel cell development and operation. *Appl Microbiol Biotechnol*. 2007;76(3):485-494. doi:10.1007/s00253-007-1027-4
149. Park M, Tsai S-L, Chen W, Park M, Tsai S-L, Chen W. Microbial Biosensors: Engineered Microorganisms as the Sensing Machinery. *Sensors*. 2013;13(5):5777-5795. doi:10.3390/s130505777
150. Pierra M, Carmona-Martínez AA, Trably E, Godon J-J, Bernet N. Microbial characterization of anode-respiring bacteria within biofilms developed from cultures previously enriched in dissimilatory metal-reducing bacteria. *Bioresour Technol*. 2015;195:283-287. doi:10.1016/J.BIORTECH.2015.07.010
151. Hong Y, Call DF, Werner CM, Logan BE. Adaptation to high current using low external resistances eliminates power overshoot in microbial fuel cells. *Biosens Bioelectron*. 2011;28(1):71-76. doi:10.1016/J.BIOS.2011.06.045
152. Zhang L, Zhu X, Li J, Liao Q, Ye D. Biofilm formation and electricity generation of a microbial fuel cell started up under different external resistances. *J Power Sources*. 2011;196(15):6029-6035. doi:10.1016/J.JPOWSOUR.2011.04.013
153. Katuri KP, Scott K, Head IM, Picioreanu C, Curtis TP. Microbial fuel cells meet with external resistance. *Bioresour Technol*. 2011;102(3):2758-2766. doi:10.1016/J.BIORTECH.2010.10.147
154. Sathish-Kumar K, Solorza-Feria O, Tapia-Ramírez J, Rinderkenecht-Seijas N, Poggi-Varaldo HM. Electrochemical and chemical enrichment methods of a sodic–saline inoculum for microbial fuel cells. *Int J Hydrogen Energy*. 2013;38(28):12600-12609. doi:10.1016/J.IJHYDENE.2012.11.147
155. Marsili E, Rollefson JB, Baron DB, Hozalski RM, Bond DR. Microbial biofilm voltammetry: Direct electrochemical characterization of catalytic electrode-attached biofilms. *Appl Environ Microbiol*. 2008. doi:10.1128/AEM.00177-08
156. Liu Y, Deng D, Lan X. A Highly Efficient Mixed-culture Biofilm as Anodic Catalyst and Insights into Its Enhancement through Electrochemistry by Comparison with G. sulfurreducens. *Electrochim Acta*. 2015;155:327-334. doi:10.1016/J.ELECTACTA.2014.12.152
157. Kim JR, Min B, Logan BE. Evaluation of procedures to acclimate a microbial fuel cell for electricity production. *Appl Microbiol Biotechnol*. 2005;68(1):23-30. doi:10.1007/s00253-004-1845-6
158. Hidalgo D, Sacco A, Hernández S, Tommasi T. Electrochemical and impedance characterization of Microbial Fuel Cells based on 2D and 3D anodic electrodes working with seawater microorganisms under continuous operation. *Bioresour Technol*. 2015;195:139-146. doi:10.1016/J.BIORTECH.2015.06.127
159. Hirschorn B, Orazem ME, Tribollet B, Vivier V, Frateur I, Musiani M. Determination of effective capacitance and film thickness from constant-phase-element parameters. *Electrochim Acta*. 2010. doi:10.1016/j.electacta.2009.10.065
160. Jung S-H, Ahn Y-H, Oh S-E, et al. Impedance and Thermodynamic Analysis

of Bioanode, Abiotic Anode, and Riboflavin-Amended Anode in Microbial Fuel Cells. *Bull Korean Chem Soc*. 2012;33(10):3349-3354. doi:10.5012/bkcs.2012.33.10.3349

161. Fricke K, Harnisch F, Schröder U. On the use of cyclic voltammetry for the study of anodic electron transfer in microbial fuel cells. *Energy Environ Sci*. 2008;1(1):144. doi:10.1039/b802363h
162. Peng L, Zhang X-T, Yin J, et al. Geobacter sulfurreducens adapts to low electrode potential for extracellular electron transfer. *Electrochim Acta*. 2016;191:743-749. doi:10.1016/J.ELECTACTA.2016.01.033
163. Li C, Lesnik KL, Fan Y, Liu H. Redox Conductivity of Current-Producing Mixed Species Biofilms. Lebedev N, ed. *PLoS One*. 2016;11(5):e0155247. doi:10.1371/journal.pone.0155247
164. Virdis B, Millo D, Donose BC, Lu Y, Batstone DJ, Krömer JO. Analysis of electron transfer dynamics in mixed community electroactive microbial biofilms. *RSC Adv*. 2016;6(5):3650-3660. doi:10.1039/C5RA15676A
165. Magnuson TS, Isoyama N, Hodges-Myerson AL, et al. Isolation, characterization and gene sequence analysis of a membrane-associated 89 kDa Fe(III) reducing cytochrome c from Geobacter sulfurreducens. *Biochem J*. 2001;359(Pt 1):147-152. doi:10.1042/BJ3590147
166. Seviour T, Doyle LE, Lauw SJL, et al. Voltammetric profiling of redox-active metabolites expressed by Pseudomonas aeruginosa for diagnostic purposes. *Chem Commun*. 2015;51(18):3789-3792. doi:10.1039/C4CC08590F
167. Sharp D, Gladstone P, Smith RB, Forsythe S, Davis J. Approaching intelligent infection diagnostics: Carbon fibre sensor for electrochemical pyocyanin detection. *Bioelectrochemistry*. 2010;77(2):114-119. doi:10.1016/J.BIOELECHEM.2009.07.008
168. Hamelers HVM, ter Heijne A, Stein N, Rozendal RA, Buisman CJN. Butler–Volmer–Monod model for describing bio-anode polarization curves. *Bioresour Technol*. 2011;102(1):381-387. doi:10.1016/J.BIORTECH.2010.06.156
169. Hong J, Ghourchian H, Moosavi–Movahedi AA. Direct electron transfer of redox proteins on a Nafion-cysteine modified gold electrode. *Electrochem commun*. 2006;8(10):1572-1576. doi:10.1016/J.ELECOM.2006.07.011
170. Sheng-Fu Wang †,‡, Ting Chen ‡, Zhi-Ling Zhang †, et al. Direct Electrochemistry and Electrocatalysis of Heme Proteins Entrapped in Agarose Hydrogel Films in Room-Temperature Ionic Liquids. 2005. doi:10.1021/LA050947K
171. Oliot M, Galier S, Roux de Balmann H, Bergel A. Ion transport in microbial fuel cells: Key roles, theory and critical review. *Appl Energy*. 2016;183:1682-1704. doi:10.1016/J.APENERGY.2016.09.043
172. Lobato J, González del Campo A, Fernández FJ, Cañizares P, Rodrigo MA. Lagooning microbial fuel cells: A first approach by coupling electricity-producing microorganisms and algae. *Appl Energy*. 2013;110:220-226. doi:10.1016/J.APENERGY.2013.04.010
173. Wang C-T, Lee Y-C, Ou Y-T, et al. Exposing effect of comb-type cathode electrode on the performance of sediment microbial fuel cells. *Appl Energy*. 2017;204:620-625. doi:10.1016/J.APENERGY.2017.07.079
174. Hong SW, Chang IS, Choi YS, Chung TH. Experimental evaluation of influential factors for electricity harvesting from sediment using microbial

fuel cell. *Bioresour Technol*. 2009;100(12):3029-3035. doi:10.1016/J.BIORTECH.2009.01.030

175. Hsu L, Mohamed A, Ha PT, et al. The Influence of Energy Harvesting Strategies on Performance and Microbial Community for Sediment Microbial Fuel Cells. *J Electrochem Soc*. 2017;164(3):H3109-H3114. doi:10.1149/2.0171703jes
176. Arias-Thode YM, Hsu L, Anderson G, et al. Demonstration of the SeptiStrand benthic microbial fuel cell powering a magnetometer for ship detection. *J Power Sources*. 2017;356:419-429. doi:10.1016/J.JPOWSOUR.2017.03.045
177. Martinucci E, Pizza F, Perrino D, et al. Energy balance and microbial fuel cells experimentation at wastewater treatment plant Milano-Nosedo. *Int J Hydrogen Energy*. 2015;40(42):14683-14689. doi:10.1016/J.IJHYDENE.2015.08.100
178. Erable B, Lacroix R, Etcheverry L, Féron D, Delia ML, Bergel A. Marine floating microbial fuel cell involving aerobic biofilm on stainless steel cathodes. *Bioresour Technol*. 2013;142:510-516. doi:10.1016/J.BIORTECH.2013.05.063
179. Tommasi T, Salvador GP, Quaglio M. New insights in Microbial Fuel Cells: novel solid phase anolyte. *Sci Rep*. 2016;6(1):29091. doi:10.1038/srep29091
180. Wetser K, Dieleman K, Buisman C, Strik D. Electricity from wetlands: Tubular plant microbial fuels with silicone gas-diffusion biocathodes. *Appl Energy*. 2017. doi:10.1016/j.apenergy.2016.10.122
181. Tommasi T, Sacco A, Armato C, et al. Dynamical analysis of microbial fuel cells based on planar and 3D-packed anodes. *Chem Eng J*. 2016;288:38-49. doi:10.1016/J.CEJ.2015.11.089
182. Velasquez-Orta SB, Werner D, Varia JC, Mgana S. Microbial fuel cells for inexpensive continuous in-situ monitoring of groundwater quality. *Water Res*. 2017;117:9-17. doi:10.1016/J.WATRES.2017.03.040
183. Eriksson S, Hurme R, Rhen M, Bowles DJ, Quick P. Low-temperature sensors in bacteria. In: *Philosophical Transactions of the Royal Society B: Biological Sciences*. ; 2002. doi:10.1098/rstb.2002.1077
184. Hall EK, Singer GA, Kainz MJ, Lennon JT. Evidence for a temperature acclimation mechanism in bacteria: An empirical test of a membrane-mediated trade-off. *Funct Ecol*. 2010. doi:10.1111/j.1365-2435.2010.01707.x
185. Huang Y, He Z, Kan J, Manohar AK, Nealson KH, Mansfeld F. Electricity generation from a floating microbial fuel cell. *Bioresour Technol*. 2012. doi:10.1016/j.biortech.2012.02.142
186. Song YC, Yoo KS, Lee SK. Surface floating, air cathode, microbial fuel cell with horizontal flow for continuous power production from wastewater. *J Power Sources*. 2010. doi:10.1016/j.jpowsour.2010.04.041
187. An J, Kim D, Chun Y, Lee SJ, Ng HY, Chang IS. Floating-type microbial fuel cell (FT-MFC) for treating organic-contaminated water. *Environ Sci Technol*. 2009. doi:10.1021/es8024337
188. Schievano A, Colombo A, Grattieri M, et al. Floating microbial fuel cells as energy harvesters for signal transmission from natural water bodies. *J Power Sources*. 2017. doi:10.1016/j.jpowsour.2016.11.037